FACULTY OF ENGINEERING OF THE UNIVERSITY OF PORTO

Simulation of Pelvic Organ Prolapse Repair Surgery Using Biodegradable Implants Mimicking Uterosacral and Cardinal Ligaments

Ana Telma Costa Silva

Dissertation elaborated within the scope of the Master's in Biomedical Engineering

Supervisor: Dra. Maria Elisabete Teixeira da Silva

Co-supervisor: Prof. Dr. Marco Paulo Lages Parente

Co-supervisor: Eng. Nuno Miguel Araújo Ferreira

July 22, 2024

Simulation of Pelvic Organ Prolapse Repair Surgery Using Biodegradable Implants Mimicking Uterosacral and Cardinal Ligaments

Ana Telma Costa Silva

Dissertation elaborated within the scope of the Master's in Biomedical Engineering

July 22, 2024

Abstract

The pelvic organs encompass the pelvic cavity, the pelvic girdle, and the pelvic floor. Pelvic Organ Prolapse is a form of Pelvic Floor Dysfunction marked by one or more pelvic organs descending from their normal position due to weakened or torn ligaments and pelvic floor muscles, which typically provide support to these organs.

This condition is particularly prevalent among older women and individuals who have undergone at least one vaginal birth, significantly impacting their quality of life.

It is anticipated that the number of women undergoing surgery with surgical meshes will continue to rise. Currently, no completely effective treatment for this dysfunction exists, as existing methods harbor several disadvantages and limitations. Therefore, the development of new alternatives that more effectively address these issues and improve the treatment of Pelvic Organ Prolapse is crucial.

An innovative approach involves the development of biodegradable meshes with properties similar to human tissue. These meshes degrade over 2-3 years and possess elastic properties suitable for prolapse repair. Different computational models were developed using Abaqus® software, integrating various biodegradable mesh geometries with square and sinusoidal configurations to mimic the uterosacral and cardinal ligaments, which are responsible for providing support and stability to the pelvic organs, especially the uterus. Supero-inferior displacement analyses were conducted to identify the most effective approaches for supporting the uterus, and these results were compared with values from models without implants and previous studies using other types of meshes. This research also allowed the investigation of different fixation methods and the comparison of results, emphasizing the importance of understanding mesh implantation techniques, including anchoring points.

In conclusion, after analyzing all the results obtained, the Model 1 and 3 implants with a square configuration exhibited the lowest supero-inferior displacement under different conditions, and the continuous suture was the most effective fixation technique. This is attributed to the square mesh being subjected to tension from the outset, unlike the sinusoidal configuration. However, to more accurately emulate the behavior of the uterosacral and cardinal ligaments, a combination of the sinusoidal and square meshes could potentially yield even better results.

Keywords: Pelvic Organ Prolapse; Biodegradable mesh; Uterosacral and Cardinal Ligaments; Computational Models.

Resumo

A anatomia dos órgãos pélvicos engloba a cavidade pélvica, a cintura pélvica e o pavimento pélvico. O Prolapso dos Órgãos Pélvicos é uma forma de Disfunção do Pavimento Pélvico caracterizada pela descida de um ou mais órgãos pélvicos da sua posição normal devido ao enfraquecimento ou rutura dos ligamentos e dos músculos do pavimento pélvico, que normalmente dão apoio a estes órgãos.

Esta condição é particularmente prevalente em mulheres mais velhas e em indivíduos que tiveram pelo menos um parto vaginal, afetando significativamente a sua qualidade de vida.

Prevê-se que o número de mulheres submetidas a cirurgia com malhas cirúrgicas continue a aumentar. Atualmente, não existe um tratamento completamente eficaz para esta disfunção, uma vez que os métodos existentes apresentam várias desvantagens e limitações. Por conseguinte, é crucial o desenvolvimento de novas alternativas que abordem mais eficazmente estas questões e melhorem o tratamento do Prolapso dos Órgãos Pélvicos.

Uma abordagem inovadora envolve o desenvolvimento de malhas biodegradáveis com propriedades semelhantes às do tecido humano. Estas malhas degradam-se ao longo de 2-3 anos e possuem propriedades elásticas adequadas para a reparação do prolapso. Foram desenvolvidos diferentes modelos computacionais utilizando o *Software* Abaqus®, integrando diferentes geometrias de malhas biodegradáveis com a configuração quadrada e sinusoidal, de forma a mimetizar os ligamentos uterossacrais e cardinais, que são responsáveis pelo suporte e estabilidade aos órgãos pélvicos, especialmente o útero. Foram efectuadas análises de deslocamento supero-inferior para identificar as abordagens que melhor suportavam o útero, tendo estes resultados sido comparados com valores de modelos sem implantes e com estudos anteriores que utilizaram outros tipos de malhas. Esta pesquisa também permitiu a investigação de diferentes métodos de fixação e a comparação de resultados, ressaltando a importância do conhecimento das técnicas de implantação de malhas, incluindo pontos de ancoragem.

Em conclusão, após a análise de todos os resultados obtidos, os implantes do Modelo 1 e 3 com uma configuração quadrada apresentaram o menor deslocamento supero-inferior em diferentes condições, e a sutura contínua foi a técnica de fixação mais eficaz. Este resultado é atribuído ao facto da malha quadrada estar sujeita a tensão desde o início, ao contrário da configuração sinusoidal. No entanto, para mimetizar com maior exatidão o comportamento dos ligamentos uterossacrais e cardinais, uma combinação das malhas sinusoidal e quadrada poderia potencialmente produzir resultados melhores.

Keywords: Prolapso dos Órgãos Pélvicos; Malha Biodegradável; Ligamentos Uterossacrais e Cardinais; Modelos Computacionais.

Acknowledgements

First and foremost, I would like to express my deepest gratitude to my supervisor, Prof. Dra. Maria Elisabete Teixeira da Silva, for her support, availability, and guidance throughout my research. I also want to thank my co-supervisors, Prof. Dr. Marco Paulo Lages Parente, for all the help whenever I asked and Eng. Nuno Miguel Araújo Ferreira, for his help, patience, expertise, valuable suggestions, and constant support.

I am deeply grateful to the Faculty of Engineering of the University of Porto and the Institute of Science and Innovation in Mechanical Engineering and Industrial Engineering for their unwavering support and provision of necessary resources.

I also want to thank my colleagues in the Laboratory of Product Development and Services, especially Ana Pais and Francisca Vaz, for all their help, encouragement, and companionship, which have made our workplace such a cozy space and made this journey much lighter.

On a deeply personal note, I am eternally grateful to my family for their unwavering support and encouragement. I especially want to thank my parents for always believing in me, giving me all the tools (and then some) to be who I am, and for all their love, patience, and pride throughout my academic career. Your love and support have been my anchor. To my uncles and cousins, for always being there and for being synonymous with home.

To my lifelong friends, for being the best and providing moments that are sometimes so simple but always unforgettable, and to the friends that university gave me that I'm sure I'll keep in my heart forever.

I also want to thank the members of Rancho DC Olival for all the wonderful laughs and for being the best possible "escape."

Lastly, I gratefully acknowledge the Emprego Científico 2021.00077.CEECIND, Funded by FCT. This work was supported by FCT, through INEGI, in the scope of LAETA, project UIDB /50022 /2020 and UIDP /50022 /2020.

"Unless you try to do something beyond what you have already mastered, you will never grow."

Rukayat

Contents

1 Introduction **1**
- 1.1 Motivation . . . 1
- 1.2 Objectives . . . 2
- 1.3 Dissertation Structure . . . 2

2 Pelvic Anatomy and Pelvic Floor Dysfunctions **5**
- 2.1 Female Pelvis Anatomy . . . 5
  - 2.1.1 Pelvic Girdle . . . 6
  - 2.1.2 Pelvic Cavity . . . 7
  - 2.1.3 Female Pelvic Floor . . . 7
- 2.2 Female Pelvic Floor Dysfunctions . . . 9
  - 2.2.1 Pelvic Organ Prolapse . . . 9

3 Computational Modelling **21**
- 3.1 Finite Element Method . . . 21
- 3.2 Abaqus® Software . . . 24
- 3.3 Simulations in previous studies . . . 24

4 Materials and Methods **29**
- 4.1 Biomechanics of the Female Pelvic Cavity . . . 29
  - 4.1.1 Constitutive Models . . . 29
  - 4.1.2 Mechanical Properties . . . 31
  - 4.1.3 Computational Modelling of the Female Pelvic Cavity . . . 32
- 4.2 Biomechanics of the implants for the uterosacral and cardinal ligaments . . . 35
  - 4.2.1 Polycaprolactone (PCL) . . . 35
  - 4.2.2 Numerical Simulation: Model 1 (USL-1) . . . 37
  - 4.2.3 Numerical Simulation: Model 2 (USL-2) . . . 40
  - 4.2.4 Numerical Simulation: Model 3 (CL-3) . . . 44
  - 4.2.5 Points of Reference . . . 47
  - 4.2.6 Study of Different Fixation Conditions . . . 48
  - 4.2.7 Stress-Strain Analysis . . . 49

5 Results **51**
- 5.1 Numerical simulations without implants . . . 51
- 5.2 Numerical simulations with implants . . . 52
  - 5.2.1 Analysis of implants behavior . . . 52
  - 5.2.2 Study the Application of Different Types of Fixations . . . 61
  - 5.2.3 Stress Concentration Analysis . . . 69

6 Discussion **75**

7 Conclusions and Future Work **81**
7.1 Conclusions 81
7.2 Further Work 82

References **83**

List of Figures

2.1 Anterior view of the female pelvis. . . . 6
2.2 Components of the pelvic bone: ilium, pubis, and ischium. . . . 6
2.3 Schematic representation of the female pelvic floor. . . . 8
2.4 The relative position of the female pelvic organs and ligaments. A: top-down view; B: lateral view. . . . 9
2.5 Types of POP. . . . 10
2.6 Parameters of the measuring points of the POP-Q system and their representation. 12
2.7 Quantitative gradings of POP. . . . 13
2.8 Baden-Walker Halfway quantification system. It consists of four different grades: grade 0 - no prolapse; grade 1 - halfway to the hymen; grade 2 - up to the hymen; grade 3 - halfway past the hymen; grade 4 - maximum descent. . . . 13
2.9 Dynamic MRI of rectal and uterine prolapse. From A to C this prolapse is getting worse. . . . 14
2.10 Kegel Exercises. A: Bridge with hip rotations; B: Side clamshell. . . . 15
2.11 The most common types of pessaries. A: cube pessary; B: shell pessary; C: ring pessary. . . . 16
2.12 Number of surgeries each 1 of the 1530 studied cases underwent before complete mesh removal. . . . 18

3.1 FEM. . . . 22
3.2 A: Reconstructed equivalent 2D geometric model; B: Finite element model of the pelvic floor; C: Comparison of morphology before (grey) and after (colored) VM in the healthy pelvic floor. AVW, anterior vaginal wall; B, bladder; C, cervix; CL; LA, levator ani; PB, indicates pubic bone; PeB, perineal body; PUL, pubic urethral ligament; PVW, posterior vaginal wall; R, rectum; RL, round ligament; S, sacrococcyx; U, uterus; USL. . . . 25
3.3 Finite element mesh and boundary conditions in the uterus. A: Posterior view; B: Lateral view. . . . 25
3.4 Implants to mimic the USL and CL after their total rupture in the pelvic cavity. A: CL implant: B: USL implant. (1) pubourethral ligaments, (2) bladder, (3) uterus, (4) USL, (5) CL site, (6) CL implant, (7) vagina, (8) urethra, (9) CL implant, (10) USL site, (11) CL. . . . 26
3.5 Uniaxial tensile test and nominal stress-stretch response for two commercial mesh implants and the numerical curves. . . . 27
3.6 The magnitude of displacement (mm) of the uterus: (a) asymptomatic case; (b) total rupture of the USL; (c) placement of mesh A to replace the USL and (d) placement of mesh B. . . . 27

4.1 3D computational model of the pelvic cavity of an asymptomatic woman. (1), symphysis pubis; (2) bladder; (3) uterus; (4) rectum; (5) LAM; (6) pelvic fascia; (7) arcus tendineous fasciae pelvis; (8) lateral ligaments of the rectum; (9) USL; (10) CL; (11) pubourethral ligaments. 33
4.2 Stress-strain curve of the healthy ligaments, and with impairments (50% and 90%). 34
4.3 Stress-strain values obtained from the uniaxial tensile test carried out on the filament. 35
4.4 PR mesh and how it can be applied to the pelvic cavity (unilateral hysterosacropexy). 37
4.5 Geometry and dimensions of the square mesh to mimic the USL behavior (USL-1Q). 38
4.6 Geometry and dimensions of the sinusoidal mesh to mimic the USL behavior (USL-1S). 39
4.7 Conformation of the USL-Model 1 to the uterus. A: Square mesh (USL-1Q); B: Sinusoidal mesh (USL-1S). 39
4.8 Incorporation of the USL-Model 1 into the computational model of the pelvic cavity. A: USL-1Q for a total rupture of the pelvic cavity; B: USL-1S for USL impairment. 40
4.9 Geometry and dimensions of the square USL mesh to realistically mimic the USL ligament. 40
4.10 A: Conformation of the mesh to the USL; B: Incorporation of both meshes conformed to the ligament in the computational model of the pelvic cavity with total rupture of the USL. 41
4.11 A: Conformation of the mesh to the USL; B: Incorporation of both meshes conformed to the ligament in the computational model of the pelvic cavity without total rupture of the USL. 42
4.12 A: Positioning of the mesh; B: Incorporation of both meshes in the computational model of the pelvic cavity without total rupture of the USL. 42
4.13 Geometry and dimensions of the square mesh to mimic the USL ligament. 43
4.14 A: Positioning of the mesh to the USL; B: Incorporation of both meshes in the computational model of the pelvic cavity without total rupture of the USL. 43
4.15 PRP mesh and how it can be applied to the pelvic cavity (pectopexy technique). . 44
4.16 Geometry and dimensions of the square mesh to mimic the CL behavior (CL3-Q). 44
4.17 Geometry and dimensions of the sinusoidal mesh to mimic the CL behavior (CL3-S). 45
4.18 A: Conformation of the arms of the CL mesh; B: Conformed CL mesh. 46
4.19 Incorporation of the implant into the computational model of the pelvic cavity. A: with total CL rupture; B: without total CL rupture. 46
4.20 Nodes in the anterior vaginal wall to measure the supero-inferior displacement. . 47
4.21 Nodes in the implants to measure the supero-inferior displacement. 47
4.22 Nodes analyzed in the ligaments. 48
4.23 Several anchoring techniques applied. A: A band of elements; B: Continuous line; C: Simple Stitch; D: Horizontal interrupted suture. 48
4.24 Comparison of stress-strain curves. 49

5.1 Different implants (Model 1 and Model 2) developed to mimic USLs 53
5.2 Representation of the supero-inferior displacements of the anterior vaginal wall in cases of total rupture of the ligaments as well as with 50% and 90% impairment with USLs implants. 55
5.3 Representation of the USL behavior mimetization. Analysis of the supero-inferior displacements of the USLs implants in cases of total rupture of the USLs as well as with 50 and 90% impairment. 56
5.4 Different implants (Model 3) developed to mimic CLs. 57

5.5 Representation of the supero-inferior displacements of the anterior vaginal wall in cases of total rupture of the ligaments as well as with 50% and 90% impairment with CLs implants. . . . 58
5.6 Representation of the supero-inferior displacements of the anterior vaginal wall in cases of impairment of 90% of the USL and impairments of 50%, 90%, and total rupture of the CLs occur with CLs implants. . . . 59
5.7 Representation of the CL behavior mimetization. Analysis of the supero-inferior displacement of Model 3 implants in cases of total rupture of the CLs as well as with 50 and 90% impairment. . . . 60
5.8 Representation of the supero-inferior displacements of the anterior vaginal wall in cases of total rupture of the ligaments as well as with 50% and 90% impairment with USLs implants with continuous line suture. . . . 62
5.9 Representation of the supero-inferior displacements of the anterior vaginal wall in cases of total rupture of the ligaments as well as with 50 and 90% impairment with CLs implants - continuous line suture. . . . 63
5.10 Representation of the supero-inferior displacements of the anterior vaginal wall in cases of total rupture of the ligaments as well as with 50 and 90% impairment with USLs implants - simple stitch suture. . . . 65
5.11 Representation of the supero-inferior displacements of the anterior vaginal wall in cases of total rupture of the ligaments as well as with 50 and 90% impairment with CLs implants - simple stitch suture. . . . 66
5.12 Representation of the supero-inferior displacements of the anterior vaginal wall in cases of total rupture of the ligaments as well as with 50 and 90% impairment with USLs implants with continuous line suture - horizontal interrupted suture. . . . 68
5.13 Representation of the supero-inferior displacements of the anterior vaginal wall in cases of total rupture of the ligaments as well as with 50 and 90% impairment with CLs implants - horizontal interrupted suture. . . . 69
5.14 Stress Concentration - Model 1 - A band of elements encastre. . . . 70
5.15 Stress Concentration - Model 1 - Continuous Line. . . . 71
5.16 Stress Concentration - Model 1 - Simple Stitch. . . . 72
5.17 Stress Concentration - Model 1 - Horizontal Interrupted Suture. . . . 73
5.18 Stress Concentration - Model 3Q - A band of elements encastre. . . . 74
5.19 Stress Concentration - Model 3S - A band of elements encastre. . . . 74

List of Tables

2.1 Examples of different synthetic meshes created with the aim of being used in surgery for POP repair. . . . 19
2.2 The most common complications reported to the FDA. . . . 20

3.1 Some of the main advantages of FEM. . . . 22
3.2 Flowchart of the Finite Element Analysis. . . . 23

4.1 Material parameters of the constitutive models applied to healthy pelvic structures. 32
4.2 Number of elements for each pelvic structure. . . . 33
4.3 Numerical parameters of the Yeoh constitutive model for healthy and impaired ligaments. . . . 34
4.4 Numerical parameters used to characterize the damage model. . . . 37

5.1 Supero-inferior displacement of the vaginal wall and respective maximum displacement magnitudes, when impairments of 50%, 90%, and total rupture of the USLs and CLs occur. . . . 51
5.2 Supero-inferior displacement of the vaginal wall and respective maximum displacement magnitudes, with 90% impairment of USL and with impairments of 50%, 90%, and total rupture of the CL. . . . 52
5.3 Supero-inferior displacement of the anterior vagina wall and respective maximum displacement magnitudes, when impairments of 50%, 90%, and total rupture of the USLs occur with USLs implants. . . . 54
5.4 Supero-inferior displacement of the USLs implants and respective maximum displacement magnitudes, when impairments of 50%, 90%, and total rupture of the USLs occur and supero-inferior displacement of this ligament (without implant) with the same conditions. . . . 56
5.5 Supero-inferior displacement and max disp. mag of the vagina, during the VM, when impairments of 50%, 90%, and total rupture of the CLs occur with CLs implants. . . . 58
5.6 Supero-inferior displacement and max disp. mag of the vagina, during the VM, when impairment of 90% of the USL and impairments of 50%, 90%, and total rupture of the CLs occur with CLs implants. . . . 59
5.7 Supero-inferior displacement of the implant and respective maximum displacement magnitudes, when impairments of 50%, 90%, and total rupture of the CLs occur and supero-inferior displacement of this ligament (without implant) with the same conditions. . . . 60
5.8 Analysis of supero-inferior displacements and respective maximum displacement magnitudes in the anterior wall of the vagina with impairment of 50%, 90% and total rupture of USLs. . . . 62

5.9 Supero-inferior displacement and max disp. mag of the vagina, during the VM, when impairments of 50%, 90%, and total rupture of the CLs occur with CLs implants - continuous line suture. 63
5.10 Analysis of supero-inferior displacements and respective maximum displacement magnitudes in the anterior wall of the vagina with impairment of 50%, 90% and total rupture of USLs - simple stitch suture. 64
5.11 Supero-inferior displacement and max disp. mag of the vagina, during the VM, when impairments of 50%, 90%, and total rupture of the CLs occur with CLs implants - simple stitch suture. 66
5.12 Analysis of supero-inferior displacements and respective maximum displacement magnitudes in the anterior wall of the vagina with impairment of 50%, 90% and total rupture of USLs - horizontal interrupted suture. 67
5.13 Supero-inferior displacement and max disp. mag of the vagina, during the VM, when impairments of 50%, 90%, and total rupture of the CLs occur with CLs implants - horizontal interrupted suture. 69

Abbreviations

2D	Two-dimensional
3D	Three-dimensional
AUGS	American Urogynecologic Society
CL	Cardinal Ligament
FDA	Food and Drug Administration
FEA	Finite Element Analysis
FEM	Finite Element Method
FI	Fecal Incontinence
Gh	Genital Hiatus
IAP	Intra-abdominal Pressure
ICS	International Continence Society
LAM	Levator Ani Muscles
MRCs	Mesh-Related Complications
MRI	Magnetic Resonance Imaging
Pb	Perineal Body
PCL	Polycaprolactone
PET	Polyethylene Terephthalate
PFD	Pelvic Floor Dysfunctions
PFM	Pelvic Floor Muscles
PLA	Polylactic Acid
POP	Pelvic Organ Prolapse
POP-Q	Pelvic Organ Prolapse Quantification
PP	Polypropylene
PTFE	Polytetrafluoroethylene
PU	Polyurethane
PVDF	Polyvinidelene Fluoride
PVM	Pubovisceralis Muscles
SP	Symphysis Pubis
Tvl	Total length of the vagina
UI	Urinary Incontinence
USL	Uterosacral Ligament
VM	Valsalva Manuever

Chapter 1

Introduction

1.1 Motivation

The anatomy of the pelvic cavity includes the pelvic organs, the pelvic girdle, and the pelvic floor. Pelvic floor dysfunctions (PFD) contain various types of clinical disorders, most notably urinary incontinence (SUI), pelvic organ prolapse (POP), and fecal incontinence (FI) [1].

POP is a type of PFD where one or more pelvic organs descend from their usual anatomical position due to the weakening or tearing of the ligaments and pelvic floor muscles (PFM) that support them. This condition is especially common in older women and those who have had at least one vaginal birth, significantly impacting their quality of life [2].

In the United States, it is predicted that between 2010 and 2050, the total number of women suffering from some form of PFD will increase from 28 million to 44 million [3]. Concerning POP, worldwide, it is estimated that 40% of women suffer from some degree of this dysfunction. In Portugal, this problem affects around 7.000 women annually, and the number is expected to rise by around 40% over the next 40 years [4]. This situation is also considered serious in developing countries, as evidenced by a study carried out in Ethiopia and Tanzania. Based on a clinical examination, 64.6% of women had some POP degree [5].

However, many women still feel embarrassed to discuss their symptoms with health professionals, convincing themselves that these are typical signs of aging, which worsens the prolapse and discomfort. When diagnosed, mild cases of the condition typically involve treatment through exercises to strengthen the PFM along with the use of vaginal devices such as pessaries to support the pelvic organs. In severe cases, surgical intervention may be necessary to reconstruct pelvic support using either body tissue or synthetic meshes [4].

In the United States, it is estimated that 3.3 million women suffer from POP every year, and it is predicted that between 2010 and 2050, the total number of women undergoing surgery using surgical meshes will increase by 48.2%. However, there are currently several postoperative complications, such as infections and erosion of the mesh tissue, resulting in a re-operation rate after surgery of around 30% [2, 6, 7].

Currently, there is no fully functional treatment for this dysfunction, so several studies are being conducted in search of a better treatment option to guarantee safety and efficacy. In April 2019, synthetic implants used to correct vaginal prolapse were banned from the market due to safety and efficacy concerns [8]. As a result, new tools, particularly in the field of biomechanics and 3D printing, are being developed to create a replacement product. This has led to the development of biodegradable meshes as a potential alternative. One promising solution being studied is biodegradable meshes with properties similar to human tissue, using the polycaprolactone (PCL) polymer, which is medically advantageous and approved by the Food and Drug Administration (FDA) for clinical purposes. Moreover, the mesh anchoring failure was observed in 38% of patients on average 1.8 years after placing the mesh [9]. Thus, it is vital to understand how meshes are implanted [4].

1.2 Objectives

The main aim of this dissertation is to develop a viable treatment to solve the problem of the lack of a sufficiently effective mesh for the surgical repair of POP in women. To this end, my work will include:

- Development of computational models with new biodegradable mesh geometries using Abaqus® software. Once these models have been properly created, they will be incorporated into the computational model of the pelvic cavity.
- Analysis of stress and displacement in the different implants developed.
- Comparison of the results obtained with those of the asymptomatic pelvic cavity model and other results obtained in previous studies using other types of meshes.
- Studying various fixation methods and comparing results with previous studies, including simple stitch, continuous line, and horizontal interrupted suture.

1.3 Dissertation Structure

The dissertation is structured as follows:

Chapter 2 — Pelvic Anatomy and Pelvic Floor Dysfunctions: This chapter introduces fundamental theoretical concepts to familiarize the reader with terms such as pelvis, pelvic girdle, and pelvic cavity. It also provides detailed information on PFD, specifically POP.

Chapter 3 – Computational Modelling: This chapter will explore the fundamental theoretical concepts underlying the finite element method (FEM), through Abaqus® software, and previous simulation studies in detail about pelvic surgery. These concepts will be thoroughly examined throughout the rest of this work to ensure a comprehensive understanding of these essential topics.

Chapter 4 - Materials and Methods: This chapter explains the methodology used for developing computer models that mimic the USL and CL, including their creation, adaptation to the uterus, and incorporation into the pelvic cavity model.

Chapter 5 - Results: In this chapter, we will discuss the outcomes of supero-inferior displacement of the anterior vaginal wall in different scenarios of ligament impairment while also examining various methods of fixation. Additionally, we'll explore the findings concerning the extent of implant displacement and the assessment of areas of high stress in implants with diverse designs.

Chapter 6 - Discussion: This chapter presents the key findings from the entire study and a discussion informed by the existing literature.

Chapter 7 - Conclusions and Future Work: This section includes the dissertation's conclusions and recommendations for future research.

Chapter 2

Pelvic Anatomy and Pelvic Floor Dysfunctions

The female pelvis not only supports the lower limbs but also contains the gastrointestinal tract, bladder, and reproductive organs. It plays a crucial role in functions such as defecation, micturition, and, potentially, childbirth. Over time, the female pelvis's bones, ligaments, and muscles have evolved from their ancestral forms. However, the adaptation of these structures from their original functions, as a supportive role, can pose limitations, potentially leading to POP, one of the most common PFD [10].

2.1 Female Pelvis Anatomy

Female pelvic anatomy is a complex interplay of muscles, ligaments, nerves, and blood vessels that provide dynamic support to the bladder, urethra, uterus, and rectum [11].

Situated centrally in the human body, the pelvis serves various functions, mainly relating to structural support and movement stabilization. The pelvic structure consists of the pelvic girdle, pelvic cavity, pelvic floor, and perineum, and is anatomically divided into two distinct regions - the upper portion, called the false (greater) pelvis, located within the abdominal cavity, and the lower section known as the true (lesser) pelvis, situated within the pelvic cavity. The true pelvis is defined by the pelvic floor [12, 13]. Figure 2.1 shows the female pelvis [14].

The perineum is a crucial anatomical region that includes the external openings of the reproductive system, the outlets of the urinary and gastrointestinal systems, and the roots of the external genital organs [12].

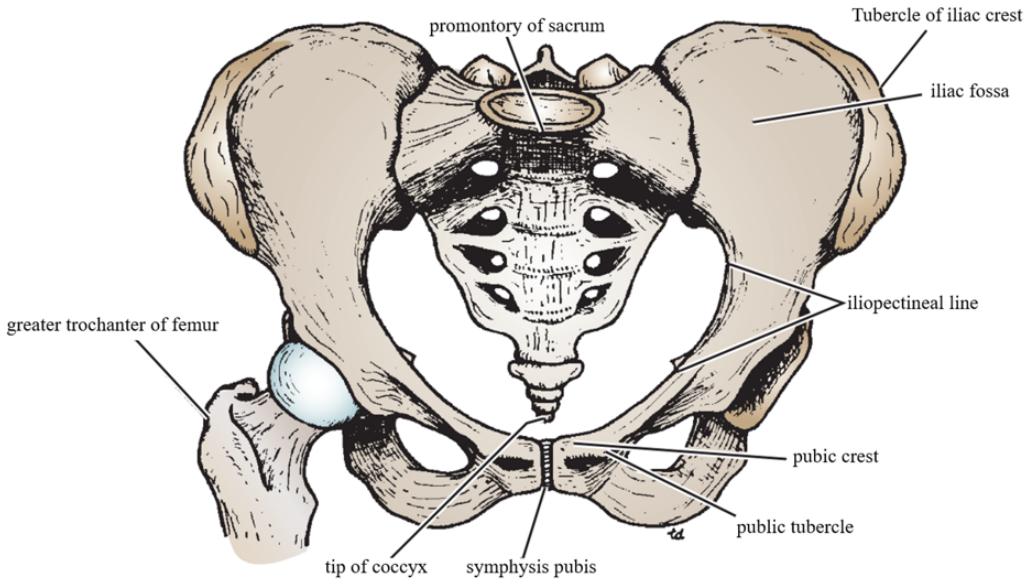

Figure 2.1 Anterior view of the female pelvis (adapted from [14]).

2.1.1 Pelvic Girdle

The pelvic girdle, a structure comprising the sacrum and coccyx bones, is formed by the ilium, ischium, and pubis bones, which connect anteriorly at the pubic symphysis and posteriorly at the sacrum via sacroiliac joints. This structure safeguards the lower parts of the urinary and intestinal tracts and the reproductive organs while also playing a crucial role in weight transmission from the spine to the femur. It provides support and protection for the pelvic viscera and stabilizes the muscles of the trunk and lower limbs. Figure 2.2 illustrates the components of the pelvic bone [13, 14, 15, 16].

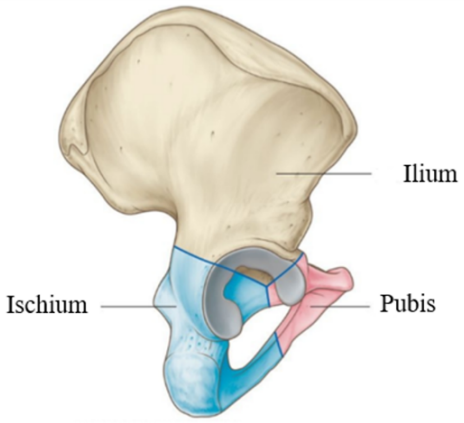

Figure 2.2 Components of the pelvic bone: ilium, pubis, and ischium (adapted from [16]).

2.1.2 Pelvic Cavity

The true pelvis is made up of three parts: the inlet, the outlet, and the cavity. The inlet, which is surrounded by the sacral promontory, iliopectineal lines, and symphysis pubis, leads to the cavity. The outlet is defined by the coccyx, ischial tuberosities, and pubic arch, which has three notches and a diamond shape. The cavity is a curved canal that connects the inlet and outlet, and it has a shallow anterior wall and a deeper posterior wall [13, 14].

Typically, the pelvic cavity is conventionally divided into two parts using the pelvic diaphragm. The upper section is known as the main pelvic cavity, and the lower section is referred to as the perineum. This space contains the urinary bladder, pelvic colon, internal reproductive organs, rectum, and other internal structures such as muscles, arteries, veins, nerves, connective tissues, and pelvic ligaments [14].

The connection between the pelvic and abdominal walls is continuous at the pelvic inlet because the pelvic cavity extends from the abdominal cavity. However, their alignment isn't perfectly vertical due to the backward tilt of the sacrum and pelvic bones along the vertebral column. This tilt causes the pelvic cavity to project backward, resulting in the inlet being oriented superiorly and anteriorly [14].

The pelvic walls (anterior, posterior, lateral, and inferior (or floor)) are composed of various elements, including bones, ligaments, muscles, fascia, and parietal peritoneum. Two important ligaments, the posterior sacrospinous and sacrotuberous ligaments, connect the iliac tuberosity to the corresponding posterior sacral cortex, forming a strong connective tissue structure. These ligaments are short and sturdy, allowing them to support the sacrum and ischium joints. Additionally, the obturator internus and piriformis muscles are key in managing lateral pressures and induced stresses within the pelvic cavity [14, 15, 17].

2.1.3 Female Pelvic Floor

The female pelvic floor is a soft tissue support structure consisting of fascia, ligaments, and muscles in the urogenital and anal regions, extending from the symphysis pubis (SP) to the coccyx. It counteracts the effects of gravity or intra-abdominal pressure (IAP) and facilitates vital bodily functions such as continence of urine and feces, childbirth, and sexual intercourse. The region serves as a convergence point for several functional systems, including the urethra, vagina, and rectum. It comprises a complex network of structures such as the pelvic diaphragm, perineal membrane, perineal body, PFM, and connective tissues such as the endopelvic fascia and pelvic ligaments [18, 19].

The PFM are unique in their ability to bear transverse loads, with contractile fibers that enclose intra-abdominal contents and maintain pelvic organ structure [20]. This group includes the *levatorani* muscle (LAM), which comprises the iliococcygeus, pubococcygeus, puborectalis muscles, and the coccygeus muscle. The pubococcygeus and puborectalis, often collectively termed pubovisceralis muscles (PVM), are U-shaped muscles originating from the inner surface of the pubic bone. The puborectalis muscle is a key constrictor of the PFM and central to active contractile

forces, with relaxation aiding the return of pelvic organs to their anatomical positions, favoring normal micturination and rectal evacuating [21].

The pelvic diaphragm, a muscular and fascial partition around the lower pelvis, includes the LAM and coccygeus muscle with their fasciae, supporting the pelvic viscera development [19, 21]. The LAM retracts the anorectal junction and narrows the genital hiatus upon activation, maintaining muscle tone during rest, contraction, and relaxation to prevent pelvic connective tissue overload. These muscles and the anterior abdominal wall muscles contribute to maintaining IAP. The posteriorly situated coccygeus muscle is vital for supporting the viscera and sustaining IAP [21, 22].

The perineal membrane fills the urogenital opening and provides support to the distal region of the urethra and vagina. The perineal body, which is made of dense connective tissue, acts as a barrier between the urogenital hiatus (the opening through which the vagina and urethra pass) and the anal hiatus. It is located between the rectum and the vagina. If the perineal body weakens, it can lead to prolapse, as the vagina and rectum are situated above it. Figure 2.3 illustrates some of the structures mentioned [21, 23].

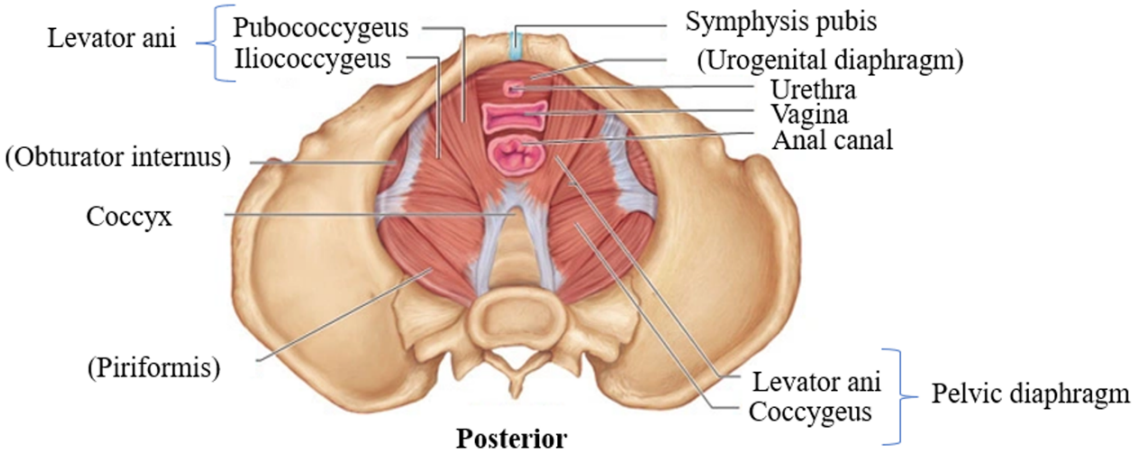

Figure 2.3 Schematic representation of the female pelvic floor (adapted from [24]).

The stability of the pelvic floor is mainly due to the presence of connective tissues. The endopelvic fascia, made up of collagen, elastin, and smooth muscle, forms a continuous layer connecting the pelvic girdle to the LAM and the viscera. The ligaments of the pelvic fascia, which are formed by the endopelvic fasciae, play a vital role in supporting the pelvic organs. These ligaments, including the pubovesical ligament, the pubourethral ligament, the anococcygeal ligament, the uterosacral ligament (USL), and the cardinal ligament (CL), are essential for maintaining the integrity of the pelvic organs [20, 25].

The CL and the USL are primary pelvic structures that provide support for the upper part of the vagina and uterus. Each ligament is represented by four ligaments, one CL and one USL, on

each side of the uterus. The USL connects the cervix to the sacrum, providing support for the uterus, while the CL is located on the lower margin of the external ligaments and contains the uterine arteries and veins. Figure 2.4 shows the positions of these ligaments [20, 25].

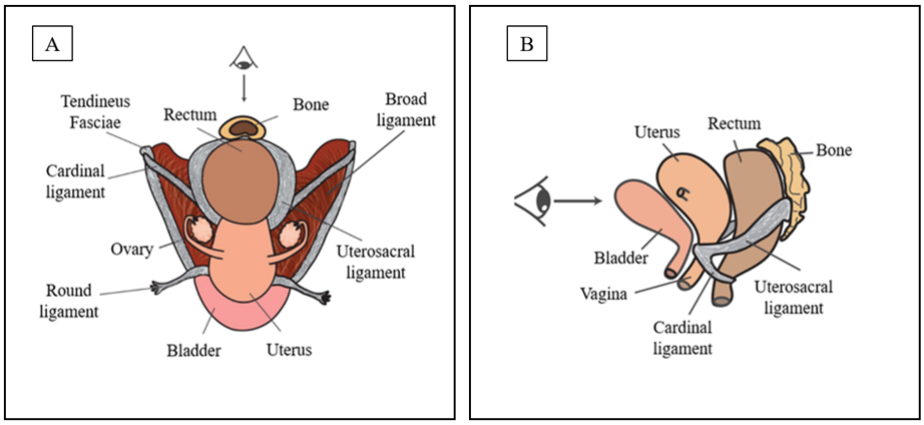

Figure 2.4 The relative position of the female pelvic organs and ligaments. A: top-down view; B: lateral view (adapted from [3]).

2.2 Female Pelvic Floor Dysfunctions

The most common PFD affecting millions of women worldwide are SUI and POP. These conditions are characterized by the weakening of the tissues that support the pelvic floor. They can compromise a woman's physical, social, psychological, and sexual health and lead to social isolation, loss of personal relationships, and reduced participation in leisure activities, thereby harming her quality of life. Other PFD are FI, sensory abnormalities of the lower urinary tract, defecation dysfunction, sexual dysfunction, and pain syndromes related to pelvic organs [26, 27].

Studies indicate that this public health issue is prevalent, especially among older women, but it affects all age groups. In the United States, around 25% of healthy, non-pregnant women are affected, and in Japan, 46.5% of adult women report experiencing at least one dysfunction [1, 26]. By the age of 80, approximately 11% of women will have undergone one or more surgical interventions for SUI or POP [28, 29].

This work's main focus is on POP; therefore, it is necessary to study it more thoroughly.

2.2.1 Pelvic Organ Prolapse

POP is a common and challenging public health issue that impacts millions of women globally. It occurs when the muscles, ligaments, and connective tissues supporting the pelvic organs become weak or injured. This can result in the bladder, cervix, uterus, vagina, rectum, and urethra shifting from their normal positions, causing discomfort, pain, incontinence, and even sexual

dysfunction. Although it can have a major impact on a woman's daily life and well-being, it is not often associated with death [30, 31].

2.2.1.1 Classification

POP is categorized based on which anatomical compartment is impacted: anterior, apical, or posterior. Anterior compartment prolapse involves the descent of the bladder (cystocele) and urethra (urethrocele), while apical compartment prolapse is characterized by the descent of the uterus or the vaginal vault. Posterior compartment prolapse involves the rectum (rectocele) or the descent of the small bowel (enterocele). Different types of prolapse can occur depending on the affected organ. A patient can experience more than one type since the pelvic organs and their supports are interconnected [32].

The most common form of POP is cystocele, which is detected twice as often as posterior vaginal prolapse (rectocele) and three times as often as vaginal dome prolapse [33, 34]. Figure 2.5 shows some of the existing prolapses.

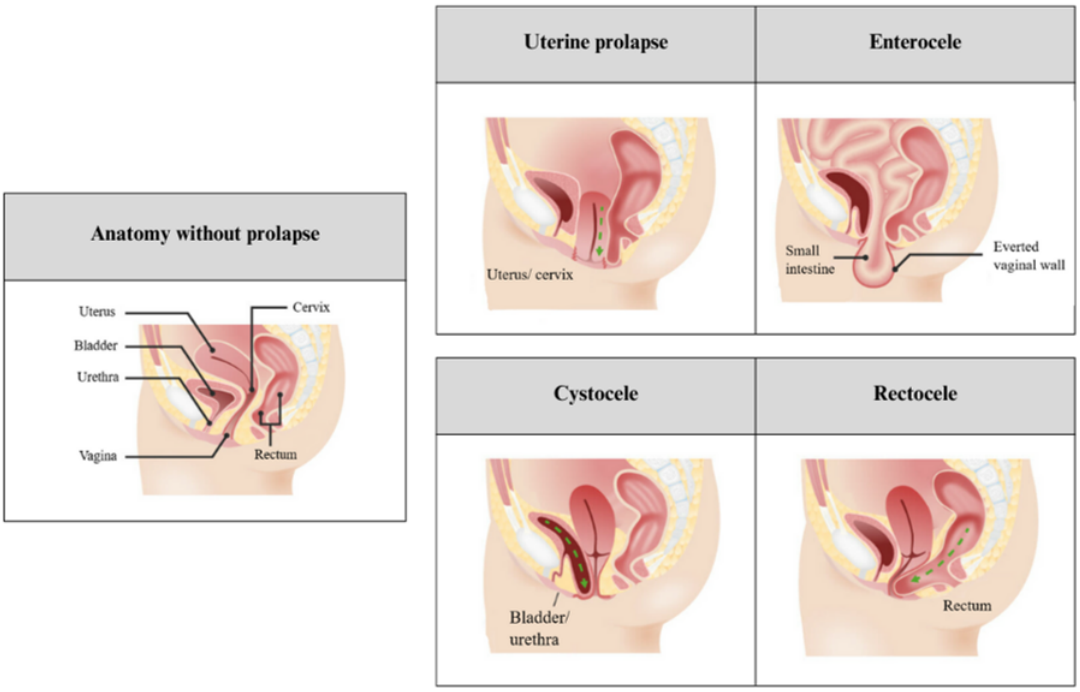

Figure 2.5 Types of POP (adapted from [23]).

2.2.1.2 Symptoms and Risk Factors

POP is a condition associated with a variety of symptoms that can vary depending on the type of prolapse. Some of the most common symptoms include a lump or feeling of swelling in the

vagina, lower back pain, difficulty or inability to have sexual intercourse, vaginal bleeding and discharge, difficulty urinating or defecating, and difficulty walking or sitting. It should be noted that SUI and FI often coexist with POP due to similar risk factors [2, 35, 36].

Several risk factors are known to contribute to the development of POP, including:

- Vaginal delivery: a study of 39617 women who underwent prolapse surgery revealed that 97.8% of them had at least one vaginal delivery, while 0.4% had at least one cesarean delivery, and 1.9% were nulliparous [37];
- Obesity: increased IAP which weakens the PFM and fascia [38];
- Menopause: estrogen deficiency during menopause causes the weakening of pelvic organ support structures and tissues [39];
- Ageing: a study of 65 women with uterine prolapse demonstrated age-related changes in pelvic ligament and muscle function, of which 90.8% were over 50 years old [40];
- Increased pressure: it can weaken the pelvic floor over time, especially if a woman has a disease causing chronic coughing or engages in activities involving heavy lifting [41];
- Hysterectomy: it can lead to pelvic floor weakness by altering anatomy and nerve supply. It appears to raise the risk of POP, even though hysterectomy has traditionally been seen as a treatment for apical prolapse. Proper support of the vaginal vault is essential in preventing POP, as the absence of apical support doubles the risk of POP recurrence [42].

2.2.1.3 Epidemiology

POP is a prevalent health concern among women globally, with a 40% prevalence rate expected to rise as the population ages. POP has a prevalence rate of 3-6% when identified through symptoms, but this figure can increase to as high as 50% when diagnosed via vaginal examination. Surgical procedures for prolapse are performed at twice the rate of those for continence issues, with prevalence rates varying significantly between 6% and 18%. The incidence of POP surgeries ranges from 1.5 to 1.8 per 1000 woman-years, peaking among women aged 60-69 [43]. A study in Gambia discovered that 46% of women had some degree of prolapse upon examination. However, only 12.5% of them reported symptoms related to this condition [44].

An analysis of the prevalence of POP across various geographic regions was conducted, involving a total of 29 studies with over 71,000 women. These studies were carried out in Europe (1-45%), the USA (16-65%), Asia (9-61%), South America (26-65%), and Africa (1-37%). The assessment of POP was done using questionnaires without physical examinations. These findings highlight that POP is a growing public health concern worldwide [45].

2.2.1.4 Quantification and Diagnoses

The POP Quantification (POP-Q) system is a recognized technique approved by the Society of Gynecologic Surgeons, the International Urogynecologic Association (IUGA), and the International Continence Society (ICS) for describing, measuring, and quantifying POP using the hymen as a reference [46, 47].

This objective, quick, and comprehensive method involves measuring the values of the genital hiatus (gh), the perineal body (pb), and the total length of the vagina (tvl) on a 3x3 grid, without straining. Additionally, points C and D should be measured and recorded at maximum effort, along with points Aa and Ba on the anterior vaginal wall and points Ap and Bp on the posterior vaginal wall. All measurements should be expressed in centimeters to the nearest 0.5 cm. These values will help accurately determine the stage of prolapse. Figure 2.6 illustrates the measurement points and their representation in the POP-Q system [33, 48, 49, 50].

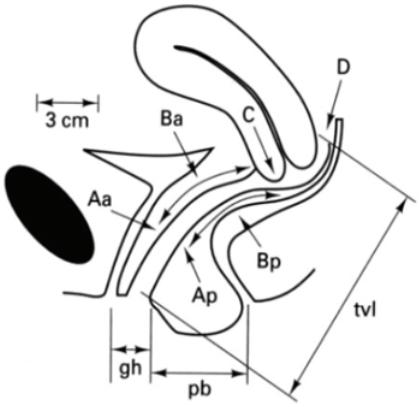

Aa Descent of fixed point on anterior wall	**Ba** The lowest part of the upper anterior vaginal wall	**C** The lowest part of the cervix
GH Genital hiatus	**PB** Perineal body	**TVL** Total vaginal length
Ap Descent of fixed point on posterior wall	**Bp** The lowest part of the upper posterior vaginal wall	**D** Vault or insertion uterosacrals

Figure 2.6 Parameters of the measuring points of the POP-Q system and their representation (adapted from [33, 48]).

According to the POP-Q, the prolapse can be classified into 5 stages, as illustrated in Figure 2.7:

- **Stage 0:** No prolapse;
- **Stage I:** The prolapse is positioned more than 1 cm above the hymen;
- **Stage II:** The prolapse is positioned approximately 1 cm, either above or below the level of the hymen;
- **Stage III:** The foremost part of the prolapse extends more than 1 cm below the hymen but does not protrude beyond 2 cm less than the entire vaginal length;
- **Stage IV:** Complete vaginal eversion.

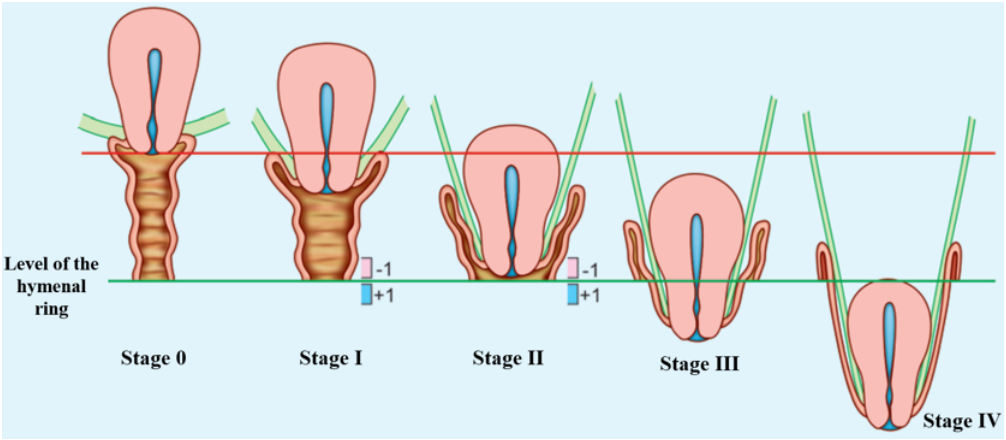

Figure 2.7 Quantitative gradings of POP (adapted from [33, 48]).

While the POP-Q system is the preferred quantification system in the medical community, alternative techniques like the Baden-Walker Halfway are also relevant. Figure 2.8 shows the scale used in this technique [33].

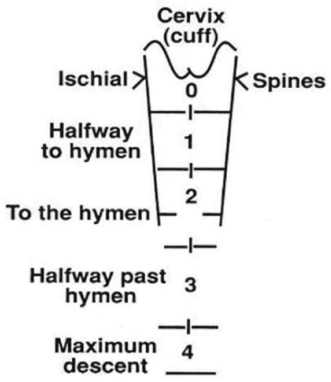

Figure 2.8 Baden-Walker Halfway quantification system. It consists of four different grades: grade 0 - no prolapse; grade 1 - halfway to the hymen; grade 2 - up to the hymen; grade 3 - halfway past the hymen; grade 4 - maximum descent (adapted from [33]).

When a patient shows symptoms of POP, the doctor conducts a medical history inquiry and a pelvic examination to evaluate the condition. During the examination, the doctor assesses the condition of pelvic organs, such as the uterus, vagina, and bladder. In complex cases, imaging methods like pelvic magnetic resonance imaging (MRI), Figure 2.9, and translabial ultrasound are valuable tools. MRI provides excellent anatomical detail and is a great preoperative tool, but it is expensive and cannot be performed regularly. On the other hand, ultrasound is a relatively inexpensive way of assessing prolapse and is widely available. However, bowel preparation is necessary to ensure accurate results as fecal content in the rectum can impair the scan's accuracy, unlike MRI [51].

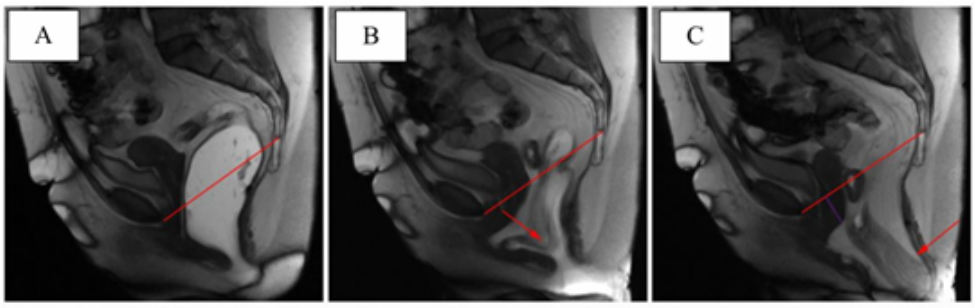

Figure 2.9 Dynamic magnetic resonance image of rectal and uterine prolapse. From A to C this prolapse is getting worse (adapted from [52]).

2.2.1.5 Treatment

The treatment of POP is a complex process that requires considering various factors, such as the severity of symptoms, age, desire for future pregnancies, and the specific organ affected. The main goal of treatment is to restore the anatomy and function that were present before the prolapse occurred [53]. Conservative treatment, a noninvasive technique, is typically the first step in treating POP. It aims to alleviate symptoms and prevent the progression of the prolapse. These treatments are effective if POP is detected early. In more severe cases (Stage 3 or 4), invasive treatments, particularly surgery, are necessary [2, 54].

Conservative treatment

The conservative management of POP, applied at an early stage of POP (Stage 1 and 2), involves making lifestyle changes. These changes include adding more dietary fiber to the diet to reduce constipation and minimize the need for straining during bowel movements. It also involves quitting smoking, as smoking doubles the risk of developing PFD. Additionally, maintaining a healthy weight or losing weight if overweight is also important [54, 55].

In cases where there are no symptoms, treatment may not be necessary. However, it is strongly recommended that women perform regular pelvic floor exercises, often referred to as Kegel exercises, especially as they age, go through menopause, or have had vaginal childbirth. These exercises help strengthen the muscles in the pelvic area, reducing the risk of POP. Figure 2.10 provides a visual guide to some of these exercises [53, 56].

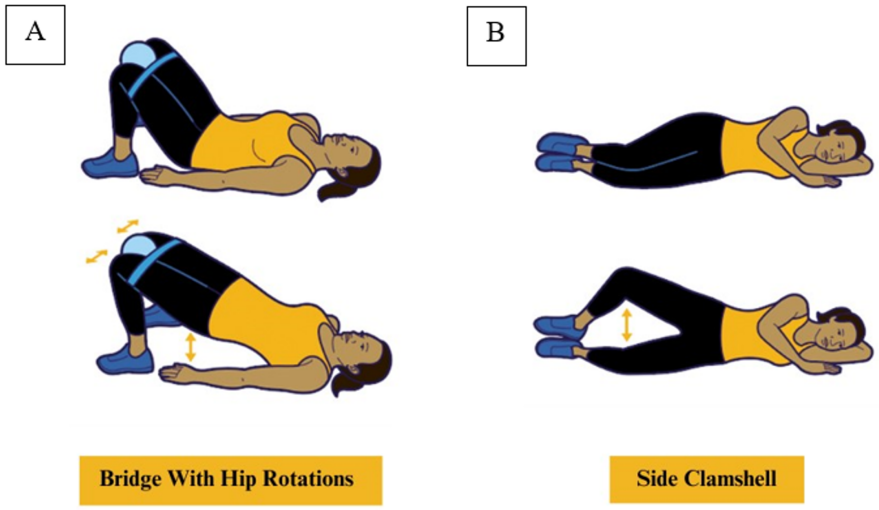

Figure 2.10 Kegel Exercises. A: Bridge with hip rotations; B: Side clamshell (adapted from [57]).

The biofeedback technique is a helpful method that enables women to strengthen and localize their PFM. This approach involves placing a sensor shaped like a tampon in the vagina or rectum while a second sensor is placed in the abdomen to monitor the pelvic floor. The patient then contracts and relaxes their PFM while observing the strength of each contraction on a computer screen. Using this technique, each contraction of the PFM can be adjusted to become stronger and more effective [54].

Electrical stimulation treatment is frequently used in combination with biofeedback to enhance the training of PFM contractions. This technique involves applying small electrical currents to directly stimulate the PFM. According to a study, combining biofeedback treatment with electrical stimulation and pelvic floor exercises has been shown to reduce the issue [58].

Pessaries are small devices primarily made of silicone or inert plastic. They are designed to prevent odors, absorb vaginal secretions, and support the bladder, uterus, or rectum. These devices come in various sizes and shapes to suit individual needs. It has been reported that two-thirds of women with POP initially opt for pessary treatment and that 77% of them continue to use it after one year. However, it is important to note that pessaries must be removed every three months to clean them and assess their condition [59].

The pessary is successful in over 85% of patients, but certain risk factors, such as having a short vaginal length, can contribute to its failure. Common complications associated with the use of pessaries include vaginal discharge, irritation, ulceration, bleeding, pain, and odor. Figure 2.11 displays the most common types of pessaries [60].

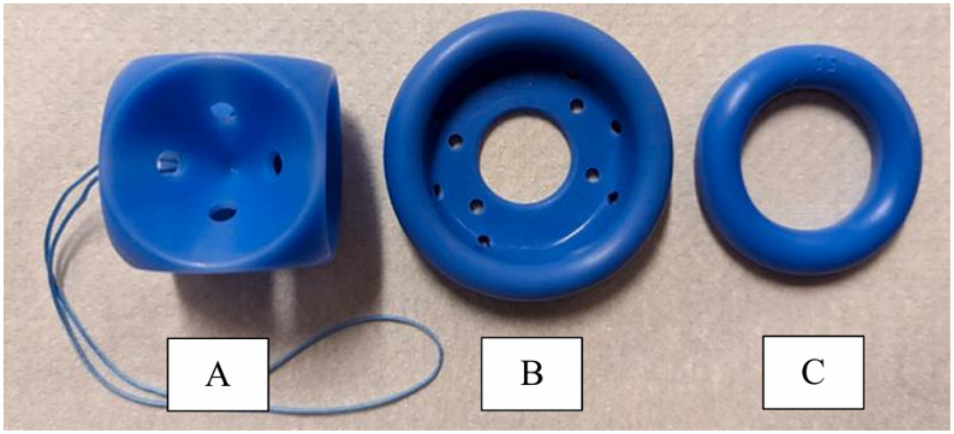

Figure 2.11 The most common types of pessaries. A: cube pessary; B: shell pessary; C: ring pessary (adapted from [61]).

Surgical treatment

For women with severe POP, surgery is the main treatment option. There are different surgical methods for POP repair, categorized by the surgical approach: vaginal or abdominal. These procedures also differ based on the materials used for repair, which can be either native tissue or non-degradable meshes. Unfortunately, repairs using native tissue carry a significant risk of anatomical and functional recurrence, ranging from 16% to 29%. Due to the high recurrence rate, surgeons have increasingly turned to the use of non-degradable meshes [18, 61, 62].

When performing reconstructive surgeries on the anterior and posterior vaginal walls, the primary method of approach is through the vagina. Repairing the anterior vaginal wall involves strengthening and tightening the connective tissue between the bladder and the vagina in order to lift and support the bladder. For the posterior vaginal wall, the main focus is on reinforcing and tightening the connective tissue between the vagina and the rectum to provide support and elevation to a section of the intestine [25, 56].

Various approaches can be used, but it is important to analyze the hypotheses in the context of several considerations thoroughly. These include evaluating surgical outcomes, comparing abdominal and vaginal approaches, and determining the use of laparoscopic or robotic techniques [63, 64].

Surgical meshes are used in medical interventions to correct POP and can be either synthetic or biological. Biological grafts fall into three categories: allografts (human donor tissue), autografts (the patient's own tissue), or xenografts (porcine or bovine donor tissue). In contrast, synthetic meshes, which have been developed to replace biological grafts, have a flat, net-like structure. This structure creates tension around body structures upon surgical implantation, supporting weak muscles and soft tissues [65, 66].

After the surgery, it was noted that approximately 80 to 90 out of every 100 women did not show any symptoms for a significant period. However, looking back at the results of the surgery over three years, it was found that nearly 38 out of every 100 women who had the procedure using their own tissue eventually had a recurrence of their condition [25, 56].

In cases of apical prolapse, such as uterine or vaginal dome prolapse, sacrocolpopexy is a commonly performed surgical procedure. It can be done through open, laparoscopic, or robotic abdominal surgery. During this procedure, a synthetic mesh is attached to the sacrum or coccyx to support the upper part of the vagina. Despite its popularity, studies have shown that around 23 out of 100 women who undergo sacrocolpopexy may experience a recurrence of uterine prolapse within two years after the surgery [64, 67, 68].

Biological grafts are often considered a favorable option for POP due to their similarity to native tissue. However, their high cost, limited availability, and increased risk of surgical complications and transmission of contagious diseases have limited their use. Synthetic meshes, on the other hand, are regarded as a more dependable alternative, given their ready availability, affordability, and reduced risk of infectious disease transmission. In addition, they allow for predicting mechanical properties and can help reduce surgical risk, making them a preferred option [65, 66].

For synthetic meshes to be deemed effective, they must exhibit mechanical and biological properties akin to those of tissues, thereby underscoring the criticality of material selection. Consequently, a myriad of factors, including but not limited to pore size, density, tensile strength and elasticity, constitution, and absorption of the material, must be taken into account following their function [23, 69, 70].

- Elasticity and Tensile strength

It is imperative for the material employed in the fabrication of surgical meshes to possess the minimum requisite properties to endure the tensions exerted by the human body. According to research, surgical meshes must withstand at least 180 mmHg pressure to handle the internal abdominal pressure during physical activities [70].

- Porosity

Mesh porosity impacts bacterial growth and cell proliferation. Microporous meshes (<10 μm) hinder cell passage and promote bacterial accumulation, leading to chronic inflammation and rejection. Macroporous meshes (>75 μm) allow cell infiltration, supporting healing and preventing infections [69, 70, 71].

- Weight (density)

Meshes are categorized by weight: heavy (>80 g/m^2), medium (50-80 g/m^2), light (35-50 g/m^2), and ultra-light (<35 g/m^2). Heavier meshes may lead to foreign body sensation and scarring, while lighter meshes promote integration and reduce inflammation [69, 71].

- Structure (type of fiber filament)

Selecting fiber filament is crucial in determining the tissue's response to mesh implantation. Meshes can be monofilament (rigid) or multifilament (flexible but higher infection risk due to smaller

pores). Multifilament meshes increase the surface area for bacterial adhesion, leading to a higher erosion rate [69, 70, 71].

- Material absorption

The material used can be absorbable (does not trigger infections but quickly loses properties such as tensile strength) or non-absorbable (maintains mechanical properties and stability for a longer period, but its greater rigidity can develop inflammatory problems) [70].

The ideal mesh for POP repair should be non-toxic, biocompatible, chemically inert, lightweight, porous, strong, non-carcinogenic, non-inflammatory, affordable, sterile, and shrinkage-resistant [65, 71].

Despite significant advancements in mesh technology for POP repair, there is still no ideal mesh due to associated complications and risks. It is estimated that 30% of women undergoing POP repair require re-operation due to mesh failure, causing the organs to return to their pre-operative position, as shown in Figure 2.12 [71, 72].

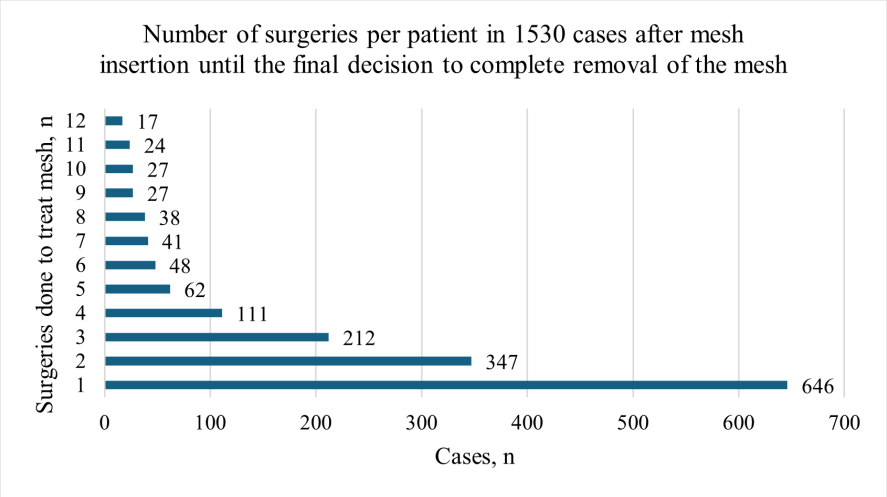

Figure 2.12 Number of surgeries each 1 of the 1530 studied cases underwent before complete mesh removal (adapted from [72]).

Synthetic mesh is commonly used in surgeries to repair POP, with polypropylene (PP) being the most commonly used material for its production. PP is a rigid, tensile-resistant, flexible, non-absorbable, non-toxic, and safe thermoplastic material suitable for use in living beings. Its popularity is also due to its low cost and wide availability. Other materials, such as polyethylene terephthalate (PET), polytetrafluoroethylene (PTFE), and polyvinylidene fluoride (PVDF), are also used, although to a lesser extent. Table 2.1 provides an analysis of some of the synthetic meshes that have been developed for use in POP repair surgery [65, 71].

Table 2.1 Examples of different synthetic meshes created with the aim of being used in surgery for POP repair (adapted from [23, 70, 71]).

UpsylonTM y-mesh (Boston scientific)	Surgipro (Autosuture)	Vicryl (Ethicon)	Restorelle (Coloplast)	Parietex (Covidien)	Dynamesh – PR soft (FEG Textiltechnik)	Uphold (Boston Scientific)	Gynecare (Gynemesh J& J)
Mesh type	**Mesh type**	**Mesh type**	**Mesh type**	**Mesh type**	**Mesh type**	**Mesh type**	**Mesh type**
PP monofilament Non-absorbable Weight: 25 g/m2 Pore size: 1.7 mm2	PP monofilament Non-absorbable Weight: 25 g/m2 Pore size: 1.7 mm2	Multifilament oiliglatina Absorbable (60-90 days) Weight: 56 g/m2 Pore size: 0.4 mm2	PP monofilament Rectangular and non-absorbable Weight: 20 g/m2 Pore size: 1.80x1.83 mm	Polyester/collagen multifilament Partially absorbable (20 days) Weight: 75 g/m2 Pore size: >3 mm	PVDF monofilament Non-absorbable	PP monofilament Non-absorbable Weight: 25 g/m2 Pore size: 2.8 mm2	PP monofilament Rectangular and non-absorbable Weight: 100 g/m2 Pore size: 2.47x1.68 mm
Advantages	**Advantages**	**Advantages**	**Advantages**	**Advantages**	**Advantages**	**Advantages**	**Advantages**
Small surface area to minimise contact with vaginal tissue	High tensile strength, malleable and retains properties in vivo	Eliminates the risk of transmitting infectious diseases	Small surface area to minimise contact with vaginal tissue	Short-term benefit for the non-stick property	Atraumatic, tissue reaction limits reaction	Small surface area to minimise contact with vaginal tissue	Very resistant, material known to surgeons, easy to cut to customise the shape
Disadvantages	**Disadvantages**	**Disadvantages**	**Disadvantages**	**Disadvantages**	**Disadvantages**	**Disadvantages**	**Disadvantages**
No prospective or retrospective studies exist	Difficult for the wound to heal completely due to the structure of the mesh	Usually results in recurrence after complete absorption	Usually results in recurrence after complete absorption	Higher infection rate (57%)	Not customisable, limited evidence	Requires sutures and a fixation device	Associated with retraction and extrusion, associations with disparenia
Design	**Design**	**Design**	**Design**	**Design**	**Design**	**Design**	**Design**

Synthetic meshes have become popular for repairing POP due to their high success rate in correcting abdominal hernias. However, in 2019, the FDA banned the marketing of meshes for transvaginal prolapse in the United States due to a high re-operation rate of 30%, and because they do not guarantee efficacy and safety (as stated in the FDA's press release on 16 April 2019), as well as, a high complication rate and numerous patient complaints [73]. These complications include, for example, pain, infections, and urinary problems. Table 2.2 shows the most common complications reported to the FDA [74].

Table 2.2 The most common complications reported to the FDA (adapted from [74]).

Complications	Number of reports
Erosion	528
Pain	472
Infection	253
Bleeding	124
Dyspareunia (painful sex)	108
Organ perforation	88
Urinary problems	80
Vaginal scarring	43
Neuro-muscular problems	38
Recurrence	32

One of the main complications caused by PP mesh is tissue erosion, which can damage adjacent soft tissues. In such cases, mesh excision is required to prevent further damage. However, complex surgeries are necessary for complete removal as the mesh is typically already integrated into the soft tissue. Nonetheless, transabdominal surgery with synthetic mesh made, for instance, through PP, remains an option of last resort for the treatment of vaginal dome prolapse and uterine prolapse [65].

Researchers are actively working to find improved treatments for POP. They mainly concentrate on regenerating pelvic tissue and creating meshes using natural polymers like PCL, polylactic acid (PLA), and polyurethane (PU). While the perfect mesh hasn't been developed yet, exploring new meshes for the pelvic region using finite element tools shows potential [65, 75].

Chapter 3

Computational Modelling

Biomechanical modeling is a powerful tool that can demonstrate PFM defects in the pelvic support system and assist surgeons in evaluating and planning surgical procedures. This work involves the development of computational mesh models, so it's essential to understand key concepts in this field, including the FEM, Abaqus® software, and previous simulation studies. These topics will be explored in detail throughout this work.

3.1 Finite Element Method

The FEM was introduced as a numerical modeling paradigm in the early 1940s through Courant's article in 1943. Courant developed the concept of minimizing a function using a linear approximation in sub-regions with values defined at discrete points, thereby laying the foundation for FEM. In the following decade, various engineers and researchers experimented with different strategies for solving practical problems in aeronautical and civil engineering. However, it wasn't until 1960, when Clought published an in-depth article on plane elasticity problems, that the name and significance of FEM were widely recognized [76, 77].

FEM is a numerical technique used to provide an approximate solution to the distribution of field variables within a given problem domain. This is especially useful when obtaining an analytical solution is difficult or impossible. FEM works by breaking down the original complex problem into a series of simpler problems, solving them sequentially, and then combining the solutions to obtain the overall solution. The first step is to divide the problem domain into small elements known as "finite elements". These elements are connected by points, called "nodes", and typically have simple geometric shapes like triangles for 2D or tetrahedrons for 3D geometries. By applying three principles of Continuous Media Mechanics (equilibrium equations, kinematic equations, and constitutive relationships), we can solve the elasticity equations in these smaller elements. The mathematical models are then established based on the constitutive relationships and boundary conditions. Figure 3.1 shows nodes and finite elements in a model [21, 78, 79].

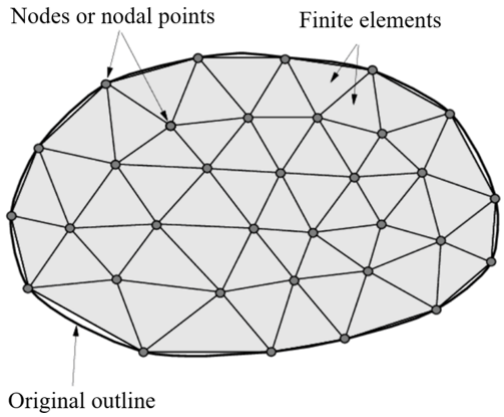

Figure 3.1 FEM (adapted from [21, 77]).

In numerical analysis, finite elements and nodal points are combined as a mesh. The number of elements in a mesh is directly linked to the desired precision level, the number of degrees of freedom, and the element size. While having more elements provides more precise solutions, there is a limit to which superior results cannot be achieved [21, 77].

The FEM is a highly versatile approach used for computing numerical solutions of differential equations. It has three key characteristics that are worth emphasizing. Firstly, FEM can handle domains with arbitrary shapes, which is particularly advantageous as differential equations are often formulated in complex domains such as the lungs. Secondly, the boundary conditions of FEM include the derivative of the solution, making them easier to deal with. Lastly, FEM can be optimized to produce highly precise solutions by either dividing the domain into smaller triangular elements or increasing the degree of polynomial approximation in each element [80]. A summary of the key advantages of FEM is provided in Table 3.1 [81].

Table 3.1 Some of the main advantages of FEM (adapted from [81]).

Modeling	Simplifies the modeling of complex and irregular shapes, allowing designers to analyze both the interior and exterior to understand critical factors and potential failures.
Adaptability	Reduces the need for physical prototypes by enabling quick and accurate modeling of various designs and materials, saving time and costs.
Accuracy	Offers high precision in solving intricate physical deformations, impractical to model manually.
Time-dependent simulation	It is effective for simulations where, for example, a deformation in one area affects the deformation in another area.
Boundaries	Designers can apply boundary conditions in FEM to define the model's response to forces, thermal effects, and constraints.
Visualization	Generates detailed visualizations that assist engineers in identifying and addressing vulnerabilities in the design.

This method is vital for understanding the complex behavior of pelvic soft tissues in biomechanics, especially in the study of PFD. The different components of this method are identified by their nodal parameters. These parameters include the nodal force vector and nodal displacement vector, which are used to obtain important information such as muscle tension and stress, reaction forces and tension during childbirth, displacement of the mid-pubic point during voluntary contraction, and the Valsalva maneuver (VM), as well as the underlying mechanisms involved in cystocele formation, among other applications [20].

In 3D structures, nodal information is key in defining crucial parameters such as the nodal force vector (f^e) and the nodal displacement vector (δ^e) for each element e. The relationship between nodal forces and nodal displacements is directly related to the deformations occurring in the elements. This important correlation is best described by Equation 3.1, which incorporates the square stiffness matrix k^e for the element e, as mentioned earlier [20].

$$f^e = k^e \times \delta^e \tag{3.1}$$

Table 3.2 represents the general steps in FEM structural analysis [82].

Table 3.2 Flowchart of the Finite Element Analysis (adapted from [82]).

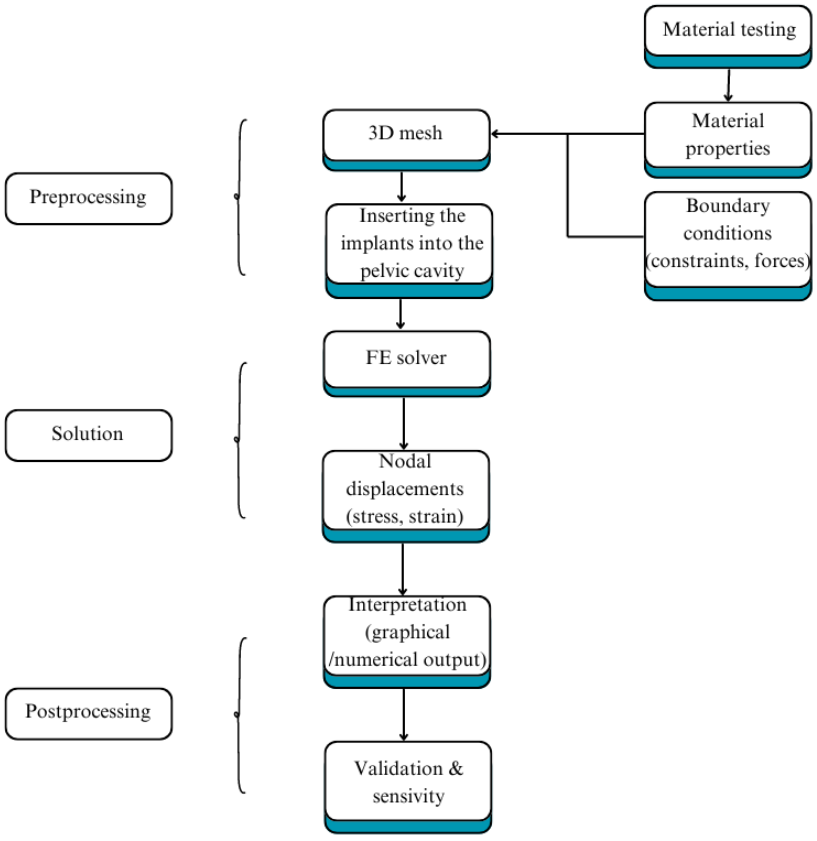

3.2 Abaqus® Software

FEM is based on mathematical equations that are used to create a simulation referred to as Finite Element Analysis (FEA). FEA is used to perform structural analysis and predict how a specific design or product will respond when exposed to real stress and strain conditions. Therefore, FEA provides a virtual model that allows engineers to test a structural design using specialized software [83].

The Abaqus® software v.2022 suite is a collection of FEA software developed by Dassault Systems and is part of the SIMULIA family of codes. This software can handle both simple linear analyses and complex non-linear problems. It comes with a wide range of pre-defined elements and materials, such as ceramics, polymers, and composites, allowing for efficient replication of virtually any required geometry. The software's accuracy depends on the number of nodes and elements in the model and the size and type of mesh. Generally, smaller elements result in better accuracy [84, 85].

An analysis in Abaqus® typically involves three stages: pre-processing, simulation, and post-processing. Pre-processing involves defining a model of the physical problem and creating an input file, usually using Abaqus/CAE. In the simulation stage, Abaqus/Standard or Abaqus/Explicit solves the numerical problem defined in the model. Post-processing involves evaluating the outcomes obtained from the completed simulation using the visualization module available in Abaqus/CAE [84, 85].

In Abaqus Standard, equilibrium is maintained at each solution step by balancing externally applied loads with internally generated reaction forces. In contrast, Abaqus Explicit does not enforce equilibrium at each step, which does not imply a lack of accuracy. While Abaqus Standard requires iterative methods to solve nonlinear problems, Abaqus Explicit advances the kinematic state from the previous increment without iteration. This makes Abaqus Explicit the preferred choice for high-speed dynamic analyses, such as crash analysis or drop tests [86].

3.3 Simulations in previous studies

POP is becoming a significant concern for women's health globally. Medical researchers have conducted several studies to comprehend better and tackle this issue. The emergence of computer models has led to the production of numerous new studies to enhance the repair of POP and ultimately ensure improved health outcomes for women in the future.

Xie et al. developed a 2D mechanical model of the pelvic floor based on MRI of a healthy 35-year-old woman. This model is a useful tool for simulating and studying the biomechanical behavior of the pelvic floor under various conditions, such as anterior vaginal prolapse due to soft tissue compromise. The study aimed to comprehend how the pelvic floor organs would deform and the patterns of increased IAP and different levels of impairment. Through simulations, the researchers could observe how different types of impairment affect pelvic floor function. The model illustrated changes in pelvic floor mechanics in response to simulated muscle weakness

and tissue damage. The study emphasizes the potential of mechanical modeling as a valuable tool for investigating pelvic floor dynamics and guiding clinical decision-making in diagnosing and treating PFD [87]. The computer model can be seen in Figure 3.2.

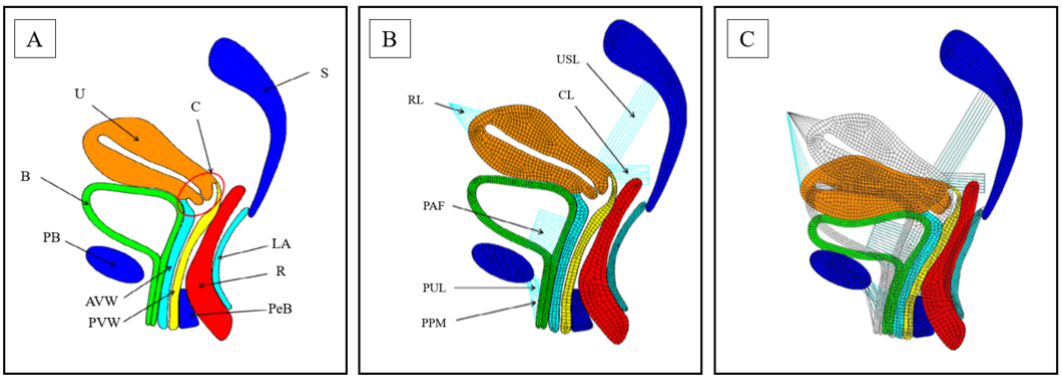

Figure 3.2 A: Reconstructed equivalent 2D geometric model; B: Finite element model of the pelvic floor; C: Comparison of morphology before (grey) and after (colored) VM in the healthy pelvic floor. AVW, anterior vaginal wall; B, bladder; C, cervix; CL; LA, levator ani; PB, indicates pubic bone; PeB, perineal body; PUL, pubic urethral ligament; PVW, posterior vaginal wall; R, rectum; RL, round ligament; S, sacrococcyx; U, uterus; USL. (adapted from [87]).

In a study by Chen et al., they used Abaqus® software and MRI of a healthy woman to create a 3D model of the inverted uterus and its ligaments. The study found that as IAP increased, the displacement of the uterus and each uterine ligament also increased. The lower USL and CL displacement were also mainly concentrated in the middle and upper segments near the cervix with increasing IAP [88]. Figure 3.3 provides a visual representation of the computer model created in the study.

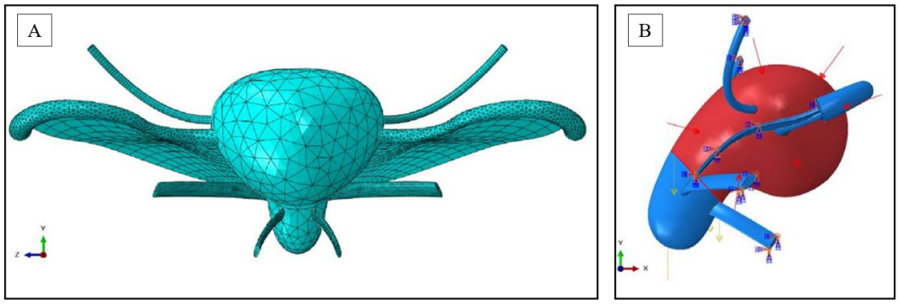

Figure 3.3 Finite element mesh and boundary conditions in the uterus. A: Posterior view; B: Lateral view (adapted from [88]).

Silva et al. have published promising studies in this area, including the development of computational models of the pelvic cavity and implants to replace CL and USL, such as the models

shown in Figure 3.4. These authors simulated the POP repair surgery with synthetic implants and simulated the VM with an IAP of 4 kPa [25].

Figure 3.4 Implants to mimic the USL and CL after their total rupture in the pelvic cavity. A: CL implant: B: USL implant. (1) pubourethral ligaments, (2) bladder, (3) uterus, (4) USL, (5) CL site, (6) CL implant, (7) vagina, (8) urethra, (9) CL implant, (10) USL site, (11) CL (adapted from [25]).

Using membrane elements, the USL implant had 396 nodes and 1952 elements, while the CL implant had 352 nodes and 1696 elements. The variation in numbers is due to the different geometries of each model [25].

The properties of the implants were determined through experimental uniaxial tensile tests using Restorelle (A, monofilament PP mesh) and Dynamesh (B, monofilament PVDF mesh) synthetic implants. Figure 3.5 shows these uniaxial tensile tests for both implants and their response to nominal uniaxial tension, with the experimental curve representing the average of the tests conducted. Therefore, based on these curves, hyperelastic mechanical behavior was considered, which is not indicative of a commercial knitted synthetic mesh, especially its porosity [25].

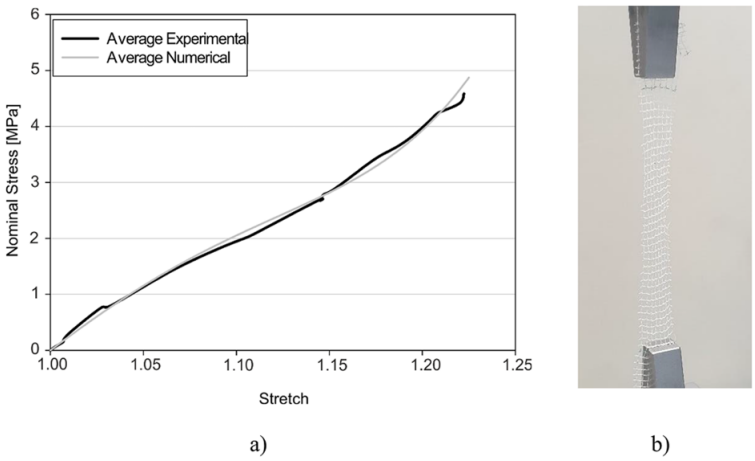

Figure 3.5 Uniaxial tensile test and nominal stress-stretch response for two commercial mesh implants and the numerical curves (adapted from [25]).

The study's results, as shown in Figure 3.6, were promising and suggested that using a synthetic mesh to replace or reinforce the USL could help provide support. However, this study was carried out using computer models of non-porous implants, and there is still significant room for improvement, as the stress/strain test values do not yet meet the required standards [25]. This present dissertation aims to develop biodegradable porous meshes and simulate surgery to correct POP using different geometries.

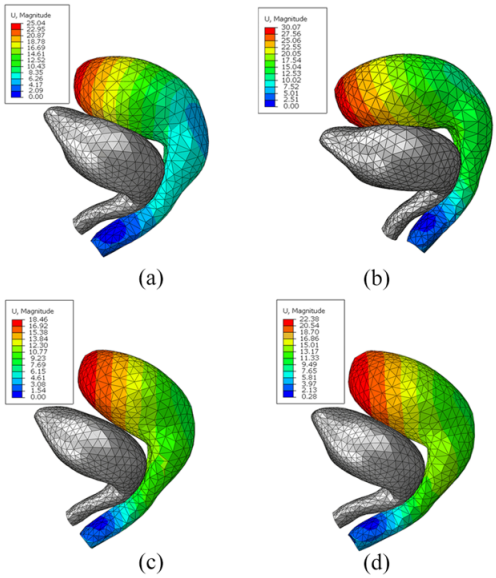

Figure 3.6 The magnitude of displacement (mm) of the uterus: (a) asymptomatic case; (b) total rupture of the USL; (c) placement of mesh A to replace the USL and (d) placement of mesh B (adapted from [6]).

Chapter 4

Materials and Methods

This section provides information on the materials and methods for creating computational models simulating the USL and CL. It includes details on building the models, assigning material properties to the implant, matching them to the uterus, and incorporating them into the pelvic cavity model.

4.1 Biomechanics of the Female Pelvic Cavity

When creating a model, it's crucial to define the mechanical properties of the materials that make up the structures and organs to ensure the simulation is as realistic as possible. This section contains detailed information on the constitutive models used and the mechanical properties associated with each organ. Finally, we present the model of the female pelvic cavity that will be used throughout the work.

4.1.1 Constitutive Models

The constitutive law of a material is essential for describing the relationship between stress (σ) and strain (ε). In linear elastic materials, this relationship is determined by parameters like Poisson's ratio and Young's modulus. On the other hand, hyperelastic materials are characterized by the concept of strain potential energy [89].

Linear Elastic

When linear elastic materials undergo uniaxial tension, it suffices to consider Young's modulus solely to illustrate the interdependence between stress and strain [90]. The constitutive law that effectively captures this correlation is presented in Equation 4.1.

$$\sigma = E\varepsilon \tag{4.1}$$

The stiffness of a material is determined by the ratio of stress to strain. Young's Modulus (or elastic modulus) represents the ratio of σ to ε under elastic deformation. It indicates the material's resistance to deformation when subjected to a force and is determined by the initial slope of the stress-strain curve. Young's Modulus is a measure of a material's stiffness. It's important to emphasize that permanent deformation occurs once the elastic limit is exceeded [91]. However, the simulations only consider behavior up to that limit for the current study.

Hiperelastic Materials

Hyperelastic materials are known for their exceptional elasticity, shock resistance, and durability, allowing them to undergo significant deformation. Materials like rubber, gels, and soft tissues (such as arteries and muscles) exhibit hyperelastic behavior in various engineering applications. In recent years, researchers have focused on studying the mechanical properties of hyperelastic materials, aiming to develop theoretical models that accurately predict and explain experimental results. Additionally, engineers have been using numerical simulations to understand the complex behaviors of hyperelastic materials in devices based on specific experimental data [92].

Like other muscle tissues, the pelvic floor is a hyperelastic material with a nonlinear stress-strain relationship. When it is stretched beyond a certain point, the stress increases significantly in a nonlinear manner until it reaches its failure strength. This could potentially seriously affect its functionality [93].

Certain materials' behavior can be described using a constitutive equation (or constitutive model), which mathematically links the observed stress and strain values in a body [92]. The hyperelastic constitutive models such as Yeoh, and Ogden were employed to replicate the mechanical behavior of pelvic cavity tissues. These models do not consider the effects of viscosity, temperature, and time dependency [94]. They utilize a nonlinear stress-strain relationship to describe incompressible hyperelastic materials. These models have been proven to accurately approximate the tensile curves of different pelvic floor tissues, allowing for the simulation of biomechanical behavior during maneuvers such as the VM and in cases of impairment of pelvic ligaments [6].

- **Yeoh Model**

The relationship between stress and strain represents a material's constitutive law. This connection is associated with Poisson's ratio and Young's modulus for linear elastic materials. In the case of hyperelastic materials, the constitutive law is defined by the strain potential energy, which can be expressed through Equation 4.2 [95].

$$U = \sum_{i+j=1}^{N} \left(C_{ij} \left(\overline{I_1} - 3 \right)^i \left(\overline{I_2} - 3 \right)^j \right) + \sum_{i=1}^{N} \left(\frac{1}{D_i} \left(J_{\text{el}} - 1 \right)^{2j} \right) \tag{4.2}$$

In this particular expression, the energy density function of the strain is denoted by U. The material constants, C_{ij} and D_i, are determined through experimental data. The first and second

invariants of the deviatoric part of the left Cauchy-Green deformation tensor are denoted by $\overline{I_1}$ and $\overline{I_2}$ respectively, and they are related to the distortional deformation. The elastic volume ratio, J_{el}, is related to the determinant of the deformation gradient tensor, F, and represents volumetric changes. The complexity and accuracy of the model are determined by the order of the series expansion, which is denoted by N. Notably, distortional (or isochoric) deformations are represented by the terms $\left(\overline{I_1}-3\right)^i$ and $\left(\overline{I_2}-3\right)^j$, while volumetric (or dilatational) deformations are represented by $\left(\overline{J_{el}}-1\right)^{2j}$ [95].

The Yeoh model, also referred to as the third-order reduced polynomial form, is widely recognized for its precision in representing material behavior, especially under large strains. Its focus on the first invariant of the deformation tensor makes it particularly suitable for isotropic materials. Like other hyperelastic models, the Yeoh model parameters are typically determined with a high degree of precision through experimental stress-strain data curve fitting. The Yeoh model is expressed by Equation 4.3 [95].

$$U = C_{10}\left(\overline{I_1}-3\right)+C_{20}\left(\overline{I_1}-3\right)^2+C_{30}\left(\overline{I_1}-3\right)^3+\frac{1}{D_1}\left(J^{\mathrm{el}}-1\right)^2+\frac{1}{D_2}\left(J^{\mathrm{el}}-1\right)^4+\frac{1}{D_3}\left(J^{\mathrm{el}}-1\right)^6 \quad (4.3)$$

C_{i0} and D_i are two temperature-dependent parameters and $\overline{I_i}$ represents the invariant of the deflection strain tensor [95].

• Ogden Model

The Ogden model is widely recognized as a versatile hyperelasticity model that accurately describes the Helmholtz free energy per reference volume based on the applied principal stretches. Ogden presents his deformation potential energy model in Equation 4.4 [95].

$$U = \sum_{i=1}^{N}\frac{2\mu_i}{\alpha_i^2}\left(\overline{\lambda_1}^{\alpha_i}+\overline{\lambda_2}^{\alpha_i}+\overline{\lambda_3}^{\alpha_i}-3\right)+\sum_{i=1}^{N}\frac{1}{D_i}\left(J^{\mathrm{el}}-1\right)^{2i} \quad (4.4)$$

Where, $\overline{\lambda_i} = J^{-1/3}\lambda_i \rightarrow \overline{\lambda_1\lambda_2\lambda_3} = 1$.

Thus, the initial portion of Ogden's strain energy function relies solely on $\overline{I_1}$ and $\overline{I_2}$. While Ogden's energy function cannot be explicitly expressed in terms of $\overline{I_1}$ and $\overline{I_2}$, it is feasible to derive closed-form expressions for the derivatives of U concerning these variables. The user specifies the value of N and provides tables that list the μ_i and a_i values as functions of temperature [95].

In the Ogden model, the initial shear modulus, μ_0, depends on all coefficients: $\mu_0 = \sum_{i=1}^{N}\mu_i$, and the initial bulk modulus, k_0, depends on D_1 as before. [95]

4.1.2 Mechanical Properties

The material parameters for the constitutive models of a range of pelvic structures are presented in Table 4.1. The parameters for the pelvic structures were determined from experimental data and were adapted from Brandão et al.. These studies utilized female cadavers without pelvic dysfunction to create stress-strain curves for the structures and organs in the model [25, 96].

Table 4.1 Material parameters of the constitutive models applied to healthy pelvic structures (adapted from [25, 96]).

Structures	α_k	μ_k		Model
Bladder and Urethra	$\alpha_1 = 0.19$	$\mu_1 = 5.14$		Ogden (N=1)
Rectum	$\alpha_1 = 4.25$ $\alpha_2 = -3.83$	$\mu_1 = 13.24$ $\mu_2 = 13.24$		Ogden (N=2)
Vagina and Uterus	$\alpha_1 = -3.41$ $\alpha_2 = -0.66$ $\alpha_3 = -6.48$	$\mu_1 = 92.24$ $\mu_2 = 39.29$ $\mu_3 = 54.68$		Ogden (N=3)
Pelvic ligaments (PUL)	$\alpha_1 = 10.95$	$\mu_1 = 1.58$		Ogden (N=1)
	$c_1\ [MPa]$	$c_2\ [MPa]$	$c_3\ [MPa]$	
Pubocervical fascia	0.93	-0.62	0.47	Yeoh
ATFP, CL, USL, LLR	1.74	6.60	4.79	Yeoh
PFM	0.003	0.002	0.001	Yeoh

4.1.3 Computational Modelling of the Female Pelvic Cavity

The 3D computational model of the pelvic cavity is an essential tool for understanding the mechanical behavior of the pelvic floor and for studying various disorders associated with this anatomical region.

The model was developed by Brandão et al. based on data from a 24-year-old nulliparous woman. It includes several important anatomical structures such as the bladder, uterus, rectum, LAM, pelvic fascia, tendon arch, lateral ligaments of the rectum, USL, and CL (Figure 4.1). High-resolution MRI were interpreted, and two experienced individuals marked the anatomical landmarks. These structures were then transformed into 3D representations using Inventor software. Finally, the 3D geometry was discretized into a finite element mesh using Abaqus® software [6, 96].

The model was recently used to simulate the surgical repair of POP and SUI during the VM. The study on prolapse also examined the impact of mesh rigidity on urethral mobility, especially when the LAM and/or ligaments were compromised [25, 96].

In the current investigation, the bladder, uterus, and rectum simulation incorporated fluid cavity interactions utilizing Abaqus® software, assuming a density of 1.0×10^{-9} ton/mm³. Table 4.2 shows the number of elements for each pelvic structure.

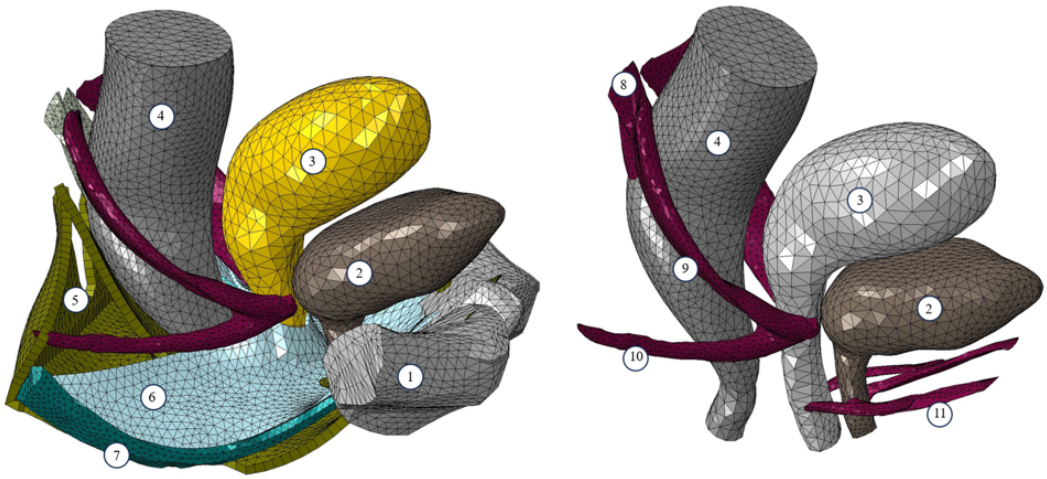

Figure 4.1 3D computational model of the pelvic cavity of an asymptomatic woman. (1), symphysis pubis; (2) bladder; (3) uterus; (4) rectum; (5) LAM; (6) pelvic fascia; (7) arcus tendineous fasciae pelvis; (8) lateral ligaments of the rectum; (9) USL; (10) CL; (11) pubourethral ligaments.

Table 4.2 Number of elements for each pelvic structure.

Structures	Number of elements
Bladder and urethra	5795
Rectum	5477
Vagina and uterus	1410
PUL	4389
Pubocervical fascia	2154
ATFP, CL, LLR, USLs	34808
LA	12635

Valsalva Maneuver

The VM involves forcefully exhaling while keeping the airway closed. This action is similar to activities like straining during bowel movements or blowing up a balloon. In urogynecology, the VM assesses patients with SUI and POP. It helps diagnose problems with the sphincter muscles during urodynamic tests and shows how far the organs move downward when IAP increases. This pressure increase typically leads to an increase in pelvic pressure and potential downward

displacement of the urethra, vagina, and uterus. This, in turn, can compress the rectum and aid in the passage of feces [97].

The VM (passive behavior) was simulated without muscle activation. It is considered an IAP of 4 kPa, which is a representative value for numerical models of young women in the supine position. The pressure was applied to the internal surface of the LAM and pelvic fascia muscles and the upper part of the bladder and uterus [25].

Impairment of the USL and the CL

In this study, simulations were performed to mimic different levels of impairment in the USLs and the CLs, including 50%, 90% (meaning a 50% and 90% reduction in stiffness compared to the healthy model), and complete (100%) impairment corresponding to total rupture. Table 4.3 presents the numerical parameters of the Yeoh constitutive model for healthy and impaired ligaments, while Figure 4.2 illustrates the stress-strain curve of the healthy ligaments, and with 50% and 90% impairment.

Table 4.3 Numerical parameters of the Yeoh constitutive model for healthy and impaired ligaments.

	C_{10} [MPa]	C_{20} [MPa]	C_{30} [MPa]
Healthy	1.74	6.60	4.79
Impairment 50%	0.87	3.30	2.40
Impairment 90%	0.17	0.66	0.48

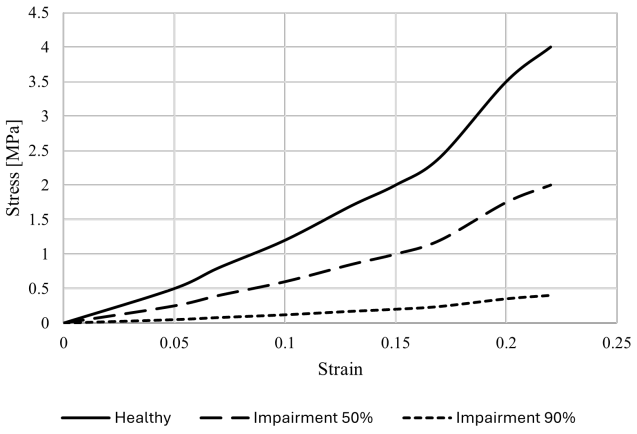

Figure 4.2 Stress-strain curve of the healthy ligaments, and with impairments (50% and 90%).

4.2 Biomechanics of the implants for the uterosacral and cardinal ligaments

Apical prolapse (uterine or vaginal apex) is a common form of POP, which involves the loss of support at the top of the vagina or uterus. This is often due to damage to the weakening of the apical ligaments, including USL and CL [98]. In this study, porous biodegradable implants were developed and subsequently incorporated into a computational model of the pelvic cavity to see how these implants behave during the VM when replacing the USL and CL after they total rupture or when they are 50% or 90% impaired.

4.2.1 Polycaprolactone (PCL)

The PCL polymer is represented by the chemical formula $C_6H_{10}O_2$ and is non-toxic, synthetic, aliphatic, and biodegradable. It is produced by the polymerization of ε -caprolactone using a catalyst. Due to its biocompatibility and biodegradability (with a lower erosion rate), PCL plays a significant role in new technological solutions in biomedical areas, such as tissue engineering, mainly because it is FDA-approved for medical use. It has a melting temperature between 59 and 64 ºC, resulting in a material with good mechanical properties at room temperature, including high strength and flexibility [65]. PCL shows potential for POP surgery and degrades over 2-3 years, which may help reduce complications such as chronic pain [99].

In Abaqus®, the material was defined with Young's modulus determined through a uniaxial tensile test on a 240 μm filament of medical-grade PCL, that is commercially available in pellets and was obtained from Corbion, under the trade name PURASORBR PC 12 polymer [100]. The experimental values obtained in the test made it possible to obtain the graph shown in Figure 4.3, resulting in a Young's modulus of 251.56 MPa.

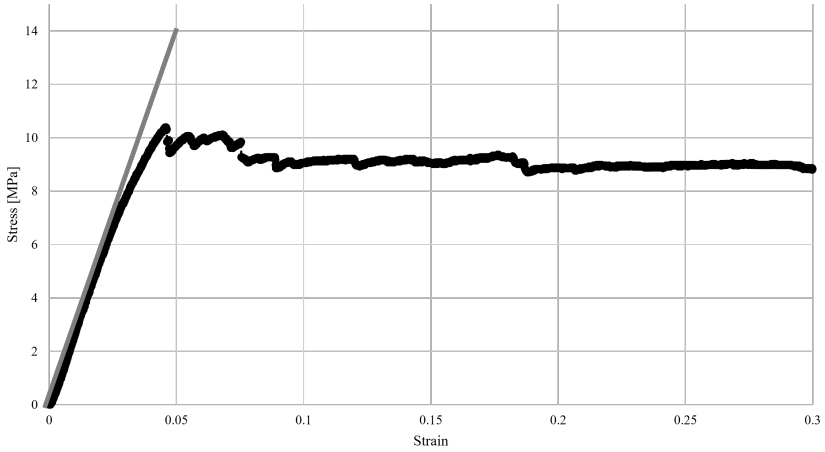

Figure 4.3 Stress-strain values obtained from the uniaxial tensile test carried out on the filament (adapted from [101]).

However, according to the literature, one would expect Young's modulus to be higher, with values ranging within the 343.9 and 363.4 MPa intervals. It should be noted that the material used for the test was exposed to temperatures of 200ºC during the printing process, which may have affected its properties and storage and usage conditions, as it is shared among different users for various tasks. The Poisson's ratio, calculated as the ratio of the change in width to the change in length of a material when subjected to a force, is 0.3 for the PCL polymer [101].

Damage Model

To improve the characterization of the material being used and make the simulations more realistic, a damage model was also defined in addition to the elastic properties mentioned earlier. This model includes a criterion for damage initiation, after which the effective plastic displacement, $\overline{\dot{u}^{pl}}$, is determined using an Evolution Equation 4.5 [102].

$$\bar{\dot{u}}^{pl} = L\bar{\dot{\varepsilon}}^{pl} \tag{4.5}$$

Where L is the characteristic length of the element.

The evolution of the damage variable concerning relative plastic displacement can be represented in tabular, linear, or exponential formats. Setting the plastic displacement at failure, $\bar{u}_f^{pl}$ to 0 causes instantaneous failure, which is not recommended due to the sudden stress drop at the material point, potentially leading to dynamic instabilities. When the effective plastic displacement at the point of failure (full degradation) is specified, the damage variable increases linearly with the displacement [102]. Then, the damage variable increases according to Equation 4.6:

$$\dot{d} = \frac{L\dot{\bar{\varepsilon}}^{pl}}{\bar{u}_f^{pl}} = \frac{\dot{\bar{u}}^{pl}}{\bar{u}_f^{pl}}. \tag{4.6}$$

This definition ensures that the material's stiffness will be completely degraded ($d = 1$) once the effective plastic displacement reaches the value $\bar{u}^{pl} = \bar{u}_f^{pl}$. The linear damage evolution law results in a truly linear stress-strain softening response. However, this only holds true if the material exhibits a perfectly plastic behavior (constant yield stress) after the onset of damage [102].

The strain rate $\bar{s}^{-1}$ is the change in strain (deformation) of a material with respect to time. In other words, is a measure of how fast or how slow deformation occurs and can be measured by: $\dot{\varepsilon} = \frac{\Delta\varepsilon}{\Delta t}$ [102].

The stress triaxility is defined as, Equation 4.7 [103]:

$$\eta = -\frac{p}{q} = \frac{1}{3} \cdot \frac{(\sigma_{xx} + \sigma_{yy} + \sigma_{zz})}{\sigma_{\text{mises}}} \tag{4.7}$$

Where $-p$ is the hydrostatic pressure stress and q is the Mises equivalent stress [103]. For uni-axial tension, the von Mises equations is $\sigma_{\text{mises}} = \sigma_{xx}$ and the $\sigma_{yy} = \sigma_{zz} = 0$.

Figure 4.3 shows the typical true stress-strain behavior of a material undergoing a uniaxial tension test. It's important to note that this curve is distinct from the nominal stress-strain response

observed in a uniaxial test. For an elastic-plastic material with isotropic hardening, damage manifests in two main ways: decreased yield stress and loss of elasticity. The solid curve in the Figure 4.3 depicts the stress-strain response.

The fracture strain, $\bar{\varepsilon}_0^{pl}$, is the equivalent plastic strain at the onset of damage. It is obtained by analyzing the graph in Figure 4.3, where the yield stress is marked by a line with a slope corresponding to Young's Modulus considered [102]. Table 4.4 shows the values of the parameters used to characterize the material damage model.

Table 4.4 Numerical parameters used to characterize the damage model.

Ductile Damage			Damage Evolution
Fracture Strain	Stress Triaxiality	Strain Rate	Displacement at Failure
0.01	0.333	0.1	0.28

4.2.2 Numerical Simulation: Model 1 (USL-1)

The mesh geometry was derived from an existing design by the manufacturer *FEG Textiltechnik mbH*, known as *Dynamesh – PR*. Comprised of PVDF, this mesh was specifically created for pelvic floor reconstruction, aiming to provide support and stability for fascial structures, connective tissue, and ligaments, as illustrated in Figure 4.4.

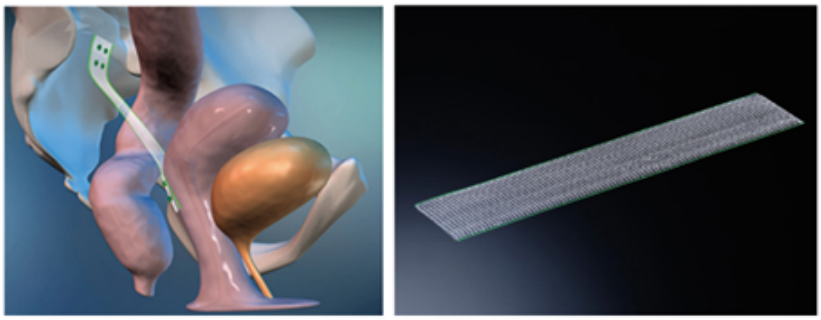

Figure 4.4 PR mesh and how it can be applied to the pelvic cavity (unilateral hysterosacropexy) (adapted from [104]).

This model was developed to mimic the USL. Two different configurations were chosen for this work: the square and the sinusoidal. The square configuration is the most common among existing synthetic meshes, while the sinusoidal configuration has shown promising results in previous studies.

4.2.2.1 Square Mesh (USL-1Q)

With the aid of the highly precise Abaqus® software, we were able to generate a 3D square mesh. This mesh, with its deformable characteristics and a planar wire shape measuring 110x40

mm, Figure 4.5, was meticulously designed to consider a pore size of 1.5 mm and a filament diameter of 240 μm. These parameters were determined based on the best results obtained from previous tests [101] and this mesh was built to mimic the USL and in order to reduce the nomenclature, it was abbreviated to USL-1Q.

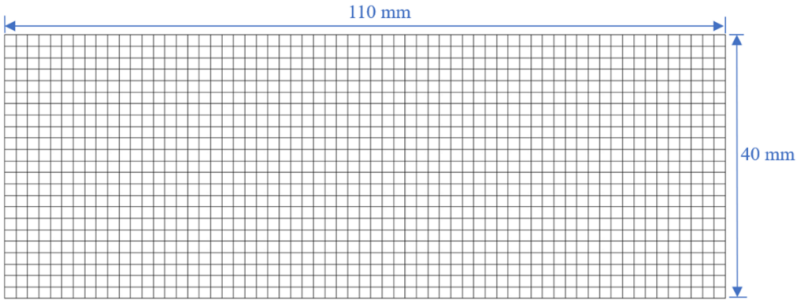

Figure 4.5 Geometry and dimensions of the square mesh to mimic the USL behavior (USL-1Q).

The mesh comprises 28392 nodes and 29840 elements, which are type B31. These beam elements use linear and quadratic interpolation and are based on the Euler-Bernoulli formulation but also incorporate "transverse shear strain". This implies that the shape of the cross-section may not remain perpendicular to the beam axis, and this concept is consistent with the Timoshenko beam theory, 1956. This is beneficial for thicker beams where shear flexibility is significant. These elements are designed to be effective for both thin (where Euler-Bernoulli theory is precise) and thick beams, making them the most efficient beam elements in Abaqus® software [105].

Our analysis is based on the well-established understanding that the Euler-Bernoulli beam theory accurately represents the behavior of beams primarily subjected to flexure, which are often referred to as 'long' beams. On the other hand, the Timoshenko theory applies to beams dominated by shear forces, commonly known as 'short' beams. In the context of our 3D square mesh model, we expect both theories to align in the intermediate length range [106].

4.2.2.2 Sinusoidal Mesh (USL-1S)

Figure 4.6 illustrates a 3D deformable mesh with a sinusoidal shape, created using Abaqus® software, also to mimic the USL behavior. The mesh is 110x40 mm in size, with a pore size of 1.58 mm. Due to the complexity of the sinusoidal geometry, it is challenging to determine a precise pore size, so the largest dimension between the sinusoidal waves is used as the reference. These parameters were determined based on the best results obtained from previous tests [101]. The purpose of creating this mesh was to replicate the USL. In order to simplify the nomenclature, it was abbreviated to USL-1S.

The mesh obtained consists of 85241 nodes and 89640 elements, which are also of type B31.

Figure 4.6 Geometry and dimensions of the sinusoidal mesh to mimic the USL behavior (USL-1S).

4.2.2.3 Conformation and incorporation of the implants

The Abaqus Explicit was used to ensure that the implants conform to the surface of the uterus. An assembly model was created to show how the mesh interacts with the uterus. A pressure was applied to the lower part of the mesh to shape it to the uterus. Boundary conditions were specified to fix the mesh's uterus and upper part. Additionally, a surface-to-surface interaction model between the two components was established. The images in Figure 4.7 show how the square and sinusoidal meshes conform to the uterus.

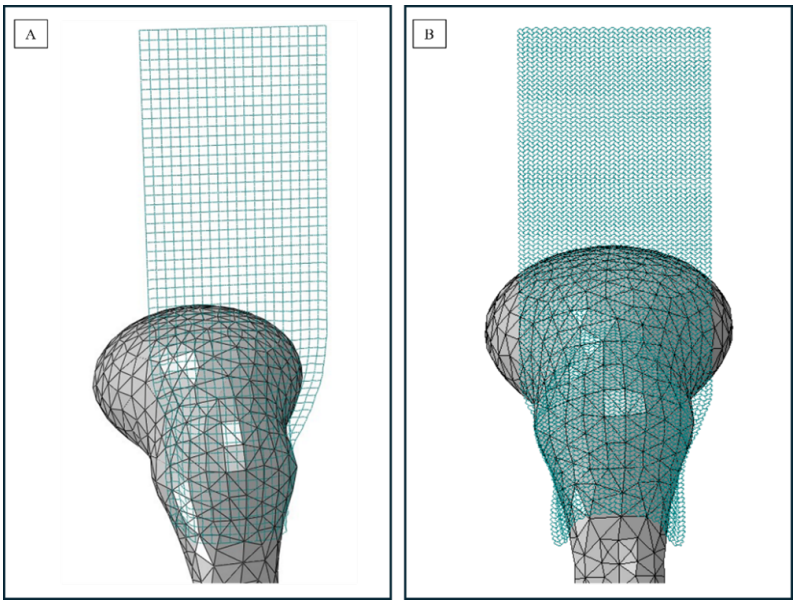

Figure 4.7 Conformation of the USL-Model 1 to the uterus. A: Square mesh (USL-1Q); B: Sinusoidal mesh (USL-1S).

Following this, the mesh was incorporated into the computational model of the pelvic cavity, and a tie constraint was applied between the mesh and the contacting part of the uterus. Figure 4.8 shows this incorporation. It is important to note that even though there seems to be some overlap

between the mesh and the organs, especially the rectum, such overlap would not actually happen in real life due to the mesh's high flexibility and easy adjustability.

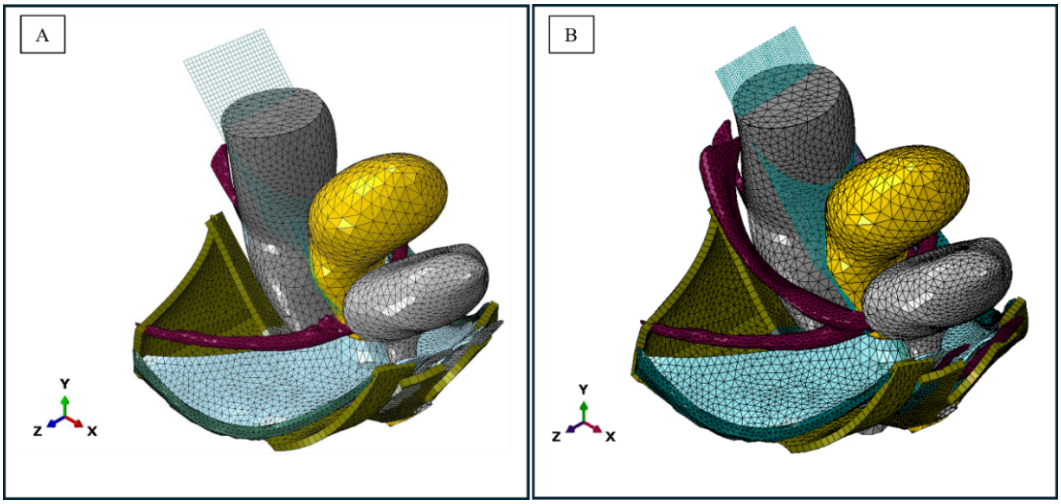

Figure 4.8 Incorporation of the USL-Model 1 into the computational model of the pelvic cavity. A: USL-1Q for a total rupture of the pelvic cavity; B: USL-1S for USL impairment.

The implants in Figure 4.8 are not fixed to any structure in the posterior region due to the model's limitation of not having a sacrum. However, different boundary conditions were applied to the posterior part of both implants, close to where fixation would be expected.

4.2.3 Numerical Simulation: Model 2 (USL-2)

This geometry is composed of two meshes to realistically mimic the USL ligament, one ligament on each side of the uterus. These meshes were designed with planar wire shapes measuring 80x25 mm, Figure 4.9, including a pore size of 1.5 mm and a filament diameter of 240 μm.

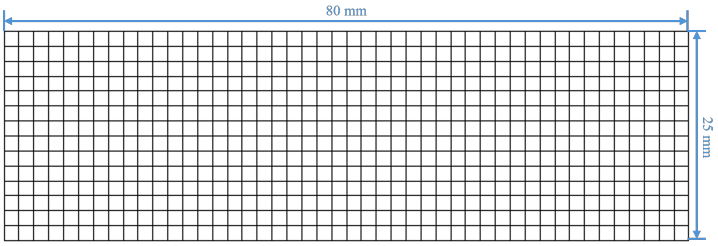

Figure 4.9 Geometry and dimensions of the square USL mesh to realistically mimic the USL ligament.

The mesh obtained consists of 12837 nodes and 13480 elements of type B31.

4.2.3.1 Model USL-2.1

Initially, the meshes created were positioned on top of the ligaments, and with the assistance of Abaqus Explicit, an assembly was conducted between the ligaments, the uterus, and the two meshes to conform the meshes to the ligaments. Pressure was applied to the mesh to conform it to the USL. Additionally, boundary conditions were defined, including the fixation of the ligaments and uterus. Furthermore, a constraint was applied at each mesh's top and bottom ends to ensure their retention in place. In addition, a general contact interaction between the parts needed to be established. Figure 4.10 shows the conformation of the square meshes to the ligaments, as well as the incorporation of these conformed meshes into the pelvic cavity model, with a tie having been applied between the parts of the mesh that come into contact with the uterus.

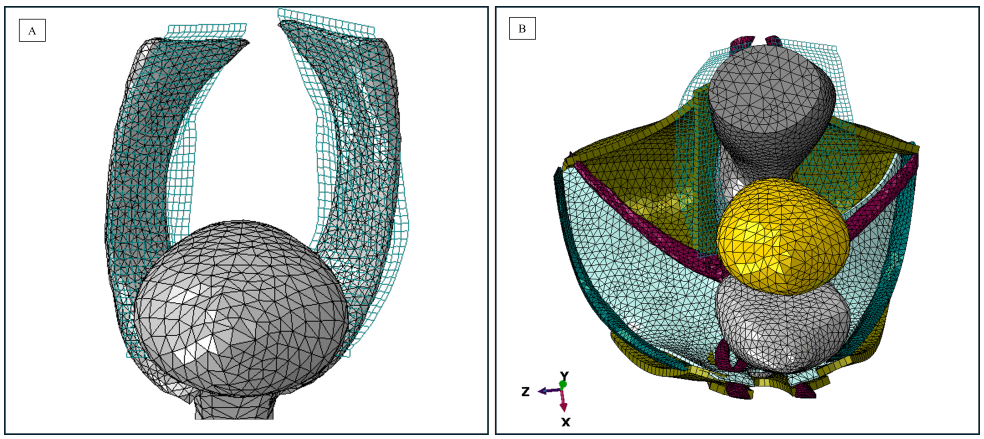

Figure 4.10 A: Conformation of the mesh to the USL; B: Incorporation of both meshes conformed to the ligament in the computational model of the pelvic cavity with total rupture of the USL.

4.2.3.2 Model USL-2.2

To create meshes that can support ligaments with associated damage, it was necessary to consider cases where the ligament is not completely ruptured. It was determined that conforming the mesh to the underside of the ligament would provide greater support and allow the mesh to start bearing load immediately as the organs begin to descend. This process was achieved using the Abaqus Explicit, following the same steps as those used for conforming the mesh to the upper part of the ligaments. Figure 4.11 shows the square meshes conforming to the ligaments and their incorporation into the pelvic cavity model. A tie constraint was applied to the lower parts of the mesh in contact with the ligament.

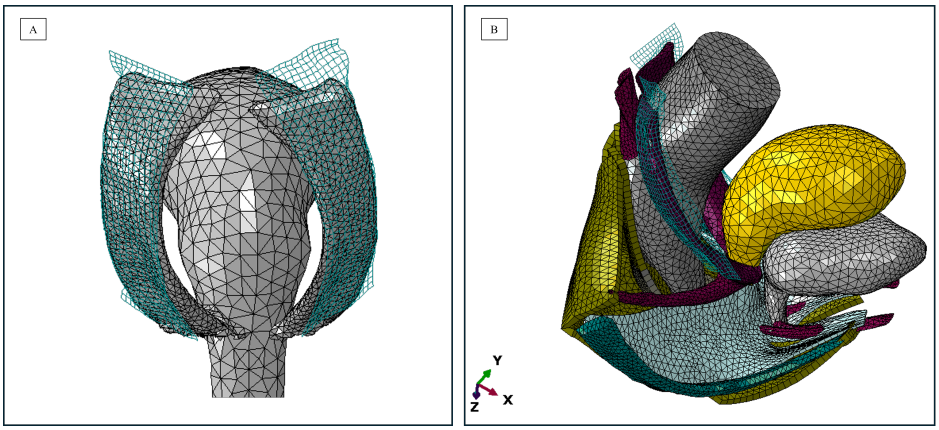

Figure 4.11 A: Conformation of the mesh to the USL; B: Incorporation of both meshes conformed to the ligament in the computational model of the pelvic cavity without total rupture of the USL.

4.2.3.3 Model USL-2.3

When the mesh is conformed to the upper part of the ligament, it is stretched for a period, but the organs' total displacement is insufficient for the mesh to support their descent. A non-conformed mesh was considered to address this issue.

The created meshes were placed in the ligament area and adjusted to the uterus without conforming. Abaqus Explicit was used for this purpose, and an assembly was created between the uterus and the two meshes. Boundary conditions were set, including constraints on the uterus and the upper and lower ends of the meshes to keep them in place. Additionally, a general contact interaction was established between the surrounding parts. Figure 4.12 shows this setup and its incorporation into the computational model of the pelvic cavity, with a tie constraint applied to the lower parts of the meshes in contact with the uterus.

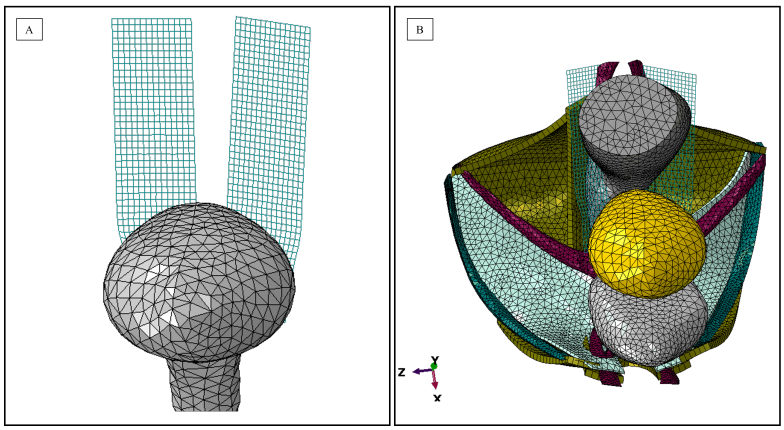

Figure 4.12 A: Positioning of the mesh; B: Incorporation of both meshes in the computational model of the pelvic cavity without total rupture of the USL.

4.2.3.4 Model USL-2.4

To explore the potential benefits of using non-conformed meshes on the uterus, we developed two deformable 3D square meshes with planar wire shapes, each measuring 80x10.50 mm. These meshes have a pore size of 1.5 mm and a filament diameter of 240 μm , Figure 4.13. The narrower mesh structure was designed to provide the same level of support as the wider meshes while minimizing interference with other organs, thus offering a more efficient and less invasive solution.

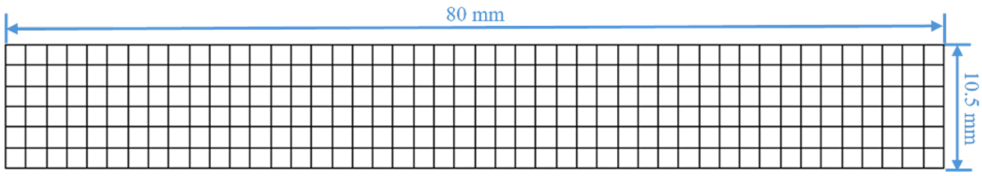

Figure 4.13 Geometry and dimensions of the square mesh to mimic the USL ligament.

The mesh obtained comprises 5765 nodes and 6040 elements, which are of type B31.

The meshes were placed around the ligaments and adjusted to the uterus without conforming. The subsequent process followed the steps described in Model 2.3, utilizing Abaqus Explicit. After assembling the meshes and the uterus, boundary conditions were defined, including fixing the uterus in place and restricting the upper and lower ends of the meshes to ensure they remained correctly positioned. Additionally, general contact interaction was established between the involved parts. Figure 4.14 shows this arrangement and its integration into the computational model of the pelvic cavity, with a tie established between the lower part of the meshes and the uterus.

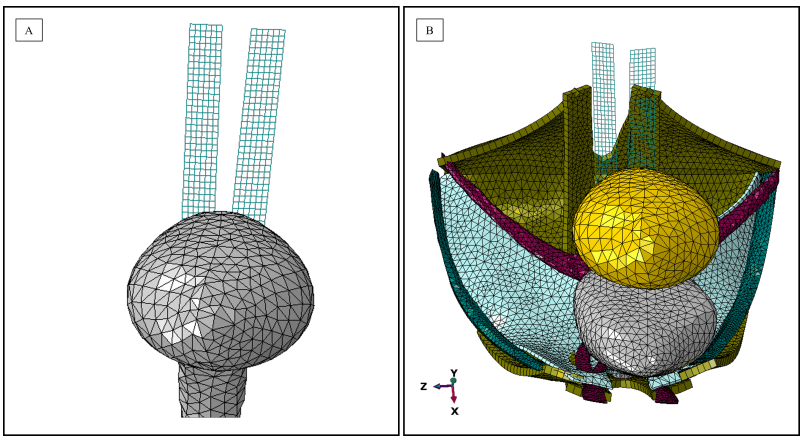

Figure 4.14 A: Positioning of the mesh to the USL; B: Incorporation of both meshes in the computational model of the pelvic cavity without total rupture of the USL.

4.2.4 Numerical Simulation: Model 3 (CL-3)

The mesh geometry was designed based on the *DynameshPRP* mesh, manufactured by FEG Textiltechnik mbH [107]. These meshes are used for POP correction in both laparoscopic and open surgical techniques, providing support and stabilization to fascial structures, connective tissue, and ligaments. The implants are utilized in the surgical treatment of vaginal/cervical stump prolapse or uterine prolapse using the pectopexy technique, as shown in Figure 4.15.

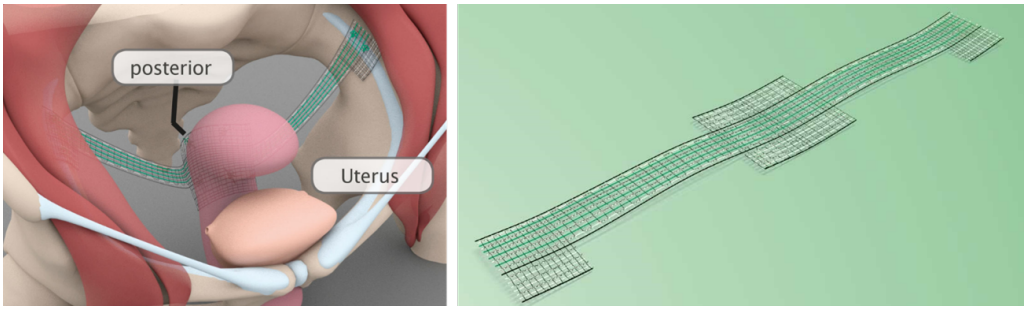

Figure 4.15 PRP mesh and how it can be applied to the pelvic cavity (pectopexy technique) (adapted from [107]).

The purpose of this mesh is to mimic the function of the CL in case of rupture or impairment. To accomplish this, it is attached to the central region of the cervix, and its ends are secured to the tendinous arch of the pelvic fascia.

Two distinct configurations were selected for this study: the square and the sinusoidal. The square configuration is the most prevalent among current synthetic meshes, whereas the sinusoidal configuration has demonstrated promising outcomes in earlier research.

4.2.4.1 Square Mesh (CL-3Q)

Using the Abaqus® software, a 3D square mesh with deformable characteristics and a planar wire shape was successfully created based on the measurements from Figure 4.16. The design considers a pore size of 1.5 mm and a filament diameter of 240 μm.

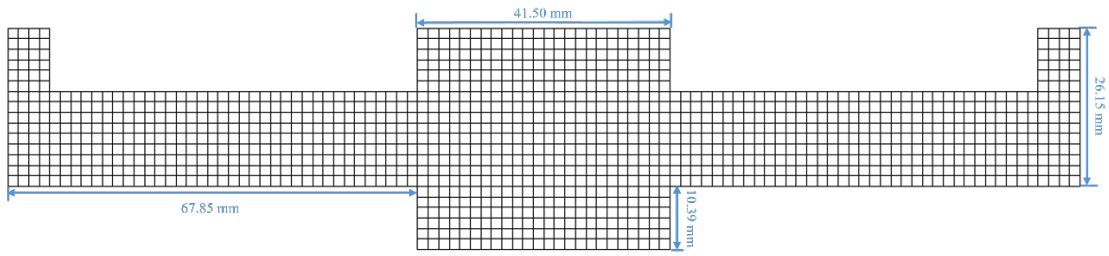

Figure 4.16 Geometry and dimensions of the square mesh to mimic the CL behavior (CL3-Q).

This mesh created consists of 25177 nodes and 26430 elements, which are type B31.

4.2.4.2 Sinusoidal Mesh (CL-3S)

Figure 4.17 depicts a 3D deformable mesh with sinusoidal geometry created using Abaqus® software. The Figure shows the mesh dimensions, with the same pore dimensions as the 1S implant. The filament diameter is 240 μm, which was selected based on the best results from previous tests.

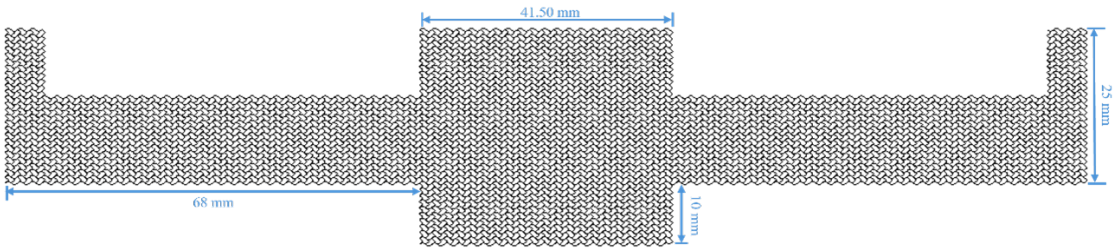

Figure 4.17 Geometry and dimensions of the sinusoidal mesh to mimic the CL behavior (CL3-S).

The mesh obtained consists of 67775 nodes and 71335 elements, which are also of type B31.

4.2.4.3 Conformation and incorporation of the implants CL

First, the Abaqus Explicit software was used to shape the central part of the mesh to fit the cervix. Pressure was applied to conform the mesh, and boundary conditions were set for the uterus and the rest of the mesh. We also established a surface-to-surface interaction between the mesh and the uterus.

Next, to shape the mesh arms at a specific angle, we placed a rigid analytics plate with the same inclination as the ligament and another rigid analytics plate to which we applied a concentrated force.

This caused the mesh arms to take on the desired shape when the plates made contact. We set up a surface-to-surface interaction between the mesh and the two plates and created boundary conditions for the plate with the desired inclination and the previously shaped mesh center. The same process was carried out for the sinusoidal mesh. Figure 4.18 illustrates the formation and final shape of the arms of the square mesh.

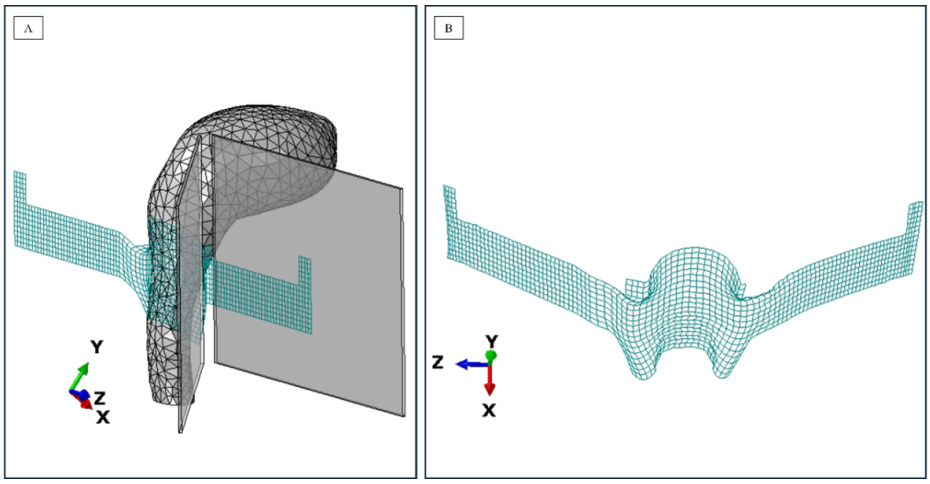

Figure 4.18 A: Conformation of the arms of the CL mesh; B: Conformed CL mesh.

Following this, the meshes were integrated into the computational model of the pelvic cavity, and a tie constraint was applied between the mesh and the contacting part of the uterus. This integration is illustrated in Figure 4.19. It should be noted that despite the apparent interference between the mesh and the organs, such interference would not manifest in practical situations owing to the high flexibility and easy adjustability of the mesh.

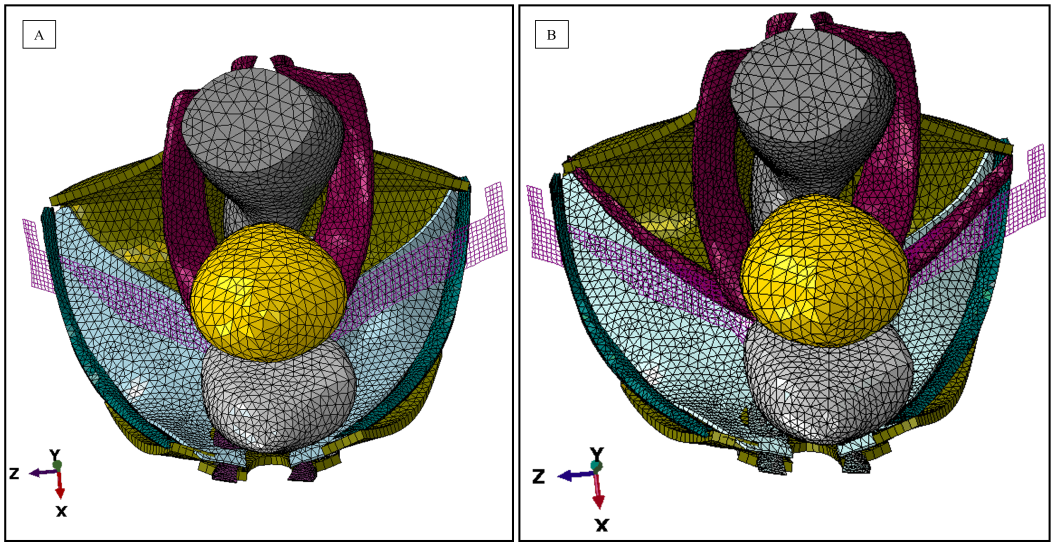

Figure 4.19 Incorporation of the implant into the computational model of the pelvic cavity. A: with total CL rupture; B: without total CL rupture.

4.2.5 Points of Reference

Parameters such as the superior-inferior displacement and magnitude of these ligaments were observed in eight nodes in the anterior vaginal wall, Figure 4.20, and the displacement values were calculated using the average of these values.

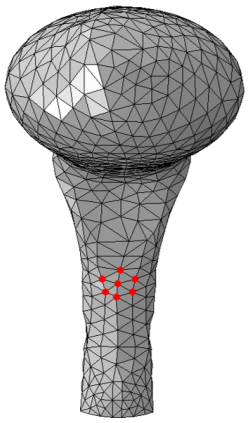

Figure 4.20 Nodes in the anterior vaginal wall to measure the supero-inferior displacement.

Points of interest to study the supero-inferior displacement and magnitude of the displacement were also established in the implants developed to understand their behavior towards the ligaments, as shown in Figure 4.21.

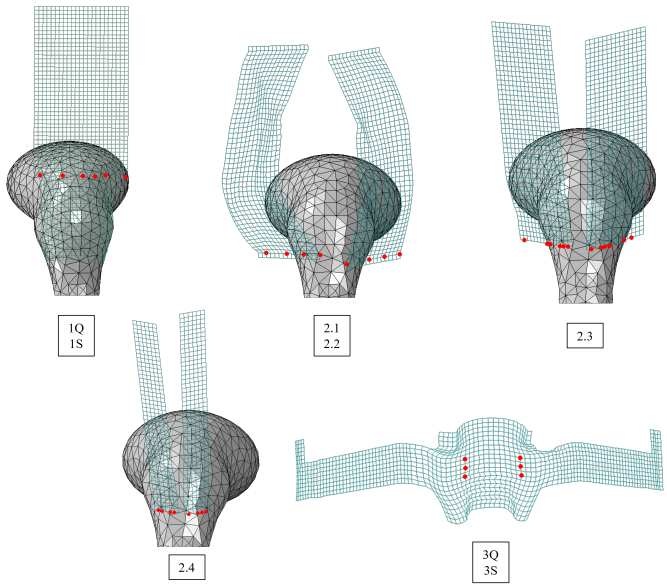

Figure 4.21 Nodes in the implants to measure the supero-inferior displacement.

The set of nodes referring to the ligaments used for comparison with the implants is depicted in Figure 4.22.

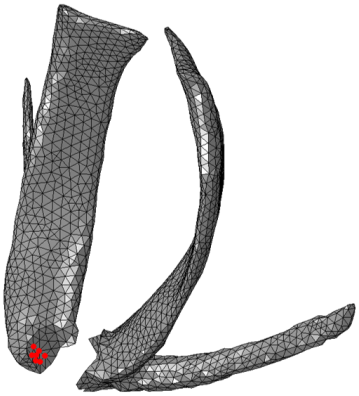

Figure 4.22 Nodes analyzed in the ligaments.

4.2.6 Study of Different Fixation Conditions

The study's initial focus was examining different implants' behavior without considering the variation in suturing techniques used by different surgeons. However, an additional analysis was conducted to investigate how implant fixation affects the supero-inferior displacement and maximum magnitude of displacement. Several anchoring techniques were defined for this purpose, including a continuous line, encasement of 8 suture elements in the center of the top of the implant, a suture of two interrupted lines horizontally. These fixation approaches are depicted in Figure 4.23.

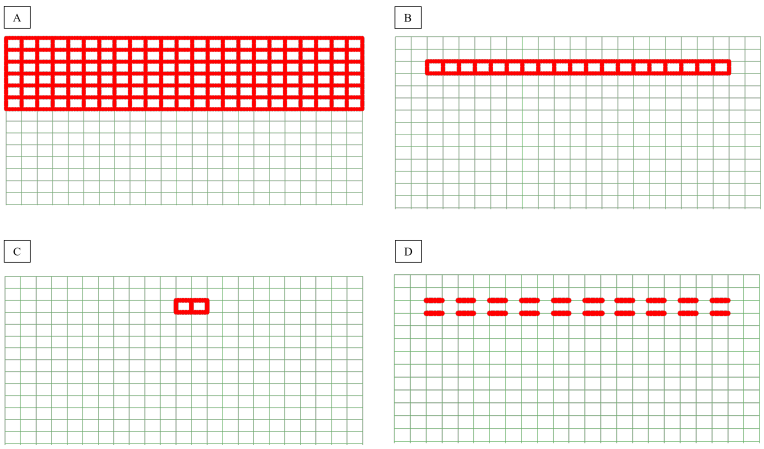

Figure 4.23 Several anchoring techniques applied. A: A band of elements; B: Continuous line; C: Simple Stitch; D: Horizontal interrupted suture.

4.2.7 Stress-Strain Analysis

The square and sinusoidal meshes had already been created and tested previously and had produced good results (in this case, better results with the sinusoidal geometry), which is why they were chosen for this study. The stress-strain curve of the ligament was obtained by Martins, 2010 and the stress-strain curves of the square and sinusoidal meshes and the Restorelle® were obtained by Vaz, 2023 [101, 108].

In Figure 4.24, the behavior of the sinusoidal and square meshes is compared to that of the ligaments and the synthetic Restorelle® mesh. It can be observed that the sinusoidal mesh initially behaves similarly to the ligament, but then deviates from the intended behavior. Restorelle®, a synthetic mesh that is no longer commercially available due to serious complications associated with its high rigidity and torsion, exhibited problematic behavior. The Restorelle® mesh does not behave like vaginal tissue or the ligament. This difference is likely a significant factor causing issues and tissue damage when this mesh is used in patients [101, 108].

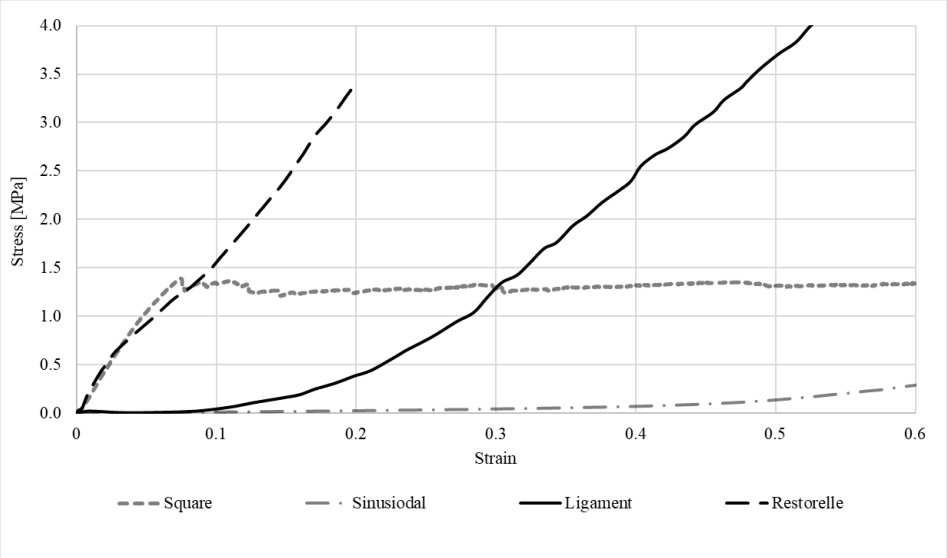

Figure 4.24 Comparison of stress-strain curves.(adapted from [101, 108]).

Chapter 5

Results

5.1 Numerical simulations without implants

Evaluating the effectiveness and performance of the implants' models requires a comprehensive comparative analysis. The values obtained from the healthy pelvic numerical model were compared with those of the developed implants. This simulation results in a supero-inferior displacement of 6.38 mm in the anterior vaginal wall, which was measured at the nodes presented in Chapter 4 - Figure 4.20. The supero-inferior displacement results show the organs' vertical descent and are taken concerning the vertical axis of the global model.

The models, which simulate the complete rupture of the USL and CL individually, provide a clear baseline for understanding the extent of damage without intervention. The supero-inferior displacement values obtained in total rupture of USL and CL, were 10.77 mm and 8.58 mm, respectively. Table 5.1 displays the supero-inferior displacement and maximum magnitude for various scenarios, including the healthy case, impairments (50% and 90%), and total rupture of the apical ligaments.

Table 5.1 Supero-inferior displacement of the vaginal wall and respective maximum displacement magnitudes, when impairments of 50%, 90%, and total rupture of the USLs and CLs occur.

	Variable	Supero-inferior disp. of the **vagina** (mm)	Max disp. mag of the **vagina** (mm)	Variation disp. of the vagina in relation to the **healthy** (%)
Healthy	**Rest**	…	…	…
	Valsalva	6.38	7.77	…
USL	**Impairment 50%**	7.03	8.53	10.19
	Impairment 90%	8.91	10.96	39.66
	Total Rupture	10.77	12.49	68.81
CL	**Impairment 50%**	6.74	8.23	5.64
	Impairment 90%	7.40	9.10	15.99
	Total Rupture	8.58	10.33	34.48

To study the effects of impairment on both ligaments, a constant 90% impairment was maintained in the USL. The supero-inferior displacement with the CL under different types of impairment (50% and 90%) and total rupture were analyzed. Table 5.2 displays the supero-inferior displacement and maximum magnitude for the different scenarios mentioned.

Table 5.2 Supero-inferior displacement of the vaginal wall and respective maximum displacement magnitudes, with 90% impairment of USL and with impairments of 50%, 90%, and total rupture of the CL.

Variable		Supero-inferior disp. of the vagina (mm)	Max disp. mag of the vagina (mm)	Variation disp. of the vagina in relation to the **healthy** (%)
		USL Impairment 90%	**USL Impairment 90%**	
CL	**Impairment 50%**	9.11	10.68	42.79
	Impairment 90%	10.23	12.55	60.34
	Total Rupture	12.37	15.49	93.89

5.2 Numerical simulations with implants

This section contains the results related to the supero-inferior displacement of the anterior wall of the vagina due to different implants, as analyzed in the specified region in Chapter 4, Figure 4.20. Table 5.1 represents the control values of the measurements without implants for comparison. The healthy supero-inferior displacement measurement is 6.38 mm. For the USL, the supero-inferior displacement was 7.03 mm for 50% impairment, 8.91 mm for 90% impairment, and 10.77 mm for total rupture. For the CL, the measurements were 6.74 mm for 50% impairment, 7.40 mm for 90% impairment, and 8.58 mm for total rupture. This study was carried out by varying the types of fixation. Additionally, the supero-inferior displacement of the implants in the region detailed in Chapter 4, Figure 4.21 was analyzed. The healthy measurement in the ligament is 8.26 mm, 9.16 mm for 50% impairment, and 10.51 mm for 90% impairment. This study was only carried out on the encastre with a band of elements. All the tables also show the maximum magnitude displacement, where it can be seen that with valving pressure, most of the displacement is in the supero-inferior direction. Finally, stress concentration in implants of Model 1 and Model 3 was also examined.

5.2.1 Analysis of implants behavior

This analysis aims to understand the behavior of the implants developed when applied to the computational model of the pelvic cavity to replace the USL and CL ligaments in the event of a total rupture and reinforce them in the event of 50% and 90% impairment.

To do this, the study focused on interpreting the supero-inferior displacements at the reference points on the anterior vaginal wall presented in Chapter 4 - Figure 4.20, as well as the supero-inferior displacement felt in each of the implants, which was measured at the nodes presented in Chapter 4 - Figure 4.21, to validate whether the implant actually fulfills any function in supporting the uterus.

Uterosacral Ligaments Implants

The implants, which are visible in Figure 5.1, were studied in their application to a computational model of the pelvic cavity. Additionally, the supero-inferior displacement associated with each implant when subjected to Valsalva pressure was analyzed. All the implants were fixed with a band of elements encastre, as shown in Chapter 4 - Figure 4.23.

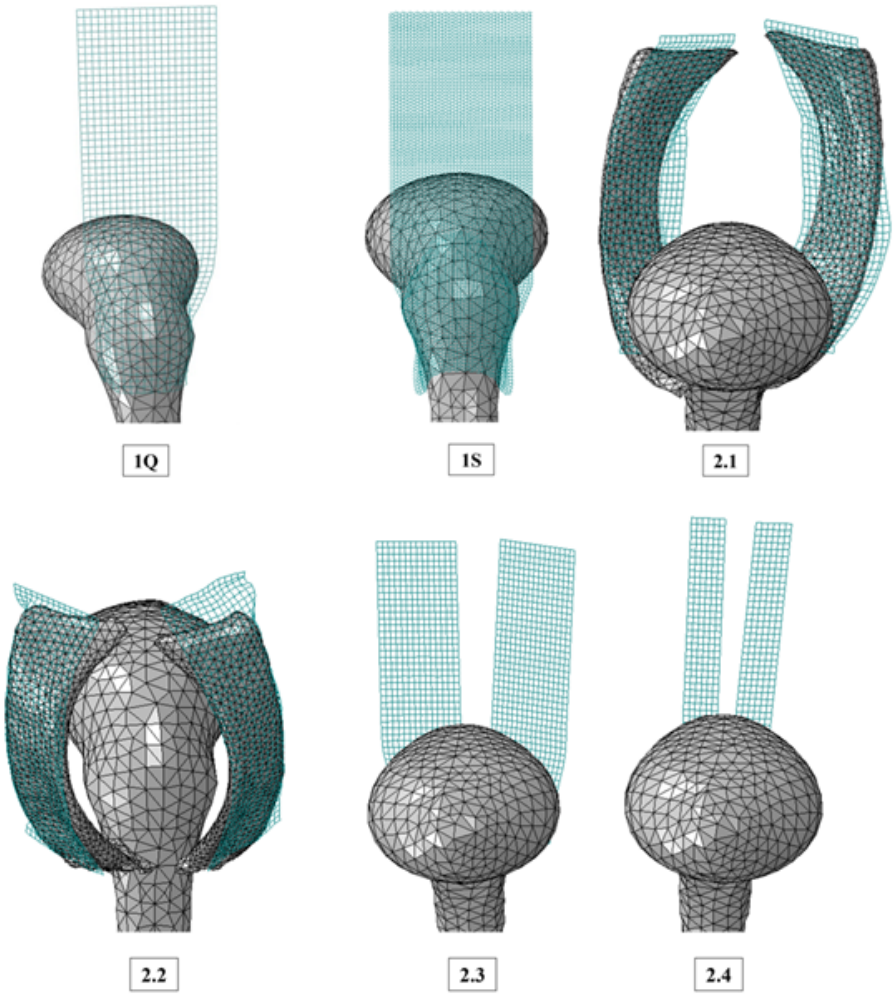

Figure 5.1 Different implants (Model 1 and Model 2) developed to mimic USLs

Anterior Vaginal Wall Supero-Inferior Displacement Analysis

The results obtained are presented in Table 5.3 and Figure 5.2. In this analysis, the control group in Figure 5.2 consists of the results obtained for the supero-inferior displacement of the healthy model (6.38 mm), 50% impairment of the USL (7.03 mm), 90% impairment of the USL (8.91 mm), and total rupture of the USL (10.77 mm). In Table 5.3, the variation in supero-inferior displacement values of the USL implants is compared to the healthy model, which measures 6.38 mm.

Table 5.3 Supero-inferior displacement of the anterior vagina wall and respective maximum displacement magnitudes, when impairments of 50%, 90%, and total rupture of the USLs occur with USLs implants.

	Variable	Supero-inferior disp. of the **vagina** (mm)	Max disp. mag of the **vagina** (mm)	Variation disp. of the vagina in relation to the **healthy** (%)
Impairment 50%	**1Q**	5.32	6.68	(-) 16.61
	1S	6.22	7.03	(-) 2.51
	2.1	7.01	8.51	9.87
	2.2	6.98	8.48	9.40
	2.3	6.83	8.34	7.05
	2.4	7.02	8.52	10.03
Impairment 90%	**1Q**	5.97	7.72	(-) 6.43
	1S	7.59	9.65	18.97
	2.1	8.89	10.35	39.34
	2.2	8.53	10.00	33.70
	2.3	8.13	9.65	27.43
	2.4	8.88	10.33	39.18
Total Rupture	**1Q**	7.01	9.29	9.87
	1S	9.29	10.77	45.61
	2.1	10.51	12.45	64.73
	2.2	10.33	12.28	61.91
	2.3	9.70	11.67	52.04
	2.4	10.50	12.47	64.58

Based on the data in Table 5.3, Model 1Q exhibits supero-inferior displacement values that are closer to those of a healthy model. This is observed in cases of total ligament rupture and cases of 50% and 90% impairment. The results indicate that implants can significantly support the uterus when ligament is impaired. In the case of 50% impairment, the 1Q and 1S implants even show a lower superior-inferior displacement than that observed in healthy ligaments.

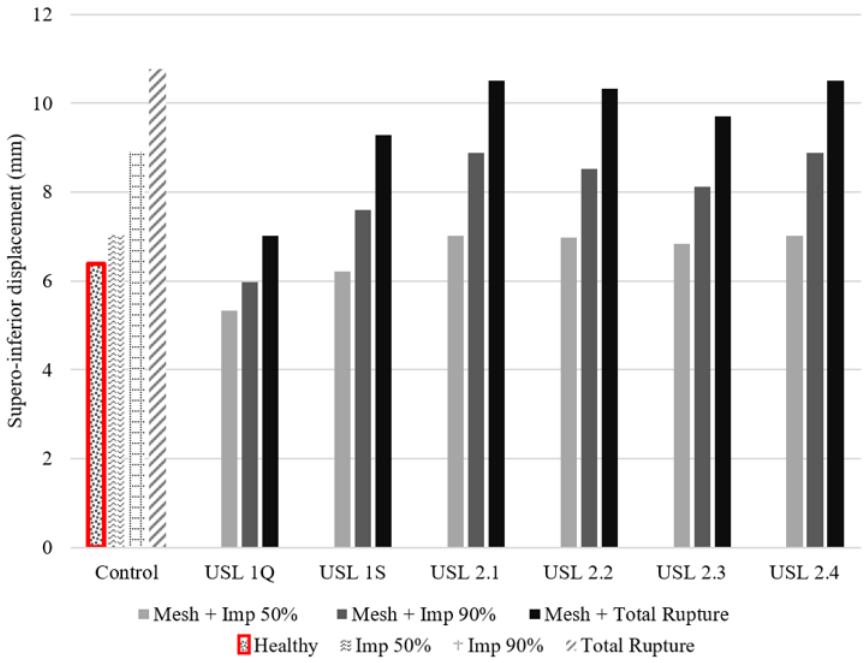

Figure 5.2 Representation of the supero-inferior displacements of the anterior vaginal wall in cases of total rupture of the ligaments as well as with 50% and 90% impairment with USLs implants.

Implant Supero-inferior Displacement Analysis

During the work, a study was carried out to compare the behavior of the implants and the ligaments. The goal was to determine which models closely matched the behavior of the USL. As a result, the values presented in Table 5.4 and Figure 5.3 focus on mimicking the USL rather than the supero-inferior descent of the vagina. These values indicate the supero-inferior displacement at the control points of the implants, Chapter 4 - Figure 4.21, and the supero-inferior displacement values of the USL, Chapter 4 - Figure 4.22. In this analysis, the control group in Figure 5.3 consists of the results obtained for the supero-inferior displacement of the healthy model (8.26 mm), 50% impairment of the USL (9.16 mm), 90% impairment of the USL (10.51 mm), and in this case, since the analysis is conducted on the ligament, it is not possible to compare the results to the total rupture value when the ligament is absent. In Table 5.3, the variation in supero-inferior displacement values of the USL implants is compared to the healthy model, which measures 8.26 mm.

Table 5.4 shows that when mimicking the USL implant, Model 1S demonstrates values closer to those of a healthy ligament than Model 1Q, for both partial and total impairment cases. However, Model 1Q exhibits lower supero-inferior displacement values, even lower than those of a healthy ligament, indicating that they provide greater stabilization under traction.

Table 5.4 Supero-inferior displacement of the USLs implants and respective maximum displacement magnitudes, when impairments of 50%, 90%, and total rupture of the USLs occur and supero-inferior displacement of this ligament (without implant) with the same conditions.

Variable		Sup-inf disp. of the **implant** (mm)	Sup-inf disp. of the **USL** (mm)	Max disp. mag of the **implant** (mm)	Max disp. mag of the **USL** (mm)	Variation sup-inf disp. of the implant in relation to the **healthy USL** (%)
Healthy			8.26		9.55	
Impairment 50%	**1Q**	3.54	9.16	4.06	10.59	(-) 57.14
	1S	5.9	9.16	6.68	10.59	(-) 28.57
	2.1	8.51	9.16	9.99	10.59	3.03
	2.2	8.75	9.16	10.35	10.59	5.93
	2.3	8.52	9.16	9.88	10.59	3.15
	2.4	8.53	9.16	9.87	10.59	3.27
Impairment 90%	**1Q**	4.40	10.51	5.07	13.20	(-) 46.73
	1S	7.87	10.51	8.70	13.20	(-) 4.72
	2.1	10.71	10.51	12.91	13.20	29.66
	2.2	11.17	10.51	12.95	13.20	35.23
	2.3	9.5	10.51	12.80	13.20	15.01
	2.4	10.91	10.51	12.82	13.20	32.08
Total Rupture	**1Q**	5.10	…	5.48	…	(-) 38.26
	1S	9.65	…	9.20	…	16.83
	2.1	14.61	…	16.17	…	76.88
	2.2	12.22	…	14.51	…	47.94
	2.3	13.21	…	15.23	…	59.93
	2.4	14.11	…	16.05	…	70.82

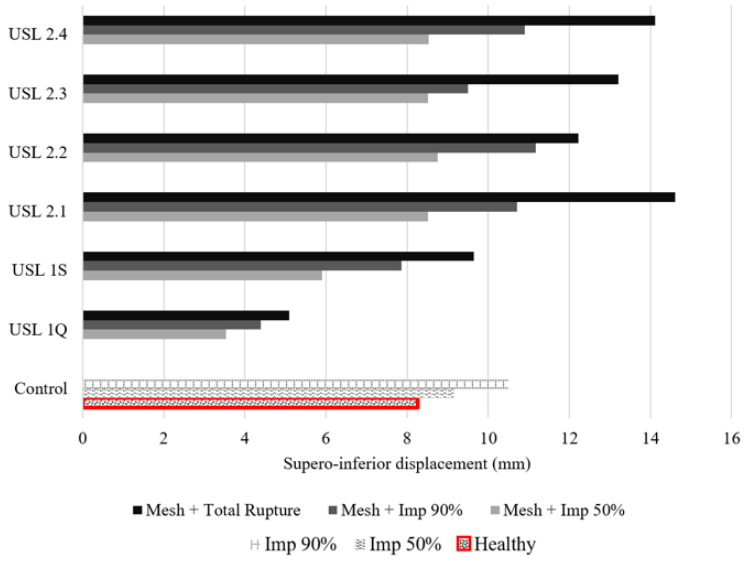

Figure 5.3 Representation of the USL behavior mimetization. Analysis of the supero-inferior displacements of the USLs implants in cases of total rupture of the USLs as well as with 50 and 90% impairment.

Cardinal Ligaments Implants

The Model 3 implants, Figure 5.4, were incorporated into the computational model of the pelvic cavity. Additionally, the supero-inferior displacement associated with each implant when subjected to Valsalva pressure was analyzed. All the implants were fixed with a band of elements encastre, as shown in Chapter 4 - Figure 4.23.

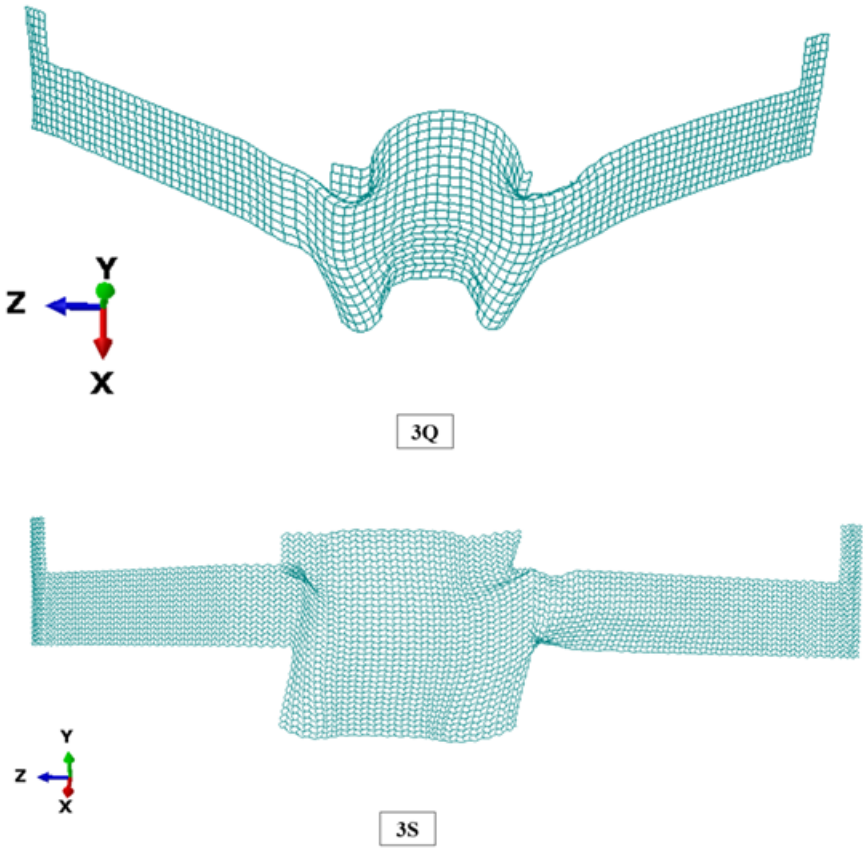

Figure 5.4 Different implants (Model 3) developed to mimic CLs.

Anterior Vaginal Wall Supero-Inferior Displacement Analysis

The results obtained are presented in Table 5.5 and Figure 5.5. Table 5.5 displays the values obtained for the supero-inferior displacement of the anterior vaginal wall in the region mentioned in Chapter 4 - Figure 4.20. The Table 5.5 also shows the values for the magnitude of displacement. In this analysis, the control group in Figure 5.5 consists of the supero-inferior displacement of the healthy model (6.38 mm), 50% impairment of the CL (6.74 mm), 90% impairment of the CL (7.40 mm), and total rupture of the CL (8.58 mm). In Table 5.5, the variation in supero-inferior displacement values of the CL implants is compared to the healthy model, which measures 6.38 mm.

Table 5.5 Supero-inferior displacement and max disp. mag of the vagina, during the VM, when impairments of 50%, 90%, and total rupture of the CLs occur with CLs implants.

Variable		Supero-inferior disp. of the **vagina** (mm)	Max disp. mag of the **vagina** (mm)	Variation disp. of the vagina concerning the **healthy** (%)
Impairment 50%	**3Q**	6.37	7.76	(-) 0.16
	3S	6.57	7.99	2.98
Impairment 90%	**3Q**	7.00	8.54	9.72
	3S	7.05	8.60	10.50
Total Rupture	**3Q**	7.18	8.42	12.54
	3S	7.42	8.84	16.30

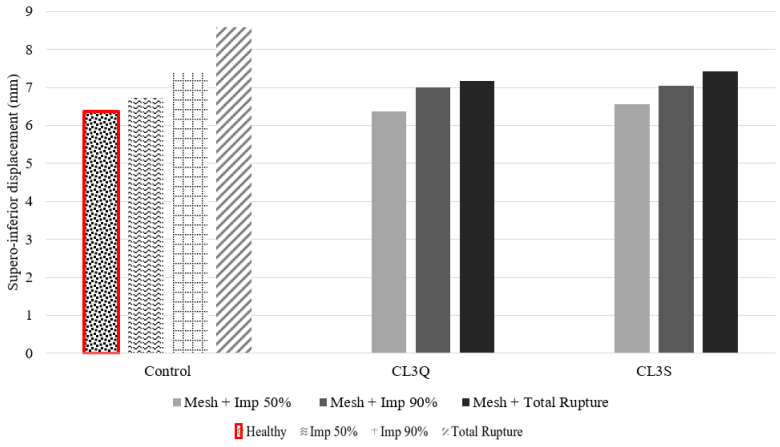

Figure 5.5 Representation of the supero-inferior displacements of the anterior vaginal wall in cases of total rupture of the ligaments as well as with 50% and 90% impairment with CLs implants.

Upon analyzing Table 5.5, it is evident that Model 3Q exhibits lower displacement values, which are close to those of the healthy model. This holds true for cases of total ligament rupture as well as for 50% and 90% impairment. The findings also indicate that implants can effectively support the uterus in instances of ligament impairment. Notably, in cases of 50% impairment, the 3Q implant demonstrates even lower superior-inferior displacement than healthy ligaments.

When the USL ligaments remain intact, and only the CL is affected, the supero-inferior displacement varies minimally compared to the control scenarios. However, when 90% of the USL is impaired, and various cases of impairment and total rupture of the CL are studied, the supero-inferior displacement varies considerably.

Table 5.6 and Figure 5.6 display the results that were obtained. In Table 5.6, the variation in supero-inferior displacement values of the CL implants is compared to the healthy model, which

measures 6.38 mm.

The control group in Figure 5.6, is shown in Table 5.2, and consists of the results obtained for the supero-inferior displacement of the healthy model (6.38 mm), 50% impairment of the CL and 90% impairment of the USL (9.11 mm), 90% impairment of the CL and 90% impairment of the USL (10.23 mm), and total rupture of the CL and 90% impairment of the USL (12.37 mm).

Table 5.6 Supero-inferior displacement and max disp. mag of the vagina, during the VM, when impairment of 90% of the USL and impairments of 50%, 90%, and total rupture of the CLs occur with CLs implants.

Variable		Supero-inferior disp. of the **vagina** (mm)	Max disp. mag of the **vagina** (mm)	Variation disp. of the vagina concerning the **healthy** (%)
Impairment 50%	**3Q**	8.20	9.95	28.53
	3S	8.49	10.26	33.07
Impairment 90%	**3Q**	9.06	10.91	42.01
	3S	9.45	11.20	48.12
Total Rupture	**3Q**	10.49	12.80	64.42
	3S	11.00	12.98	72.41

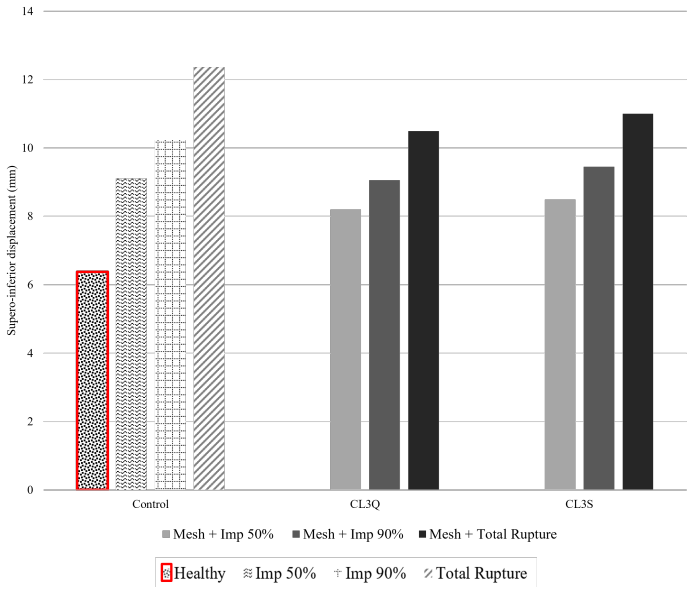

Figure 5.6 Representation of the supero-inferior displacements of the anterior vaginal wall in cases of impairment of 90% of the USL and impairments of 50%, 90%, and total rupture of the CLs occur with CLs implants.

Implants Supero-Inferior Displacement Analysis

The values presented in Table 5.7 and Figure 5.7 focus on mimicking the behavior of the CL. These values indicate the supero-inferior displacement at the control points of the implants, Chapter 4, Figure 4.21 and the supero-inferior displacement values of the CL, Chapter 4, Figure 4.22. In Figure 5.7, the control group shows the supero-inferior displacement for the healthy model (8.26 mm), and varying degrees of CL impairment: 50% (9.16 mm) and 90% (10.51 mm). Table 5.7 compares the variation in supero-inferior displacement values of the CL implants to the healthy model (8.26 mm).

Table 5.7 Supero-inferior displacement of the implant and respective maximum displacement magnitudes, when impairments of 50%, 90%, and total rupture of the CLs occur and supero-inferior displacement of this ligament (without implant) with the same conditions.

Variable		Sup-inf disp. of the **implant** (mm)	Sup-inf disp. of the **CL** (mm)	Max disp. mag of the **implant** (mm)	Max disp. mag of the **CL** (mm)	Variation sup-inf disp. of the implant in relation to the **healthy CL** (%)
Healthy			8.26		9.55	
Impairment 50%	**3Q**	7.02	9.16	8.00	10.59	(-) 15.01
	3S	7.80	9.16	9.04	10.59	(-) 5.57
Impairment 90%	**3Q**	7.96	10.51	8.86	13.20	(-) 3.63
	3S	8.85	10.51	9.88	13.20	7.14
Total Rupture	**3Q**	9.15	…	9.38	…	10.77
	3S	10.11	…	10.67	…	22.40

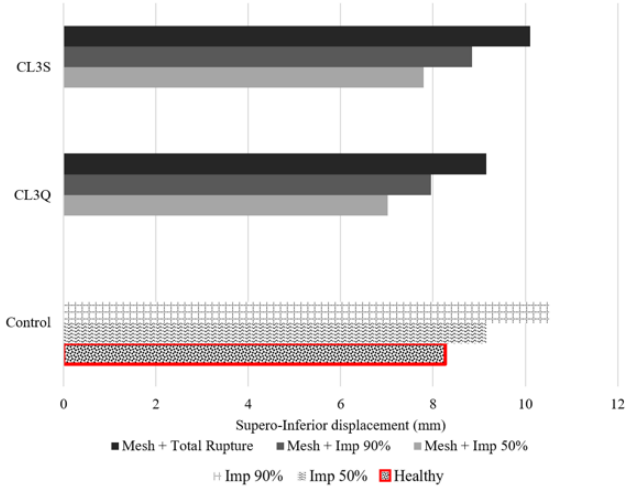

Figure 5.7 Representation of the CL behavior mimetization. Analysis of the supero-inferior displacement of Model 3 implants in cases of total rupture of the CLs as well as with 50 and 90% impairment.

Table 5.7 indicates that Model 3Q closely mimics the behavior of a healthy ligament more accurately in most of the scenarios, and, as in the case of USL, Model 3Q shows lower supero-inferior displacement values, which are even less than those of a healthy ligament in cases of partial impairment, suggesting that it offers better stabilization under traction.

5.2.2 Study the Application of Different Types of Fixations

Proper anchoring points and suture fixation are crucial to prevent post-surgery mesh-related complications (MRCs). In this regard, the primary function is to keep the mesh in place until tissue ingrowth is completed. The mesh anchoring failure was observed in 38% of patients, on average 1.8 years after placing the mesh. Thus, it is vital to understand how meshes are implanted. The anchoring points applied in the simulation will be the same as those used in the surgery [9].

The goal of analyzing the results from numerical simulations using the developed implants is to gain insight into their performance under different fixation approaches, which can vary based on the surgeon's preference. This analysis also aims to understand how the implants behave when mimicking different ligament conditions (impairment of 50%, 90%, and total rupture).

5.2.2.1 Fixation with continuous line suture

Continuous Line Suture - USL Implants

All the implants were fixed with a continuous line, which was measured at the nodes presented in Chapter 4 - Figure 4.23.

Anterior Vaginal Wall Supero-Inferior Displacement Analysis

The supero-inferior displacement in the region mentioned in Chapter 4 - Figure 4.20 for different implants was analyzed. The results are presented in Table 5.8 and Figure 5.8. As previously noted, the control group in Figure 5.8 includes the results for the supero-inferior displacement of the healthy model (6.38 mm), 50% impairment of the USL (7.03 mm), 90% impairment of the USL (8.91 mm), and total rupture of the USL (10.77 mm). Table 5.8 details the variations in supero-inferior displacement values of the USL implants compared to the healthy model, which has a displacement of 6.38 mm.

After analyzing Table 5.8, we can observe that the Model 1Q implant exhibits significantly lower displacement values, which align closely with those of the healthy model, in cases of both total rupture and 50% and 90% ligament impairment. Despite the good results of Implant 1S in cases of partial impairment, looking at cases of total rupture, the sinusoidal mesh doesn't seem to work.

Table 5.8 Analysis of supero-inferior displacements and respective maximum displacement magnitudes in the anterior wall of the vagina with impairment of 50%, 90% and total rupture of USLs.

Variable		Supero-inferior disp. of the **vagina** (mm)	Max disp. mag of the **vagina** (mm)	Variation disp. of the vagina concerning the **healthy** (%)
Impairment 50%	**1Q**	5.43	6.80	(-) 14.89
	1S	6.40	7.83	0.31
	2.1	7.02	8.52	10.03
	2.2	6.99	8.49	9.56
	2.3	6.86	8.37	7.52
	2.4	7.03	8.52	10.19
Impairment 90%	**1Q**	6.10	7.68	(-) 4.39
	1S	7.80	9.14	22.26
	2.1	8.90	10.10	39.50
	2.2	8.87	10.08	39.18
	2.3	8.70	9.93	36.36
	2.4	8.90	10.11	39.50
Total Rupture	**1Q**	7.10	9.04	11.29
	1S	10.10	11.91	58.31
	2.1	10.68	12.62	67.40
	2.2	10.33	12.26	61.91
	2.3	9.15	10.94	43.42
	2.4	9.78	11.57	53.29

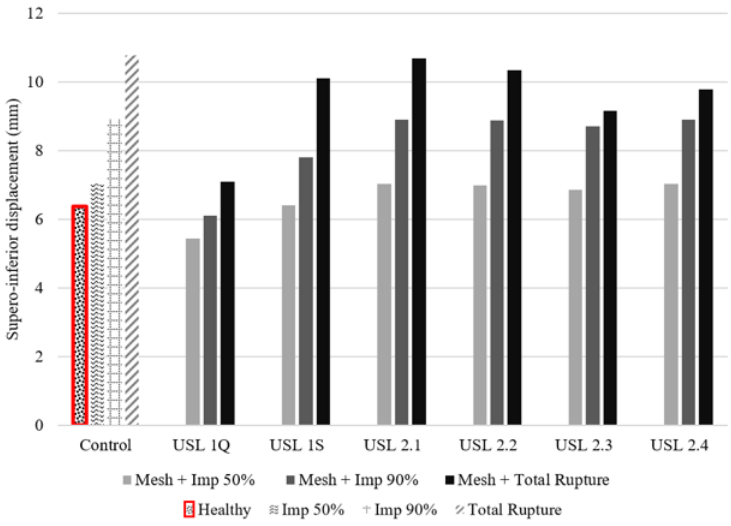

Figure 5.8 Representation of the supero-inferior displacements of the anterior vaginal wall in cases of total rupture of the ligaments as well as with 50% and 90% impairment with USLs implants with continuous line suture.

Conversely, implants 2.1, 2.2, and 2.4 are associated with results that are the furthest from those of the healthy model. Implants 2.1 and 2.2 were designed to provide support when the USL

is impaired, so it was anticipated that they would yield these values in cases of total USL rupture.

Continuous Line Suture - CL Implants

All the implants were fixed with a continuous line, which was measured at the nodes presented in Chapter 4 - Figure 4.23.

Anterior Vaginal Wall Supero-Inferior Displacement Analysis

Table 5.9 and Figure 5.9 show the results for the supero-inferior displacement of the anterior vaginal wall in the area mentioned in Chapter 4 - Figure 4.20. The control group in Figure 5.9 includes the supero-inferior displacement results for the healthy model (6.38 mm), 50% CL impairment (6.74 mm), 90% CL impairment (7.40 mm), and complete CL rupture (8.58 mm). Table 5.9 compares the supero-inferior displacement values of the CL implants to the healthy model (6.38 mm).

Table 5.9 Supero-inferior displacement and max disp. mag of the vagina, during the VM, when impairments of 50%, 90%, and total rupture of the CLs occur with CLs implants - continuous line suture.

Variable		Supero-inferior disp. of the **vagina** (mm)	Max disp. mag of the **vagina** (mm)	Variation disp. of the vagina concerning the **healthy** (%)
Impairment 50%	**3Q**	6.37	7.76	(-) 0.16
	3S	6.56	7.99	2.82
Impairment 90%	**3Q**	7.00	8.43	9.72
	3S	7.05	8.60	10.50
Total Rupture	**3Q**	7.36	8.41	15.36
	3S	7.40	9.53	15.99

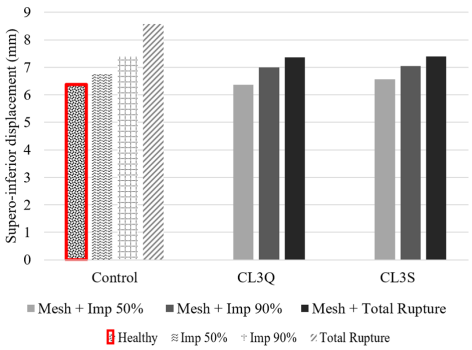

Figure 5.9 Representation of the supero-inferior displacements of the anterior vaginal wall in cases of total rupture of the ligaments as well as with 50 and 90% impairment with CLs implants - continuous line suture.

When analyzing Table 5.9, it's evident that the implant with square geometry exhibits lower displacement values, resembling those of the healthy model. This holds true for cases of total ligament rupture as well as 50% and 90% impairment. Interestingly, in the case of 50% impairment, the 3Q implant showcases even lower supero-inferior displacement values compared to the healthy ligaments.

5.2.2.2 Fixation with Simple Stitch Suture

Simple Stitch Suture - USL Implants

Different fixation methods can result in variations in the behavior of the implants. As a result, the encastre in USLs implants was modified to one with only 8 elements, as shown in Chapter 4 - Figure 4.23.

Anterior Vaginal Wall Supero-Inferior Displacement Analysis

Table 5.10 and Figure 5.10 present the study results on supero-inferior displacement from Chapter 4 - Figure 4.20. The control group includes supero-inferior displacement for the healthy model (6.38 mm), 50% USL impairment (7.03 mm), 90% USL impairment (8.91 mm), and total USL rupture (10.77 mm). Table 5.10 compares the supero-inferior displacement variations of USL implants to the healthy model (6.38 mm).

Table 5.10 Analysis of supero-inferior displacements and respective maximum displacement magnitudes in the anterior wall of the vagina with impairment of 50%, 90% and total rupture of USLs - simple stitch suture.

Variable		Supero-inferior disp. of the **vagina** (mm)	Max disp. mag of the **vagina** (mm)	Variation disp. of the vagina concerning the **healthy** (%)
Impairment 50%	**1Q**	6.35	7.72	(-) 0.47
	1S	6.4	7.77	0.31
	2.1	7.02	8.52	10.03
	2.2	7.03	8.53	10.19
	2.3	6.91	8.42	8.31
	2.4	7.03	8.52	10.19
Impairment 90%	**1Q**	6.58	8.91	3.13
	1S	7.10	9.05	11.29
	2.1	8.86	9.97	38.87
	2.2	8.90	9.98	39.50
	2.3	8.76	9.92	37.30
	2.4	8.88	10.05	39.18
Total Rupture	**1Q**	10.34	11.91	62.07
	1S	10.45	12.26	62.23
	2.1	10.74	12.67	68.34
	2.2	10.76	12.71	68.65
	2.3	9.35	11.14	46.55
	2.4	9.79	11.58	53.45

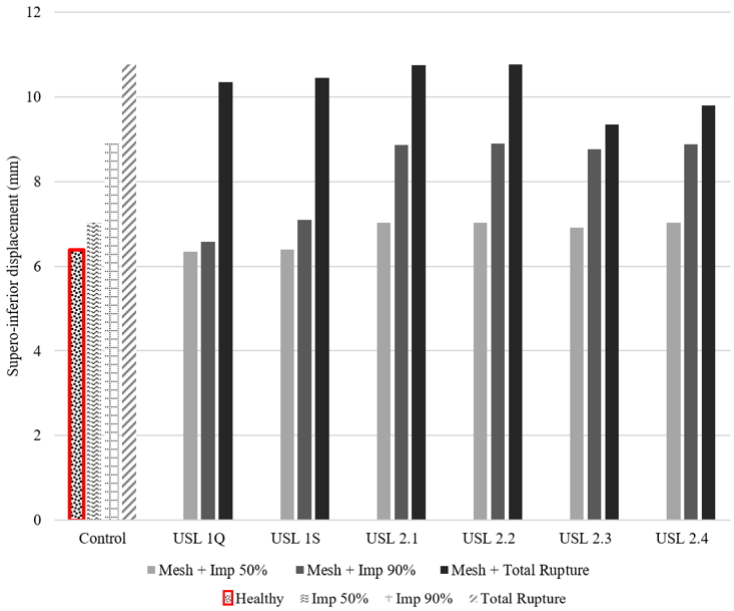

Figure 5.10 Representation of the supero-inferior displacements of the anterior vaginal wall in cases of total rupture of the ligaments as well as with 50 and 90% impairment with USLs implants - simple stitch suture.

In Table 5.10, Model 1Q has significantly lower displacement values, similar to the healthy model, particularly when the ligament impairment is at 50% and 90%. However, in cases of total rupture, implant 2.3 demonstrates values closest to the healthy model. The results for implants 2.1 and 2.2 differ the most from those of the healthy model. This was expected as these implants are meant to support the USL, and in cases of complete USL rupture, they are not effective. Instead, implants 2.3 and 2.4 were used in such cases. In cases of 50% impairment, these results indicate that the implants can be essential in supporting the uterus due to their minimal variation compared to the healthy model.

Simple Stitch Suture - CL Implants

Variations in fixation types for the implants alter their behavior. Consequently, the encastre type in Model 3 was modified to include only 8 elements, as illustrated in Capther 4 - Figure 4.23.

Anterior Vaginal Wall Supero-Inferior Displacement Analysis

Table 5.11 presents the study's results on supero-inferior displacement in the region specified in Chapter 4 - Figure 4.20. In this analysis, Figure 5.11 shows the results for the supero-inferior displacement of the healthy model (6.38 mm) and different levels of impairment of the CL implants: 50% impairment (6.74 mm), 90% impairment (7.40 mm), and total rupture (8.58 mm). In

Table 5.11, the supero-inferior displacement values of the CL implants are compared to the healthy model's 6.38 mm measurement.

Table 5.11 Supero-inferior displacement and max disp. mag of the vagina, during the VM, when impairments of 50%, 90%, and total rupture of the CLs occur with CLs implants - simple stitch suture.

Variable		Supero-inferior disp. of the **vagina** (mm)	Max disp. mag of the **vagina** (mm)	Variation disp. of the vagina concerning the **healthy** (%)
Impairment 50%	**3Q**	6.37	7.76	(-) 0.16
	3S	6.56	7.99	2.82
Impairment 90%	**3Q**	7.08	8.61	10.97
	3S	7.18	8.98	12.54
Total Rupture	**3Q**	7.98	9.70	25.08
	3S	8.35	9.98	30.88

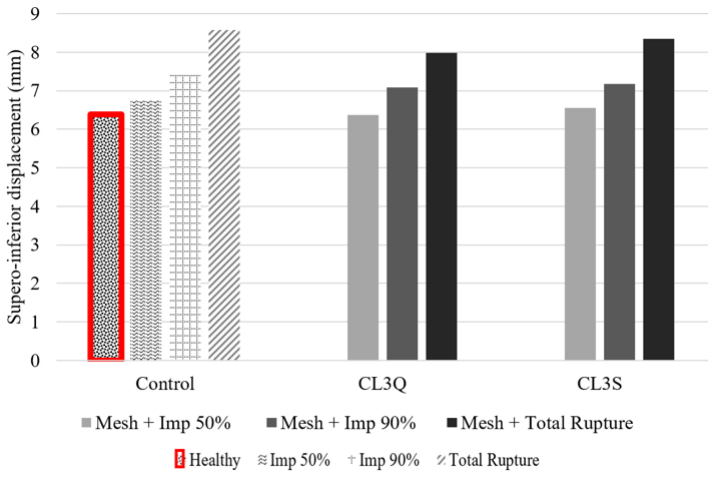

Figure 5.11 Representation of the supero-inferior displacements of the anterior vaginal wall in cases of total rupture of the ligaments as well as with 50 and 90% impairment with CLs implants - simple stitch suture.

In Table 5.11, it is evident that the 3Q implant has much lower displacement values, which are closer to those of the healthy model. This pattern was also seen in previous cases with a band of elements and continuous suture. However, the values recorded by the 3S implant are very similar. This trend holds true for both partial and total ligament rupture. Notably, in the case of 50% impairment, the 3Q implant shows even lower displacement than healthy ligaments.

5.2.2.3 Fixation with Horizontal Interrupted Suture

Horizontal Interrupted Suture - USL Implants

Tests were repeated to mimic the interrupted suture fixation depicted in Chapter 4 - Figure 4.23.

Anterior Vaginal Wall Supero-Inferior Displacement Analysis

Table 5.12 and Figure 5.12 present the results for the supero-inferior displacement in the area indicated in Chapter 4 - Figure 4.20. As previously noted, the control group in Figure 5.12 includes the results for the supero-inferior displacement of the models without implants, as shown in Table 5.1. Table 5.12 details the variations in supero-inferior displacement values of the USL implants compared to the healthy model, which has a displacement of 6.38 mm.

Table 5.12 Analysis of supero-inferior displacements and respective maximum displacement magnitudes in the anterior wall of the vagina with impairment of 50%, 90% and total rupture of USLs - horizontal interrupted suture.

Variable		Supero-inferior disp. of the **vagina** (mm)	Max disp. mag of the **vagina** (mm)	Variation disp. of the vagina concerning the **healthy** (%)
Impairment 50%	**1Q**	5.43	6.80	6.58
	1S	6.41	7.84	0.47
	2.1	7.02	8.52	10.03
	2.2	7.03	8.53	10.19
	2.3	6.86	8.37	7.52
	2.4	7.03	8.52	10.19
Impairment 90%	**1Q**	6.02	7.48	(-) 5.64
	1S	7.45	8.86	16.77
	2.1	8.11	9.73	27.12
	2.2	8.12	9.74	27.27
	2.3	7.97	9.55	24.92
	2.4	8.12	9.76	27.27
Total Rupture	**1Q**	6.74	7.67	5.64
	1S	7.78	8.10	21.94
	2.1	10.58	12.52	65.83
	2.2	10.77	12.71	68.81
	2.3	9.15	10.94	43.42
	2.4	9.78	11.57	53.29

In Table 5.12, the implants in Model 1Q exhibit supero-inferior displacement values that are closer to the healthy model in cases of partial and total impairment of the USL. This similarity has been observed when compared to other fixation methods. The supero-inferior displacement values observed by the 1S Model are also low and close to healthy, especially in cases of 50% impairment. Implants 2.1 and 2.2 demonstrate the most pronounced deviation from the healthy model. Nevertheless, these outcomes were anticipated in instances of total USL rupture, given that these implants were specifically designed to provide support to the USL following impairment.

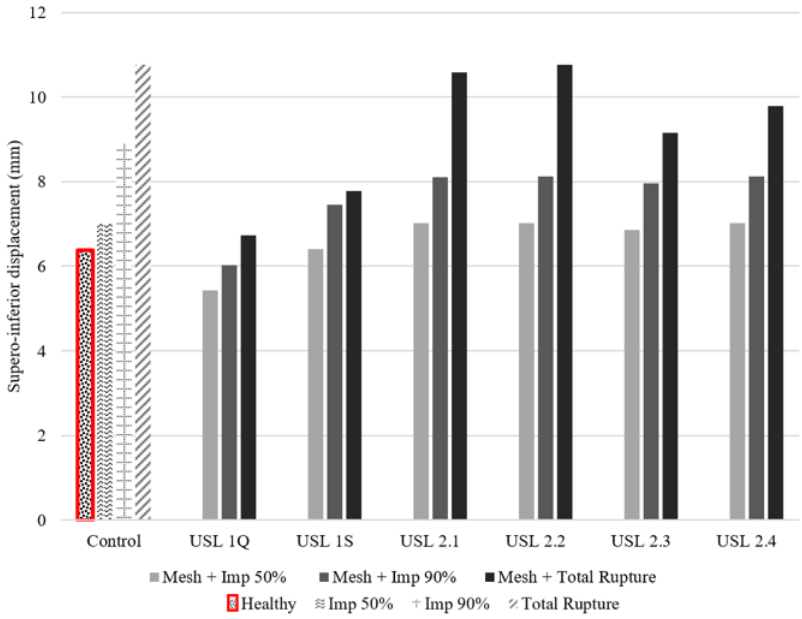

Figure 5.12 Representation of the supero-inferior displacements of the anterior vaginal wall in cases of total rupture of the ligaments as well as with 50 and 90% impairment with USLs implants with continuous line suture - horizontal interrupted suture.

Horizontal Interrupted Suture - CL Implants

Variations in boundary conditions for the implants can influence their behavior. Consequently, the encastre in Model 3 was modified to incorporate horizontal interrupted suture fixation, as illustrated in Chapter 4 - Figure 4.23.

Anterior Vaginal Wall Supero-Inferior Displacement Analysis

Table 5.13 and Figure 5.13 present the results of the study on supero-inferior displacement in the region specified in Chapter 4 - Figure 4.20. In Figure 5.13, the control group illustrates the supero-inferior displacement for the healthy model (6.38 mm) and varying degrees of CL impairment: 50% (6.74 mm), 90% (7.40 mm), and total rupture (8.58 mm). Table 5.13 compares the variation in supero-inferior displacement values of the CL implants to the healthy model (6.38 mm).

From the analysis of Table 5.13 and Figure 5.13, it is clear that the implant with square geometry has supero-inferior displacement values that closely match those of the healthy model, especially in scenarios of total ligament rupture and 50% and 90% impairments. The sinusoidal geometry also shows similar values. Notably, in the 50% impairment case, the 3Q implant exhibits a supero-inferior displacement even lower than that of the healthy ligaments.

Table 5.13 Supero-inferior displacement and max disp. mag of the vagina, during the VM, when impairments of 50%, 90%, and total rupture of the CLs occur with CLs implants - horizontal interrupted suture.

Variable		Supero-inferior disp. of the vagina (mm)	Max disp. mag of the vagina (mm)	Variation disp. of the vagina concerning the healthy (%)
Impairment 50%	**3Q**	6.37	7.76	(-) 0.16
	3S	6.56	7.99	2.82
Impairment 90%	**3Q**	6.88	8.41	7.84
	3S	7.28	8.81	14.11
Total Rupture	**3Q**	7.47	9.17	17.08
	3S	7.88	9.83	23.51

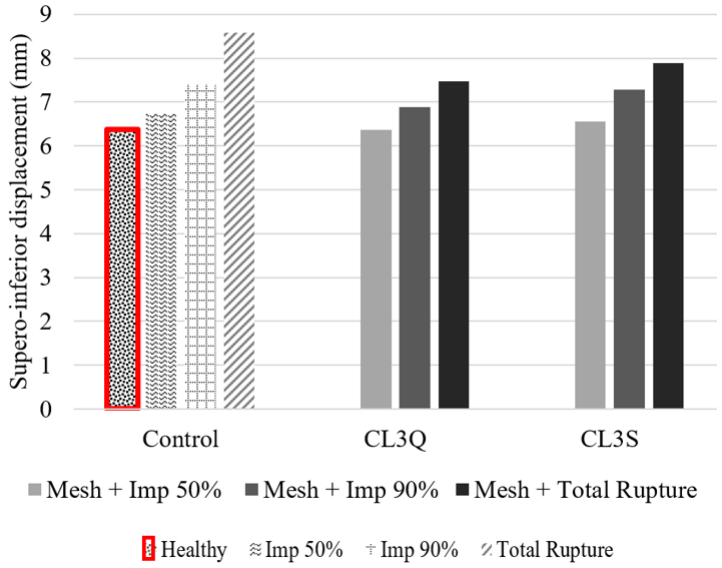

Figure 5.13 Representation of the supero-inferior displacements of the anterior vaginal wall in cases of total rupture of the ligaments as well as with 50 and 90% impairment with CLs implants - horizontal interrupted suture.

5.2.3 Stress Concentration Analysis

Figures 5.14, 5.15, 5.16, and 5.17 display the stress concentration experienced by Model 1 implants under various impairment scenarios (50%, 90% and total rupture). These figures allow for a comparison between the two selected configurations and enable an analysis of the different types of fixation.

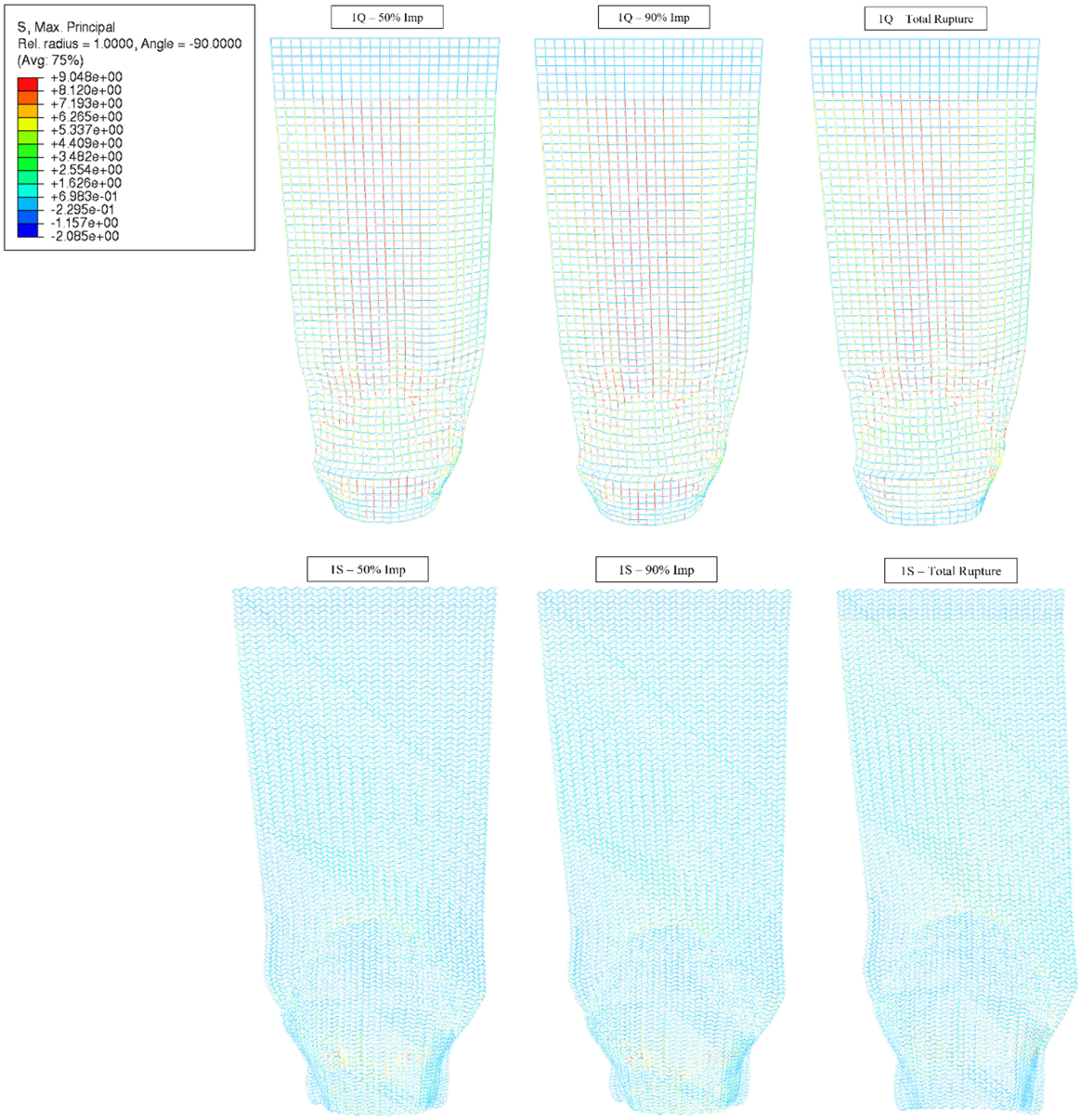

Figure 5.14 Stress Concentration - Model 1 - A band of elements encastre.

In Figure 5.14, it is demonstrated that when the implant is fixed with a band of elements, in the 1Q implant, tension is evenly distributed across the center of the mesh in all cases. However, observing areas of high tension in the sinusoidal configuration is difficult because they are less pronounced, but the areas around the uterus are where the highest values are observed.

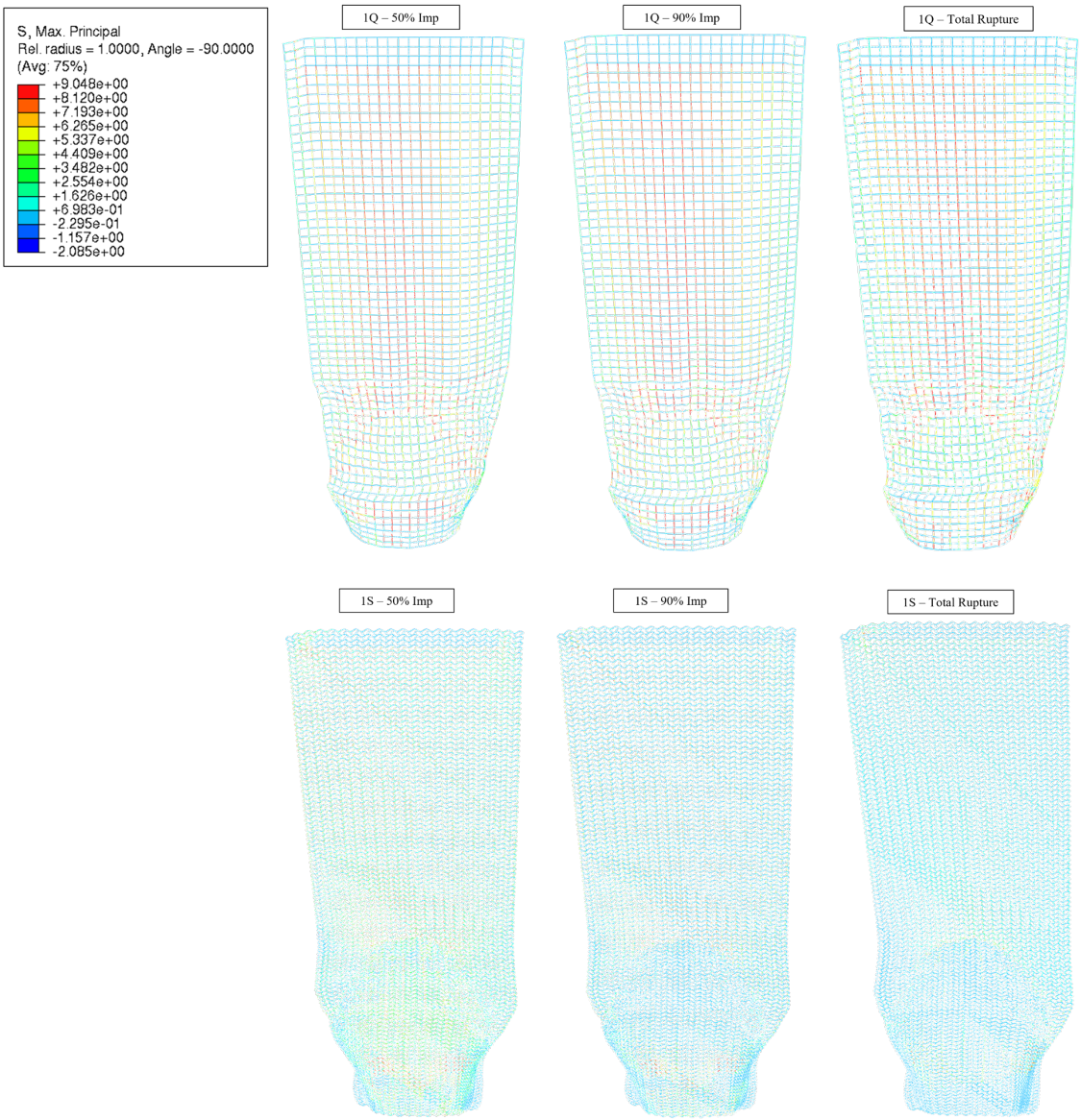

Figure 5.15 Stress Concentration - Model 1 - Continuous Line.

Based on the analysis shown in Figure 5.15, when the implant is fixed with a continuous line in a square configuration, the stress concentration is along the center of the mesh, similar to what was reported with the element band encastre. In the sinusoidal configuration, the highest values are felt in the area around the uterus, although much less obvious.

In Figure 5.16, it is evident that when the implants in Model 1 are fixed with a simple stitch, there is a different stress concentration compared to the previous fixing methods. In both the square and sinusoidal configurations, the highest stress areas are located around the embedded elements and in the area that comes into contact with the uterus.

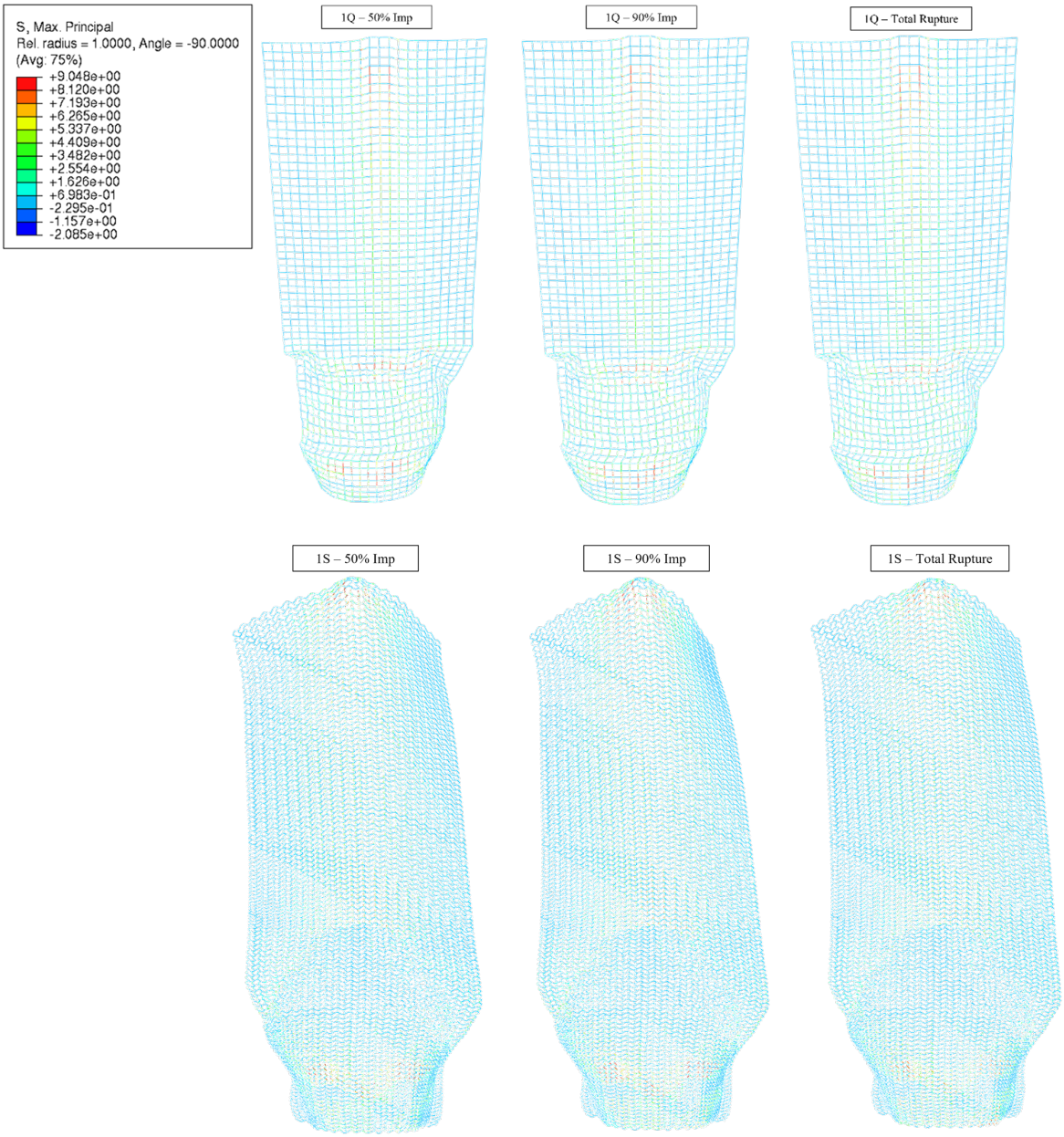

Figure 5.16 Stress Concentration - Model 1 - Simple Stitch.

In Figure 5.17, it is possible to observe that, similar to the continuous and band fixation methods, when the implant is secured with a horizontal interrupted suture, the highest tension area in the square configuration is located at the center of the implant. In contrast, the highest concentration values are observed around the uterus in the sinusoidal configuration, although they are significantly less pronounced.

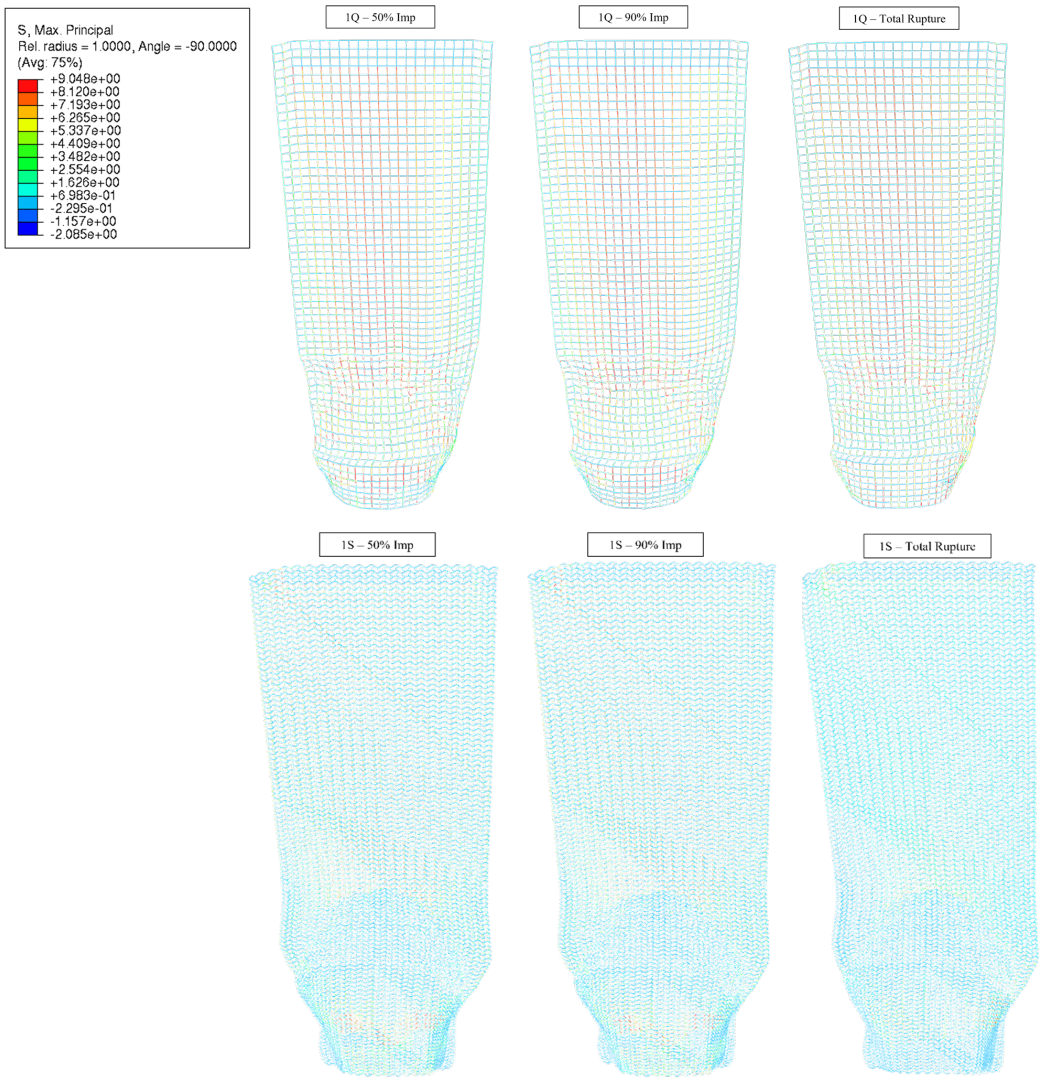

Figure 5.17 Stress Concentration - Model 1 - Horizontal Interrupted Suture.

Figures 5.18 and 5.19 show the stress concentration experienced by Model 3 implants under different impairment scenarios (50%, 90%, and total rupture). A comparison between the two selected configurations can be made using these figures.

The stress concentration was analyzed for various types of fastening. However, Figures 5.18 and 5.19 only pertain to the encastre of a band of elements because the values turned out to be practically the same when using different types.

For both the square and sinusoidal configurations, the highest stress zone is in the region in contact with the uterus. Furthermore, similar to Model 1Q and 1S, there are no significant differences across the various cases (50%, 90%, and total rupture).

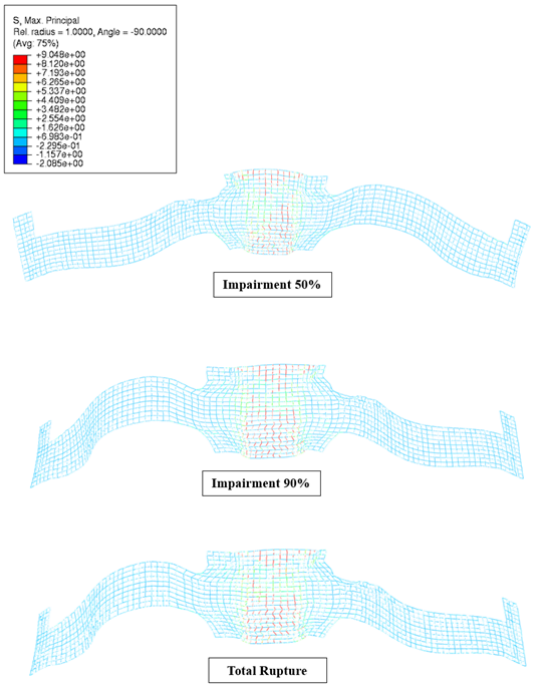

Figure 5.18 Stress Concentration - Model 3Q - A band of elements encastre.

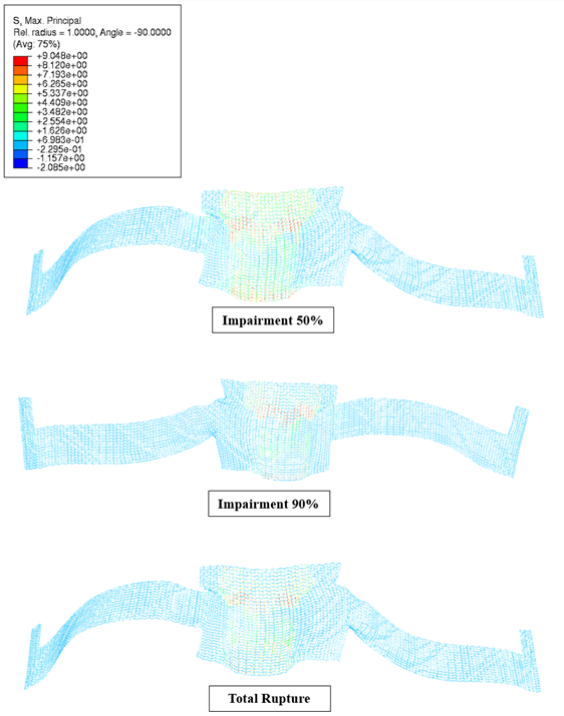

Figure 5.19 Stress Concentration - Model 3S - A band of elements encastre.

Chapter 6

Discussion

POP is a common chronic disorder in women, affecting the quality of life of millions worldwide. Surgical therapy using vaginal meshes or native tissues has encountered adverse effects post-procedure, and currently, there is no optimal solution for prolapse repair surgery [71].

This study aimed to advance research and use biodegradable meshes with properties associated with PCL polymer. The primary objective was to investigate the performance of porous biodegradable implants under Valsalva pressure in a pelvic cavity model, building upon previous research in the field.

The supero-inferior displacement of the anterior vaginal wall varies when comparing partial impairment (50% and 90%) and complete rupture of the USL and CL with a healthy model. Essentially, when the USL and CL are completely ruptured, there is an increase in this displacement of 4.39 mm and 2.2 mm, respectively, compared to the healthy model, which is why it is greater in cases of total rupture. These findings are consistent with the research of Chen et al. 2006, which indicates that the extent of impairment directly correlates with the degree of prolapse [109].

In the available literature, no studies have been found on using biodegradable meshes to repair POP. However, according to Röhrnbauer et al. 2017, a technique involving aspiration was used to measure tissue displacement of the anterior vaginal wall. The clinical results indicated that the tissue displacement, as well as the initial displacement, were smaller after surgery to repair POP [110].

In this study, the inclusion of various implants designed to mimic the USL and CL resulted in a reduced supero-inferior displacement of the vaginal wall compared to the control model, which had no implants, as well as compared to models with partial and total impairment.

In the context of USL, the findings suggest that the use of implants leads to reduced descent of the anterior vaginal wall, resulting in increased support for the uterus.

When there was a 50% impairment in the USL, the vaginal canal showed a displacement of 7.03 mm. After applying Model 1 implants, there was a 24.32% decrease in displacement for Model 1Q and a 11.52% decrease for Model 1S, compared to the mentioned displacement. Upon implanting Model 2 implants, there was a less pronounced decrease of 0.28%, 0.71%, 2.84%, and 0.14% for Models 2.1, 2.2, 2.3, and 2.4, respectively.

With 90% impairment in the USL, there was a supero-inferior displacement of the vaginal canal of 8.91 mm. When the Model 1Q and 1S implants were implanted, there was a 33% and 14.81% reduction, respectively, in the mentioned displacement. With the implantation of Model 2, there was also a reduction in the supero-inferior displacement. However, as with the 50% impairment, this variation was less pronounced, 0.22%, 4.26%, 8.75%, and 0.34% with the Models 2.1, 2.2, 2.3, and 2.4, respectively.

In cases of complete rupture of USL, there was a 10.77 mm superior-inferior displacement of the vaginal canal. When Model 1Q and 1S implants were used, there was a 34.91% and 13.74% reduction in this displacement. With the implantation of Model 2, there was also a reduction in the superior-inferior displacement. The reduction was less noticeable than with Model 1 but more noticeable than with partial impairment, with reductions of 34.91%, 13.74%, 2.41%, 9.94%, and 2.51% in relation to Models 2.1, 2.2, 2.3, and 2.4, respectively.

The results from the CL show that when implants are used, there is less descent of the vaginal canal. For instance, in cases of 50% impairment in the CL, the vaginal canal experienced a supero-inferior displacement of 6.74 mm. This value decreased by 5.49% and 2.52% with the 3Q and 3S implants, respectively. In cases of 90% impairment, the displacement was 7.40 mm and with the 3Q and 3S implants, this value decreased by 5.41% and 4.73%, respectively. In cases of total CL rupture, the displacement of the vaginal canal of 7.48 mm decreased by around 16.32% and 13.52% with the incorporation of the 3Q and 3S implants, respectively.

However, this ligament plays more of a stabilizing role in the uterus than a supporting one. It was expected that this displacement would not be so influenced by the insertion of the implants.

In the analysis of the supero-inferior displacement recorded on the implants, it was observed that while the values associated with the sinusoidal configuration were in closer proximity to those of the healthy implants, the square configuration adopted in Models 1 and 3 exhibited even lower values. This observation suggests that these implants demonstrate the capacity to provide greater stabilization under traction.

After applying a constant 90% impairment to the USL and conducting tests with implants in cases of impairment and total rupture of the CLs, it was found that the supero-inferior displacement increased by approximately 2 mm compared to cases with only damage to the CLs. However, the supero-inferior displacement value of the vaginal canal with 90% impairment to the USL and total rupture of the CL was 12.37, while the highest supero-inferior displacement value was 11.00. This indicates that the implant provided some support to the uterus.

In studying Model 2, we expected to see results that would reduce the supero-inferior displacement of the anterior vaginal wall, essentially providing more support for the uterus. However, this wasn't the case. We noticed irregular behavior and differences between the two meshes when we looked at the resulting U-vectors. For example, in implant 2.1, there were even vectors pointing upwards, which is opposite to what we would expect. Model 1, however, exhibits more stable behavior.

In the scenarios mentioned above, implants with a square shape demonstrated lower supero-inferior displacement values. This is because the square configuration is more rigid when under

tension, and the vertical fibers resist the force from the beginning. On the other hand, implants with a sinusoidal shape experience an initial stretching phase when force is applied, and maximum fiber resistance occurs later.

Previous studies by Vaz, 2023 have shown that the sinusoidal mesh behaves more similarly to vaginal tissue, in contrast to the square mesh which shows a significant difference [101]. This study is in line with the results obtained because in the study, the results were compared with vaginal tissue, and the behavior of the sinusoidal mesh is closer to the tissue, so it won't be able to support as much as the square mesh. However, the meshes developed should not be compared to vaginal tissue but rather to the supporting structures, which in this case are the ligaments and which have a higher stiffness. The two mesh configurations being studied exhibit very different mechanical behaviors, and the optimal mesh could be an optimization of the sinusoidal and square mesh to mimic the ligament's behavior closely. In Chapter 4 - Figure 4.24, it's evident that the sinusoidal mesh initially moves closer to the ligament. Utilizing fibers with a lower amplitude in the sinusoidal mesh will result in a stiffer behavior, which is desirable for mimicking the behavior of the ligament, as demonstrated by Sterk, 2023. [111].

Considering the same mesh geometry using Restorelle® and biodegradable properties, the Restorelle® properties are much stiffer than the biodegradable ones. It could be inferred that using a Restorelle® mesh would lead to better performance in terms of supporting the uterus. However, because it is more stiffer and has a twisting behavior, which makes it even more stiffer, and results in many complications related to the graft, unlike biodegradable meshes. In addition, the non-biodegradable nature of these meshes exacerbates the problem. Unlike biodegradable meshes, which, even though they are rigid, degrade over time [25]. Chen et al. 2023, proved that absorbable sutures reduce the risk of complications such as infections and erosions when compared to permanent sutures [112].

In the clinic, the surgeon may not be able to determine the number of elements fixed in the type of embedment initially used. Therefore, a more realistic analysis was conducted, and three different types of fixation were selected: continuous, simple, and interrupted. Although the choice of suture used in the surgical repair of apical prolapse, according to Pollack et al., has traditionally been based on institutional and personal preferences rather than data, more research has been conducted to inform these clinical decisions better [113]. It has been observed that different types of sutures can result in different surgical outcomes, particularly the integration of tissue with the implant material. According to Raalte et al, precise and reliable fixation is crucial for positive surgical outcomes, and various suturing and anchoring devices have been introduced over the years to facilitate precise and reliable fixation [114].

When the fixation was used with a continuous encastre, the supero-inferior displacement values were higher than those obtained with a band of elements encastre, although the difference was small. These results were expected, as when the fixation area is reduced, the implants have more freedom to move.

With a 50% impairment in the USL, there was a 7.03 mm supero-inferior displacement of the anterior vaginal wall. However, when the implants with continuous encastre were applied in Model

1, there was a reduction of 22.76% and 8.96% in Model 1Q and 1S, respectively, compared to the mentioned displacement. With the implantation of Model 2 implants, there was also a decrease, though less pronounced, of 0.14%, 0.57%, 2.42%, and 0% in relation to Models 2.1, 2.2, 2.3, and 2.4, respectively.

For cases of 90% impairment of the USL, there was an 8.91 mm supero-inferior displacement of the anterior vaginal wall. When using continuous encastre implants in Model 1Q and 1S, there was a 31.54% and 12.46% reduction, respectively, in the displacement mentioned above. With the implantation of Model 2, there was also a reduction in the displacement, with reductions of 0.11%, 0.45%, 2.36%, and 0.11% in relation to Models 2.1, 2.2, 2.3, and 2.4 respectively.

In cases of total rupture of the USL, there was a 10.77 mm supero-inferior displacement of the anterior vaginal wall. When Model 1Q and 1S implants were used, there was a 34.08% and 6.22% reduction, respectively in this displacement. With the implantation of Model 2, there was also a reduction in the supero-inferior displacement, which was less pronounced than with Model 1Q, but more noticeable than in cases of partial impairment, with reductions of 0.84%, 4.09%, 15.04%, and 9.19% in relation to Models 2.1, 2.2, 2.3, and 2.4 respectively.

When using simple encastre fixing, the supero-inferior displacement values are higher than those obtained with continuous encastre. These results align with the findings in the literature. In a study by Silva et al. 2021, comparing these two types of sutures while maintaining all other factors constant, variations of around 10% were observed [25].

In this study, a 50% impairment in the USL resulted in a supero-inferior displacement of the anterior vaginal wall by 7.03 mm. When Model 1 implants were used with simple encastre, there was a reduction of 9.67% and 8.96% in Model 1Q and 1S, respectively, compared to the mentioned displacement. The implantation of Model 2 implants also showed a decrease, with reductions of 0.14%, 0%, 1.71%, and 0% in Models 2.1, 2.2, 2.3, and 2.4, respectively. When comparing simple suture with continuous suture, the maximum variation in the implants of Models 1 and 2 was 16.94%, which corresponds to Implant 1Q.

In cases of 90% USL impairment, the supero-inferior displacement of the anterior vaginal wall was 8.91 mm. The use of implants with a simple fixation in Model 1Q and 1S resulted in reductions of 26.15% and 20.31%, respectively, in the mentioned displacement. With Model 2 implants, there was a reduction of 0.56%, 0.11%, 1.68%, and 0.34% in Models 2.1, 2.2, 2.3, and 2.4 respectively. When comparing the simple suture with the continuous suture, the maximum variation in Models 1 and 2 implants was 8.97%, corresponding to Implant 1S.

In cases of a total rupture of the USL, there was a 10.77 mm supero-inferior displacement of the anterior vaginal wall. When a simple suture was applied to the Model 1Q and 1S implants, there was a 3.99% and 2.97% reduction, respectively, in this displacement. When Model 2 implants were used, there was a reduction in the displacement of 0.27%, 0.09%, 13.18%, and 9.09%, in relation to Models 2.1, 2.2, 2.3, and 2.4, respectively. Comparing the simple suture with the continuous suture, the maximum variation in the implants of Models 1 and 2 is 45.63%, and this corresponds to Implant 1Q.

When using fixation with an interrupted horizontal encastre, the supero-inferior displacement values are very similar to those obtained with the continuous encastre. These results were interesting because they showed that even with fewer sutured nodes, it is possible to obtain equally good fixation.

In this study, when there was a 50% impairment in the USL, the anterior vaginal wall experienced a supero-inferior displacement of 7.03 mm. However, when implants with interrupted horizontal encastre were used, there was a 22.76% and 8.82% decrease in Model 1Q and 1S respectively, compared to the mentioned displacement. With the implantation of Model 2 implants, there was also a decrease, although less pronounced, of 0.14%, 0%, 2.42%, and 0% in Models 2.1, 2.2, 2.3, and 2.4, respectively. Comparing the interrupted horizontal suture to the continuous suture, the maximum variation in Model 1 and 2 implants is 0.57% and corresponds to Implant 2.2.

In cases of 90% USL impairment, the anterior vaginal wall experienced a supero-inferior displacement of 8.91 mm. When implants with a interruped encastre were used in Model 1Q and 1S, there was a 26.15% and 20.31% reduction, respectively, in the displacement mentioned. With the implantation of Model 2, there was also a reduction in the supero-inferior displacement of 0.56%, 0.11%, 1.68%, and 0.34% in Models 2.1, 2.2, 2.3, and 2.4, respectively. Comparing the interrupted horizontal suture with the continuous suture, the maximum variation in Model 1 and 2 implants is 8.88% and corresponds to Implant 2.1.

In cases of total rupture of USL, there was a 10.77 mm superior-inferior displacement of the anterior vaginal wall. However, when an interrupted horizontal encastre was applied to the Model 1Q and 1S, there was a 37.42% and 27.76% reduction, respectively, in this displacement. With the implantation of Model 2, there was also a reduction in the superior-inferior displacement of 3.62%, 0%, 15.04%, and 9.04% in Models 2.1, 2.2, 2.3, and 2.4, respectively. Comparing the single suture with the continuous suture, the maximum variation in the Model 1 and 2 implants is 22.97% and corresponds to Implant 1S.

When it comes to implants that mimic the CL the values obtained with different types of fixation did not vary significantly. This is expected because these ligaments are subject to compression, so the method of fixation has minimal impact on the supero-inferior displacement achieved.

There is a scarcity of information on the type of suture used in prolapse correction surgeries. The surgical techniques used to repair POP with native tissue and implants vary from surgeon to surgeon. According to Meyer et al., differences in the anchoring sites of the vaginal apex can impact surgical results over time. Therefore, we believe that the results of the present study demonstrate the importance of the mesh anchoring technique as a crucial point for improving the results of prolapse surgery [115]. However, more studies need to be carried out to prove these results.

Through an analysis of stress concentration, it is evident that the square shape exhibits a larger area of red coloration due to a more even tension distribution. Consequently, the fibers are brought to rupture almost uniformly and simultaneously. This is in contrast to the behavior of the sinusoidal shape, which deviates from this pattern due to its unique geometry.

During this study, the use of a pelvic cavity model was restricted by certain limitations, such as the absence of the sacrum. Furthermore, the pelvic cavity model represents a healthy woman but has been modified to simulate a woman with apical prolapse (specifically involving the USL and CL with ruptures and impairments). However, it is suggested that with prolapse, other structures such as the muscles, which were presumed healthy in this study, may also be affected.

The sinusoidal mesh pore is positioned diagonally and may not have been adequately accounted for. Furthermore, there is a percentage difference in density between the various meshes, limiting the comparability and applicability of the results.

Chapter 7

Conclusions and Future Work

7.1 Conclusions

Presently, POP significantly impacts the quality of life for a substantial number of women globally. In Portugal, the prevalence of this condition is anticipated to escalate by 40% over the next 40 years. Unfortunately, severe cases of POP are compounded by the absence of effective treatment modalities, notably due to the substantial drawbacks associated with synthetic meshes, such as tissue erosion, pain, and discomfort. These issues have prompted the FDA to prohibit the commercialization and dissemination of synthetic meshes for transvaginal prolapse treatment. Furthermore, reoperation is necessitated in 30% of surgical instances.

The investigation presented herein delved into the advancement of diverse computational models of biodegradable implants for POP repair utilizing Abaqus® software. The findings, which focused on the analysis of supero-inferior displacement, revealed that a mesh featuring a square configuration, when integrated into a computational model of the pelvic cavity, yielded lower displacement compared to other geometric configurations. This finding implies greater effectiveness in simulating the USLs and CLs. Furthermore, the study underscored the significance of fixation techniques, singling out continuous sutures as the most optimal method.

One limitation that should be considered is the discrepancy in the density of the two configurations, which may have impacted the results. This suggests the necessity for additional research.

Future studies should aim to investigate the synergistic effects of diverse mesh geometries on pelvic organ support enhancement. Moreover, computational modeling must be advanced by integrating all pertinent anatomical considerations and physiological parameters to further enrich our understanding in this area.

In practical terms, biodegradable meshes demonstrate significant potential for enhancing surgical outcomes and mitigating complications such as chronic pain and erosion. The implementation of more streamlined fixation techniques could further augment the efficacy of prolapse repairs utilizing these novel meshes.

In conclusion, this study's results add to the increasing evidence backing the use of biodegradable meshes in POP surgery. Addressing current limitations and conducting further research can

enhance treatment options and improve outcomes for women with this condition.

7.2 Further Work

It would be interesting to test different ideas in the future to create a mesh that better mimics the USLs and CLs.

- Develop meshes that incorporate both the sinusoidal and square meshes;
- Study other fixation techniques that can lead to better results;
- Develop implant models by varying the filament thickness;
- Evaluate the performance of the implants using a more accurate and detailed model of the pelvic cavity;
- Create a model of a patient with prolapse, considering that the current one is designed for a healthy woman and needs to be adapted for a woman with apical prolapse;
- As POP and SUI are often closely associated and the two dysfunctions can occur simultaneously, it would be interesting to study and develop computational models capable of mimicking the pubourethral ligaments.

References

[1] Rocío Adriana Peinado-Molina, Antonio Hernández-Martínez, Sergio Martínez-Vázquez, Julián Rodríguez-Almagro, and Juan Miguel Martínez-Galiano. Pelvic floor dysfunction: prevalence and associated factors. *BMC Public Health*, 23, 12 2023. ISSN 14712458. doi: 10.1186/s12889-023-16901-3.

[2] Coloplast. Pelvic organ prolapse (pop) - a patient guide, 2018. URL https://www.femalepelvicsolutions.com/wp-content/uploads/2020/11/USUC_POP-Education-PM-02911.pdf. Accessed: 2024-06-22.

[3] Adwoa Baah-Dwomoh and Raffaella De Vita. Effects of repeated biaxial loads on the creep properties of cardinal ligaments. *Journal of the Mechanical Behavior of Biomedical Materials*, 74:128–141, 10 2017. ISSN 18780180. doi: 10.1016/j.jmbbm.2017.05.038.

[4] João Ferreira. Biomecânica: Combinar engenharia e experiência clínica para melhorar o tratamento do prolapso de órgãos pélvicos femininos, 5 2020. URL https://www.inegi.pt/pt/noticias/biomecanica-combinar-engenharia-e-experiencia-clinica-para-/melhorar-o-tratamento-do-prolapso-de-orgaos-pelvicos-femininos. Accessed: 2024-06-20.

[5] Abdul Hakeem Jokhio, Raheela Mohsin Rizvi, and Christine MacArthur. Prevalence of pelvic organ prolapse in women, associated factors and impact on quality of life in rural pakistan: Population-based study. *BMC Women's Health*, 20, 4 2020. ISSN 14726874. doi: 10.1186/s12905-020-00934-6.

[6] Maria Elisabete Teixeira da Silva, Jorge Nuno Machado Bessa, Rita Rynkevic, Marco Paulo Lages Parente, Maria Teresa da Quinta Costa Mascarenhas Saraiva, Renato Manuel Natal Jorge, and António Augusto Fernandes. Simulation of vaginal uterosacral ligament suspension damage, mimicking a mesh-augmented apical prolapse repair. *Proceedings of the Institution of Mechanical Engineers, Part H: Journal of Engineering in Medicine*, 236:573–582, 4 2022. ISSN 20413033. doi: 10.1177/09544119221074567.

[7] Saya Segal, Lily A. Arya, and Ariana L. Smith. Functional outcomes for incontinence and prolapse surgery. *Current Bladder Dysfunction Reports*, 7:179–186, 9 2012. ISSN 19317220. doi: 10.1007/s11884-012-0136-9.

[8] Shagnik Ray, Marisa M. Clifton, and Kevin Koo. Inaccuracies in news media reporting about the 2019 us food and drug administration ban on transvaginal mesh for pelvic organ prolapse repair. *Urology*, 150:194–200, 4 2021. ISSN 15279995. doi: 10.1016/j.urology.2020.05.009.

[9] K. L. Shek, V. Wong, J. Lee, A. Rosamilia, A. J. Rane, H. Krause, J. Goh, and H. P. Dietz. Anterior compartment mesh: A descriptive study of mesh anchoring failure. *Ultrasound in Obstetrics and Gynecology*, 42:699–704, 12 2013. ISSN 09607692. doi: 10.1002/uog.12577.

[10] Megan Schimpf and Paul Tulikangas. Evolution of the female pelvis and relationships to pelvic organ prolapse. *International Urogynecology Journal*, 16:315–320, 2005. ISSN 09373462. doi: 10.1007/s00192-004-1258-1.

[11] Mélanie Roch, Nathaly Gaudreault, Marie Pierre Cyr, Gabriel Venne, Nathalie J. Bureau, and Mélanie Morin. The female pelvic floor fascia anatomy: A systematic search and review. *Life*, 11, 9 2021. ISSN 20751729. doi: 10.3390/life11090900.

[12] Sandip Vasavada, Rodney Appell, Peter Sand, and Shlomo Raz. *Female Urology, Urogynecology, and Voiding Dysfunction*. Springer, 2005.

[13] Khalid Chaudhry Shazia R. Chaudhry Ahmed Nahian. *Anatomy, Abdomen and Pelvis, Pelvis*. StatPearls, 2023.

[14] Snell S. Richard, M.R.C.S., L.R.C.P., M.B., B.S., and M.D. *Clinical Anatomy by Regions*. Lippincott Williams & Wilkins, 9 edition edition, 2011.

[15] Dr. Samanthi. Difference between pelvis and pelvic girdle, 8 2013. URL https://www.differencebetween.com/difference-between-pelvis-and-vs-pelvic-girdle/. Accessed: 2024-06-20.

[16] Adam W. M. Mitchell Richard Drake A. Wayne Vogl. *Gray's Anatomy for Students*. Elsevier, 2015.

[17] Maria Elisabete Teixeira Da Silva. *Evaluating the mechanical properties of biological soft tissues using inverse methods: application to the pelvic floor muscles*. PhD thesis, Faculty of Engineering, University of Porto, 2017.

[18] Micaela Isabel and Almeida Pinto. Melt electrowriting prototype optimization for medical-grade polycaprolactone mesh printing. Master's thesis, Faculty of Engineering, University of Porto, 2022.

[19] Sender Herschorn. Female pelvic floor anatomy: the pelvic floor, supporting structures, and pelvic organs. *REVIEWS IN UROLOGY*, 6, 2004.

[20] Rafaela Figueiredo Ferreira. Development of a computational tool to simulate the use of synthetic meshes for pelvic organ prolapse repair. Master's thesis, Faculty of Engineering, University of Porto, 2020.

[21] Maria Campos and Dulce Alves De Oliveira. Impacto biomecânico de um parto subsequente no pavimento pélvico feminino. Master's thesis, Faculty of Engineering, University of Porto, 2023.

[22] Peter Petros. *The Female Pelvic Floor - Function, Dysfunction and Management According to the Integral Theory - 3rd edition*. Springer, 2010.

[23] Gonçalo Henrique Lourenço Sá Rios. Biomechanical study of pelvic organ prolapse and correction under application of urogynecologic surgical meshes. Master's thesis, Faculty of Engineering - University of Porto, 2013.

[24] Brooks Rehabilitation Dr. Marie K. Bogh. What women need to know about their pelvic floor and how physical therapy can help, 12 2022. URL https://brooksrehab.org/blog/pelvic-floor-education/. Accessed: 2024-06-20.

[25] M. E.T. Silva, J. N.M. Bessa, M. P.L. Parente, T. Mascarenhas, R. M. Natal Jorge, and A. A. Fernandes. Effect of mesh anchoring technique in uterine prolapse repair surgery: A finite element analysis. *Journal of Biomechanics*, 127, 10 2021. ISSN 18732380. doi: 10.1016/j.jbiomech.2021.110649.

[26] Rocío Adriana Peinado Molina, Antonio Hernández Martínez, Sergio Martínez Vázquez, and Juan Miguel Martínez Galiano. Influence of pelvic floor disorders on quality of life in women. *Frontiers in Public Health*, 11, 2023. ISSN 22962565. doi: 10.3389/fpubh.2023.1180907.

[27] Alejandra M. Ruiz-Zapata, Andrew J. Feola, John Heesakkers, Petra de Graaf, Mija Blaganje, and Karl Dietrich Sievert. Biomechanical properties of the pelvic floor and its relation to pelvic floor disorders[figure presented]. *European Urology, Supplements*, 17:80–90, 4 2018. ISSN 18781500. doi: 10.1016/j.eursup.2017.12.002.

[28] Zahra Hadizadeh-Talasaz, Talat Khadivzadeh, Hossein Ebrahimipour, and Nayereh Khadem Ghaebi. The experiences of women who live with pelvic floor disorders: A qualitative study. *International Journal of Community Based Nursing and Midwifery*, 9:159–171, 4 2021. ISSN 23224835. doi: 10.30476/ijcbnm.2021.87275.1422.

[29] Stratton M. Grimes WR. *Pelvic Floor Dysfunction*. StatPearls Publishing, 2023. URL https://www.ncbi.nlm.nih.gov/books/NBK559246/. Accessed: 2024-06-20.

[30] Food and Drug Administration (FDA). Pelvic organ prolapse (pop), 2023. URL https://www.fda.gov/medical-devices/urogynecologic-surgical-mesh-implants/pelvic-organ-prolapse-pop. Accessed: 2024-06-20.

[31] Diogo Vilas Boas Rodrigues Pinheiro. Structure design optimisation of biodegradable implants for melt electrowriting. Master's thesis, Faculty of Engineering, University of Porto, 2022.

[32] Pamela Moalli and Shaniel Bowen. *Chapter 2 - Epidemiology & pathophysiology of pelvic organ prolapse & urinary incontinence in women*, pages 27–57. Biomechanics of Living Organs. Academic Press, 2023. doi: https://doi.org/10.1016/B978-0-12-823403-7.00013-0. URL https://www.sciencedirect.com/science/article/pii/B9780128234037000130.

[33] Persu Cristian. Pelvic organ prolapse quantification system (pop-q)-a new era in pelvic prolapse staging. *Journal of Medicine and Life*, 4:75–81, 2011.

[34] Evelin Maza Stanley Oiseth Lindsay Jones. Achieve mastery of medical concepts - pelvic organ prolapse (lecturio medical), 1 2024. URL https://www.lecturio.com/concepts/pelvic-organ-prolapse/. Accessed: 2024-06-20.

[35] Gleneagles Hospital Singapore. Pelvic organ prolapse (pop). URL https://www.gleneagles.com.sg/conditions-diseases/pelvic-organ-prolapse/symptoms-causes. Accessed: 2024-06-20.

[36] Cleveland Clinic. Pelvic organ prolapse, 2023. URL https://my.clevelandclinic.org/health/diseases/24046-pelvic-organ-prolapse.

[37] Jennie Larsudd-Kåverud, Julia Gyhagen, Sigvard Åkervall, Mattias Molin, Ian Milsom, Adrian Wagg, and Maria Gyhagen. The influence of pregnancy, parity, and mode of delivery on urinary incontinence and prolapse surgery—a national register study. *American Journal of Obstetrics and Gynecology*, 228:61.e1–61.e13, 1 2023. ISSN 10976868. doi: 10.1016/j.ajog.2022.07.035.

[38] Lee Una J.a; Kerkhof Manon H.b; van Leijsen Sanne A.c; Heesakkers John P.d. Obesity and pelvic organ prolapse. *Current Opinion in Urology*, pages 428–434, 9 2017.

[39] Urogynecology University of Colorado. Menopause & prolapse. URL https://urogyn.coloradowomenshealth.com/conditions/pelvic-floor-disorders/menopause-prolapse.html. Accessed: 2024-06-20.

[40] Shervil Kagayaita Sayko, Eighty Mardiyan Kurniawati, and Pudji Lestari. Age as the risk factor that affected the increased degree of uterine prolapse. *Biomolecular and Health Science Journal*, 1:20, 5 2018. doi: 10.20473/bhsj.v1i1.8210.

[41] Elizabeth Culleton-Quinn, Kari Bø, Neil Fleming, David Mockler, Cinny Cusack, and Déirdre Daly. Elite female athletes' experiences of symptoms of pelvic floor dysfunction: A systematic review. *International Urogynecology Journal*, 33:2681–2711, 10 2022. ISSN 14333023. doi: 10.1007/s00192-022-05302-6.

[42] Tea Kuittinen, Sari Tulokas, Päivi Rahkola-Soisalo, Tea Brummer, Jyrki Jalkanen, Eija Tomas, Juha Mäkinen, Jari Sjöberg, Päivi Härkki, and Maarit Mentula. Pelvic organ prolapse after hysterectomy: A 10-year national follow-up study. *Acta Obstetricia et Gynecologica Scandinavica*, 102:556–566, 5 2023. ISSN 16000412. doi: 10.1111/aogs.14542.

[43] Matthew D. Barber and Christopher Maher. Epidemiology and outcome assessment of pelvic organ prolapse. *International Urogynecology Journal and Pelvic Floor Dysfunction*, 24:1783–1790, 11 2013. ISSN 09373462. doi: 10.1007/s00192-013-2169-9.

[44] Sumaira Mubarik, Kristina Allen-Brady, Salvatore Giovanni Vitale, and Mingfu Wu. Global burden and trends of pelvic organ prolapse associated with aging women: An observational trend study from 1990 to 2019. *Frontiers in public health*, 2022.

[45] Heidi W. Brown, Aparna Hegde, Markus Huebner, Hedwig Neels, Hayley C. Barnes, Gisele Vissoci Marquini, Narmin Mukhtarova, Bernard Mbwele, Visha Tailor, Ervin Kocjancic, Elisa Trowbridge, and Lynsey Hayward. International urogynecology consultation chapter 1 committee 2: Epidemiology of pelvic organ prolapse: prevalence, incidence, natural history, and service needs, 2 2022. ISSN 14333023.

[46] Bernard T. Haylen, Christopher F. Maher, Matthew D. Barber, Sérgio Camargo, Vani Dandolu, Alex Digesu, Howard B. Goldman, Martin Huser, Alfredo L. Milani, Paul A. Moran,

Gabriel N. Schaer, and Mariëlla I.J. Withagen. An international urogynecological association (iuga) / international continence society (ics) joint report on the terminology for female pelvic organ prolapse (pop), 2 2016. ISSN 15206777.

[47] International Urogynecological Association (IUGA). Pelvic organ prolapse, 6 2024. URL https://www.iuga.org/news/news/june-is-pelvic-organ-prolapse-pop-awareness-month. Accessed: 2024-06-20.

[48] Fiona Reid. Assessment of pelvic organ prolapse: a practical guide to the pelvic organ prolapse quantification. *Obstetrics, Gynaecology & Reproductive Medicine*, 2014.

[49] Chendrimada Madhu, Steven Swift, Sophie Moloney-Geany, and Marcus J. Drake. How to use the pelvic organ prolapse quantification (pop-q) system? *Neurourology and Urodynamics*, 37:S39–S43, 8 2018. ISSN 15206777. doi: 10.1002/nau.23740.

[50] Anuja Bhalerao Vaidehi A Duddalwar. Comparative study to evaluate intersystem association between pelvic organ prolapse quantification system and simplified pelvic organ prolapse scoring system. *Journal of South Asian Federation of Obstetrics and Gynaecology*, 13, 2021.

[51] Yoon I; Gupta N. *Pelvic Prolapse Imaging*. StatPearls, 1 2023. URL https://www.ncbi.nlm.nih.gov/books/NBK551513/. Accessed: 2024-06-20.

[52] João Cunha Salvador, Mónica Portela Coutinho, José Marques Venâncio, and Bárbara Viamonte. Dynamic magnetic resonance imaging of the female pelvic floor—a pictorial review. *Insights into Imaging*, 10, 12 2019. ISSN 18694101. doi: 10.1186/s13244-019-0687-9.

[53] InformedHealth.org. Pelvic organ prolapse: Overview. *Journal of Medicine and Life*, 8 2018. URL https://www.ncbi.nlm.nih.gov/books/NBK525783/.

[54] UChicagoMedicine. Pelvic organ prolapse, 2023. URL https://www.uchicagomedicine.org/conditions-services/obgyn/urogynecology/pelvic-organ-prolapse. Accessed: 2024-06-20.

[55] Kari Bø, Sònia Anglès-Acedo, Achla Batra, Ingeborg Hoff Brækken, Yi Ling Chan, Cristine Homsi Jorge, Jennifer Kruger, Manisha Yadav, and Chantale Dumoulin. International urogynecology consultation chapter 3 committee 2; conservative treatment of patient with pelvic organ prolapse: Pelvic floor muscle training. *International Urogynecology Journal*, 33:2633–2667, 10 2022. ISSN 14333023. doi: 10.1007/s00192-022-05324-0.

[56] J. E. Jelovsek, C. Maher, and M. D. Barber. Pelvic organ prolapse. *Lancet (London, England)*, 369(9566):1027–1038, 2007. doi: 10.1016/S0140-6736(07)60462-0. URL https://doi.org/10.1016/S0140-6736(07)60462-0.

[57] Wendy Watkins. How to strengthen your pelvic-floor muscles, 12 2024. URL https://experiencelife.lifetime.life/article/fitness-fix-strengthening-your-pelvic-floor-muscles/. Accessed: 2024-06-20.

[58] Fulian Zhong, Wenbin Miao, Zhixia Yu, Lu Hong, and na Deng. Clinical effect of electrical stimulation biofeedback therapy combined with pelvic floor functional exercise on postpartum pelvic organ prolapse. *Am J Transl Res*, 13:6629–6637, 2021. URL www.ajtr.org.

[59] Barbara Bevilacqua Zeiger, Silvia da Silva Carramão, Carlos Antônio Del Roy, Thais Travassos da Silva, Susane Mei Hwang, and Antonio Pedro Flores Auge. Vaginal pessary in advanced pelvic organ prolapse: impact on quality of life. *International Urogynecology Journal*, 33:2013–2020, 7 2022. ISSN 14333023. doi: 10.1007/s00192-021-05002-7.

[60] C. B. Iglesia and K. R. Smithling. Pelvic organ prolapse. *American family physician*, 96 (3):179–185, 2017.

[61] Marianne Koch; Greta Carlin; Sören Lange; Wolfgang Umek; Christoph Krall; Barbara Bodner-Adler. Long-term adherence to pessary use in women with pelvic organ prolapse: A retrospective cohort study. *Maturitas*, 178, 2023. URL https://www.sciencedirect.com/science/article/pii/S0378512223004346.

[62] U. Kalkan, T. Yoldemir, E. S. Ozyurek, and A. Daniilidis. Native tissue repair versus mesh repair in pelvic organ prolapse surgery. *Climacteric*, 20:510–517, 11 2017. ISSN 14730804. doi: 10.1080/13697137.2017.1366978.

[63] Soo Young Jeong, Kyoungseon Kim, Ji Won Ryu, Jieum Cha, Sung Taek Park, and Sung Ho Park. Comparison of surgical outcomes of robotic versus conventional laparoscopic hysterectomy of large uterus with gynecologic benign disease. *Journal of Personalized Medicine*, 12, 12 2022. ISSN 20754426. doi: 10.3390/jpm12122042.

[64] Informed. Pelvic organ prolapse: Learn more – surgery for pelvic organ prolapse, 2021. URL https://www.ncbi.nlm.nih.gov/books/NBK525780/. Accessed: 2024-06-20.

[65] Amelia Seifalian, Zeinab Basma, Alex Digesu, and Vikram Khullar. Polypropylene pelvic mesh: What went wrong and what will be of the future? *Biomedicines*, 11, 3 2023. ISSN 22279059. doi: 10.3390/biomedicines11030741.

[66] S. Todros, P. G. Pavan, and A. N. Natali. Synthetic surgical meshes used in abdominal wall surgery: Part i—materials and structural conformation. *Journal of Biomedical Materials Research - Part B Applied Biomaterials*, 105:689–699, 4 2017. ISSN 15524981. doi: 10.1002/jbm.b.33586.

[67] Hirotaka Sato, Shota Otsuka, Hirokazu Abe, and Tomoaki Miyagawa. Medium-term risk of recurrent pelvic organ prolapse within 2-year follow-up after laparoscopic sacrocolpopexy. *Gynecology and Minimally Invasive Therapy*, 12:38–43, 1 2023. ISSN 22133089. doi: 10.4103/gmit.gmit_59_22.

[68] Silveira Brazão Júnior, Zanettini Riccetto, Cássio Luís, and Rodrigues Palma. Controvérsias com o emprego de malhas no tratamento de problemas do assoalho pélvico. *Revista Peruana de Ginecología y Obstetricia*, 2016. ISSN 2304-5124. URL http://www.redalyc.org/articulo.oa?id=323445253009. Accessed: 2024-06-20.

[69] Mengqin Yuan, Min Hu, Fangfang Dai, Yaqi Fan, Zhimin Deng, Hongbing Deng, and Yanxiang Cheng. Application of synthetic and natural polymers in surgical mesh for pelvic floor reconstruction. *Materials and Design*, 209, 11 2021. ISSN 18734197. doi: 10.1016/j.matdes.2021.109984.

[70] Karen Baylón, Perla Rodríguez-Camarillo, Alex Elías-Zúñiga, Jose Antonio Díaz-Elizondo, Robert Gilkerson, and Karen Lozano. Past, present and future of surgical meshes: A review. *Membranes*, 7, 9 2017. ISSN 20770375. doi: 10.3390/membranes7030047.

[71] Elena Mancuso, Candice Downey, Elizabeth Doxford-Hook, Michael G. Bryant, and Peter Culmer. The use of polymeric meshes for pelvic organ prolapse: Current concepts, challenges, and future perspectives. *Journal of Biomedical Materials Research - Part B Applied Biomaterials*, 108:771–789, 4 2020. ISSN 15524981. doi: 10.1002/jbm.b.34432.

[72] Paulo Rodrigues and Shlomo Raz. The burden of reoperations and timeline of problems in 1,530 cases of mesh-related complications. *Urologia Internationalis*, 106:235–242, 3 2022. ISSN 14230399. doi: 10.1159/000514389.

[73] FDA. Fda takes action to protect women's health, orders manufacturers of surgical mesh intended for transvaginal repair of pelvic organ prolapse to stop selling all devices, 4 2019. URL https://www.fda.gov/news-events/press-announcements/fda-takes-action-protect-womens-health-orders-manufacturers-/surgical-mesh-intended-transvaginal. Accessed: 2024-06-20.

[74] BCPA Michelle Llamas. Transvaginal mesh complications: Pelvic organ prolapse, 9 2023. URL https://www.drugwatch.com/transvaginal-mesh/complications-and-problems/. Accessed: 2024-06-20.

[75] R. Rynkevic, M. E.T. Silva, P. Martins, T. Mascarenhas, J. L. Alves, and A. A. Fernandes. Characterisation of polycaprolactone scaffolds made by melt electrospinning writing for pelvic organ prolapse correction - a pilot study. *Materials Today Communications*, 32, 8 2022. ISSN 23524928. doi: 10.1016/j.mtcomm.2022.104101.

[76] Wing Kam Liu, Shaofan Li, and Harold S. Park. Eighty years of the finite element method: Birth, evolution, and future. *Archives of Computational Methods in Engineering*, 29:4431–4453, 10 2022. ISSN 18861784. doi: 10.1007/s11831-022-09740-9.

[77] Vishal Jagota, Aman Preet, Singh Sethi, and Khushmeet Kumar. Finite element method: An overview. *Walailak J Sci & Tech*, 10:1–8, 2013. URL http://wjst.wu.ac.th.

[78] G.R. Liu and S.S. Quek. *Chapter 1 - Computational Modeling*, pages 1–11. Elsevier, 2014. doi: 10.1016/B978-0-08-098356-1.00001-1. URL https://linkinghub.elsevier.com/retrieve/pii/B9780080983561000011.

[79] A.J. Peyton. *3 - Electromagnetic induction tomography*, pages 61–107. Woodhead Publishing Series in Electronic and Optical Materials. Woodhead Publishing, 2015. ISBN 978-1-78242-118-4. doi: https://doi.org/10.1016/B978-1-78242-118-4.00003-4. URL https://www.sciencedirect.com/science/article/pii/B9781782421184000034.

[80] Jonathan Whiteley. *Mathematical Engineering - Finite Element Methods: A Practical Guide*, chapter An Overview of the Finite Element Method. Springer, 2017. URL http://www.springer.com/series/8445.

[81] IEEE. The advantages of the finite element method, . URL https://innovationatwork.ieee.org/the-advantages-of-fem/. Accessed: 2024-06-20.

[82] Kornelius Kupczik. Virtual biomechanics: basic concepts and technical aspects of finite element analysis in vertebrate morphology. *Journal of anthropological sciences*, 86, 2008.

[83] IEEE. How the finite element method (fem) and finite element analysis (fea) work together, . URL https://innovationatwork.ieee.org/how-the-finite-element-method-fem-and-finite-element-analysis-//fea-work-together/. Accessed: 2024-06-20.

[84] Johannes Reiner and Reza Vaziri. *Structural Analysis of Composites With Finite Element Codes: An Overview of Commonly Used Computational Methods*, chapter 8.4, pages 61–84. Elsevier, 2018.

[85] SIMULIA. Abaqus, . URL https://www.3ds.com/products/simulia/abaqus. Accessed: 2024-06-20.

[86] SIMULIA. Differences between abaqus standard & abaqus explicit, . URL https://caeassistant.com/blog/abaqus-standard-or-abaqus-explicit/#3_Explicit_or_Standard_Which_one_should_I_use. Accessed: 2024-06-20.

[87] Jiachen Xie, Song Li, Tingqiang Yao, and Jihong Shen. A 2d equivalent mechanical model of the whole pelvic floor and impairment simulation. *International Journal for Numerical Methods in Biomedical Engineering*, 39, 1 2023. ISSN 20407947. doi: 10.1002/cnm.3659.

[88] Jialan Chen, Junfeng Zhang, and Fan Wang. A finite element analysis of different postures and intra-abdominal pressures for the uterine ligaments in maintaining the normal position of uterus. *Scientific Reports*, 13, 12 2023. ISSN 20452322. doi: 10.1038/s41598-023-32368-z.

[89] Jorge Nuno and Machado Bessa. Modelação numérica de redes sintéticas para correção de prolapso uterino. Master's thesis, Faculty of Engineering, University of Porto, 2020.

[90] Jörgen Bergström. *Elasticity/Hyperelasticity*, pages 209–307. Elsevier, 2015. doi: 10.1016/b978-0-323-31150-2.00005-4.

[91] Hoss Belyadi, Ebrahim Fathi, and Fatemeh Belyadi. *Rock mechanical properties and in situ stresses*, pages 215–231. Elsevier, 2019. doi: 10.1016/b978-0-12-817665-8.00013-8.

[92] Junling Hou, Xuan Lu, Kaining Zhang, Yidong Jing, Zhenjie Zhang, Junfeng You, and Qun Li. Parameters identification of rubber-like hyperelastic material based on general regression neural network. *Materials*, 15, 6 2022. ISSN 19961944. doi: 10.3390/ma15113776.

[93] Ekaterina Stansfield, Krishna Kumar, Philipp Mitteroecker, and Nicole D S Grunstra. Biomechanical trade-offs in the pelvic floor constrain the evolution of the human birth canal. *PNAS*, 2021. doi: 10.1073/pnas.2022159118/-/DCSupplemental.

[94] D. P. Rosen and J. Jiang. A comparison of hyperelastic constitutive models applicable to shear wave elastography (swe) data in tissue-mimicking materials. *Physics in Medicine and Biology*, 64, 2019. ISSN 13616560. doi: 10.1088/1361-6560/ab0137.

[95] Hyperelastic material behavior, 2022. URL https://help.3ds.com/2022x/english/dsdoc/SIMA3DXMATRefMap/simamat-c-damageevolductile.htm?contextscope=cloud&format=P&value=undâĂę. Accessed: 2024-06-20.

[96] Sofia Brandão, Marco Parente, Thuane Huyer Da Roza, Elisabete Silva, Isabel Maria Ramos, Teresa Mascarenhas, and Renato Manuel Natal Jorge. On the stiffness of the mesh and urethral mobility: A finite element analysis. *Journal of Biomechanical Engineering*, 139, 8 2017. ISSN 15288951. doi: 10.1115/1.4036606.

[97] Helena Talasz, Christian Kremser, Markus Kofler, Elisabeth Kalchschmid, Monika Lechleitner, and Ansgar Rudisch. Proof of concept: Differential effects of valsalva and straining maneuvers on the pelvic floor. *European Journal of Obstetrics and Gynecology and Reproductive Biology*, 164:227–233, 2012. ISSN 18727654. doi: 10.1016/j.ejogrb.2012.06.019.

[98] Emmanuel Payebto Zoua, Michel Boulvain, and Patrick Dällenbach. The distribution of pelvic organ support defects in women undergoing pelvic organ prolapse surgery and compartment specific risk factors. *International Urogynecology Journal*, 2022. doi: 10.1007/s00192-021-04826-7.

[99] Monica V. Deshpande, Arjunsing Girase, and Martin W. King. Degradation of poly(ε-caprolactone) resorbable multifilament yarn under physiological conditions. *Polymers*, 15, 9 2023. ISSN 20734360. doi: 10.3390/polym15183819.

[100] Corbion C.P. what matters. Bioresorbable polymers. URL https://www.corbion.com/. Accessed: 2024-06-20.

[101] Maria Francisca Reis Rabaça Vaz. 3d printing and development of 3d computational models of biodegradable meshes. Master's thesis, Faculty of Engineering - University of Porto, 2023.

[102] SIMULIA. Damage evolution and element removal for ductile metals, 2022. URL https://help.3ds.com/2022x/english/dsdoc/SIMA3DXMATRefMap/simamat-c-damageevolductile.htm?contextscope=cloud&format=P&value=undâĂę. Accessed: 2024-06-20.

[103] Ronald Wagner. Abaqus tutorial: Damage for ductile metals - material model explained - ductile damage, 03 2021. URL https://www.researchgate.net/publication/350124892_ABAQUS_Tutorial_Damage_for_Ductile_Metals_-_Material_Model_Explained_-_Ductile_Damage. Accessed: 2024-06-20.

[104] DynaMesh® Tailored Implants Made of PVDF. Dynamesh pr, . URL https://en.dyna-mesh.com/dynamesh-pr-gb/. Accessed: 2024-06-20.

[105] Simulia Abaqus. Abaqus theory manual: 3.5.1. beam element overview. URL https://classes.engineering.wustl.edu/2009/spring/mase5513/abaqus/docs/v6.6/books/stm/default.htm?startat=ch03s05ath73.html.

[106] André Teófilo Beck and Cláudio R.A. da Silva. Timoshenko versus euler beam theory: Pitfalls of a deterministic approach. *Structural Safety*, 33:19–25, 1 2011. ISSN 01674730. doi: 10.1016/j.strusafe.2010.04.006.

[107] DynaMesh® Tailored Implants Made of PVDF. Dynamesh prp, . URL https://en.dyna-mesh.com/dynamesh-prp-gb/. Accessed: 2024-06-20.

[108] Pedro Alexandre Lopes and Sousa Martins. *Experimental and numerical studies of soft biological tissues*. PhD thesis, Faculty of Engineering, University of Porto, 2010.

[109] Luyun Chen, James A. Ashton-Miller, Yvonne Hsu, and John O.L. DeLancey. Interaction among apical support, levator ani impairment, and anterior vaginal wall prolapse. *Obstetrics and Gynecology*, 108:324–332, 8 2006. ISSN 00297844. doi: 10.1097/01.AOG.0000227786.69257.a8.

[110] Barbara Röhrnbauer, Cornelia Betschart, Daniele Perucchini, Michael Bajka, Daniel Fink, Caroline Maake, Edoardo Mazza, and David Amos Scheiner. Measuring tissue displacement of the anterior vaginal wall using the novel aspiration technique in vivo. *Scientific Reports*, 7, 12 2017. ISSN 20452322. doi: 10.1038/s41598-017-16083-0.

[111] Sebastian Sterk. Development of new surgical mesh geometries with different mechanical properties using the design freedom of 3d printing master of mechanical engineering. Master's thesis, Faculty of Engineering, University of Porto, 2023.

[112] Shuang Chen, Yuhao Liu, Liao Peng, Yuanzhuo Chen, Hong Shen, and Deyi Luo. Comparative study of absorbable suture and permanent suture in sacrocolpopexy: a meta-analysis and systematic review. *International Urogynecology Journal*, 34:993–1000, 5 2023. ISSN 14333023. doi: 10.1007/s00192-022-05427-8.

[113] Bracha L. Pollack, Patrick Popiel, Miriam C. Toaff, Elizabeth Drugge, Adrienne Bielawski, Ashley Sacks, Moses Bibi, Rebecca Friedman-Ciment, Kira Lebron, Leael Alishahian, Dena Phillips, Sara R. Rubino, Sela Pollack, Rida S. Khan, Eesha S. Khan, Dominique Malacarne Pape, and Cara L. Grimes. Permanent compared with absorbable suture in apical prolapse surgery: A systematic review and meta-analysis. *Obstetrics and Gynecology*, 141:268–283, 2 2023. ISSN 1873233X. doi: 10.1097/AOG.0000000000005032.

[114] Heather van Raalte, Nina Bhatia, Jeffrey Mangel, Hugo Ryckebusch, and Jan Paul Roovers. A novel anchoring system for pelvic organ prolapse repair: an observational study. *International Urogynecology Journal*, 34:1593–1598, 7 2023. ISSN 14333023. doi: 10.1007/s00192-022-05444-7.

[115] Isuzu Meyer, Christina T. Blanchard, Jeff M. Szychowski, and Holly E. Richter. Five-year surgical outcomes of transvaginal apical approaches in women with advanced pelvic organ prolapse. *International Urogynecology Journal*, 34:2171–2181, 9 2023. ISSN 14333023. doi: 10.1007/s00192-023-05501-9.